Science Advances
AAAS

advances.sciencemag.org/cgi/content/full/5/6/eaaw5873/DC1

# Supplementary Materials for

## Nuclear DNA from two early Neandertals reveals 80,000 years of genetic continuity in Europe

Stéphane Peyrégne*, Viviane Slon, Fabrizio Mafessoni, Cesare de Filippo, Mateja Hajdinjak, Sarah Nagel, Birgit Nickel, Elena Essel, Adeline Le Cabec, Kurt Wehrberger, Nicholas J. Conard, Claus Joachim Kind, Cosimo Posth, Johannes Krause, Grégory Abrams, Dominique Bonjean, Kévin Di Modica, Michel Toussaint, Janet Kelso, Matthias Meyer, Svante Pääbo, Kay Prüfer*

*Corresponding author. Email: stephane_peyregne@eva.mpg.de (S.Pe.); pruefer@eva.mpg.de (K.P.)

Published 26 June 2019, *Sci. Adv.* **5**, eaaw5873 (2019)
DOI: 10.1126/sciadv.aaw5873

**This PDF file includes:**

Table S7. Present-day human DNA contamination estimates from *Scladina I-4A* mtDNA based on differences between Neandertals and modern humans.
Table S8. Sequencing summary statistics for *HST* with the following filters: length (≥35 bp) and mapping quality (≥25).
Table S9. Sequencing summary statistics for *HST* with the following filters: length (≥30 bp) and mapping quality (≥25).
Table S10. Sequencing summary statistics for *Scladina I-4A* with the following filters: length (≥35 bp) and mapping quality (≥25).
Table S11. Sequencing summary statistics for *Scladina I-4A* with the following filters: length (≥30 bp) and mapping quality (≥25).
Table S12. Sequencing statistics of the negative controls for *HST* (see table S1).
Table S13. Sequencing statistics of the negative controls for *Scladina I-4A* (see table S2).
Table S14. Summary of *HST* mtDNA sequencing.
Table S15. Summary of *Scladina I-4A* mtDNA sequencing.
Table S16. Coverage statistics for all sequences from *HST* within the alignability track, map35_L100.
Table S17. Coverage statistics for *HST* sequences with a C-to-T substitution within the three first or last positions of either ends.
Table S18. Coverage statistics for all sequences from *Scladina I-4A* within the alignability track, map35_L100.
Table S19. Coverage statistics for *Scladina I-4A* sequences with a C-to-T substitution within the three first or last positions of either ends.
Table S20. Present-day human DNA contamination estimates from *HST* mtDNA.
Table S21. Present-day human DNA contamination estimates from *Scladina I-4A* mtDNA based on differences between Neandertals and modern humans.
Table S22. Present-day human DNA contamination estimates from *Scladina I-4A* mtDNA based on differences between *Scladina I-4A* and modern humans.
Table S23. Present-day human DNA contamination estimates on mtDNA in the blank libraries of *HST* based on differences between *HST* and modern humans.
Table S24. Present-day human DNA contamination estimates on mtDNA in the blank libraries of *Scladina I-4A* based on differences between Neandertals and modern humans.
Table S25. Best substitution models according to the three model selection measures computed by jModelTest 2.1.10.
Table S26. Marginal likelihoods of the different tested clock and tree models obtained from a path sampling approach using only the coding region of the mitochondrial sequences.
Table S27. Marginal likelihoods of the different tested clock and tree models obtained from a path sampling approach using the full mitochondrial genome sequences.
Table S28. Estimates of molecular age and divergence times.
Table S29. Present-day human DNA contamination estimates for *HST* nuclear DNA based on deamination rates on the last positions of the molecules.
Table S30. Present-day human DNA contamination estimates for *Scladina I-4A* nuclear DNA based on deamination rates on the last positions of the molecules.
Table S31. Relationship between sequence length and present-day human DNA contamination estimate based on deamination rates in *HST* nuclear DNA sequences.
Table S32. Present-day human DNA contamination estimates based on the sharing of derived alleles with a modern human.
Table S33. Genome-wide counts of the three possible allelic configurations informative about the underlying topologies relating *Vindija 33.19* and the Altai Neandertal to *HST* and *Scladina I-*

*4A* before correcting for reference bias or contamination (see tables S40 and S41 for corrected results and fig. S17 for a description of these allelic configurations).
Table S34. Comparison of alignments to hg19 and panTro4.
Table S35. Excess of ancestral alleles in Late Neandertals compared to *Vindija 33.19* at sites that are derived in the Altai Neandertal genome but ancestral in the genomes of an Mbuti and a Denisovan.
Table S36. Effect of the modified alignment procedure on the allele sharing with the Altai Neandertal.
Table S37. Alleles seen in *Vindija 87* at positions that are heterozygous in *Vindija 33.19*.
Table S38. Sequencing and alignment errors of *Vindija 87* sequences at positions where *Vindija 33.19* is homozygous different from the Altai Neandertal, comparing the original alignments to hg19 with our modified alignment procedure.
Table S39. Summary of the alignments to the two references.
Table S40. Applying different sequence lengths cutoffs does not affect the allele sharing with the Altai Neandertal after realignments.
Table S41. Genome-wide counts of the three possible allelic configurations informative about the underlying topologies relating *Vindija 33.19* and the Altai Neandertal to *HST* and *Scladina I-4A* after correcting for reference bias (see table S33 to compare with uncorrected results and table S42 for results corrected for contamination).
Table S42. Counts of the three possible allelic configurations informative about the underlying topologies relating *Vindija 33.19* and the Altai Neandertal to *HST* and *Scladina I-4A* after correcting for both reference bias and contamination.
Table S43. Summary statistics about the physical distance between the positions used to infer the genetic relationship of *HST* to *Vindija 33.19* and the Altai Neandertal.
Table S44. Summary statistics about the physical distance between the positions used to infer the genetic relationship of *Scladina I-4A* to *Vindija 33.19* and the Altai Neandertal.
Table S45. Effective number of independent positions.
Table S46. Comparison between split time estimates from the Vindija population based on a coalescent divergence model and the F(A|B) statistic for five low-coverage Neandertal genomes.
Table S47. Split time estimates from the Vindija population based on a coalescent divergence model.
Table S48. Age estimate for individual B (branch shortening) used to convert the F(A|B) values shown in table S47 into time before present.
Table S49. Summary of the number of sites and blocks used to compute the F(A|B) statistic and CIs.
Table S50. Split time estimates between *HST* or *Scladina I-4A* and different populations (population B) based on the calibration of the F(A|B) statistic.
Table S51. Predictions of the mitochondrial TMRCA given different split times between the populations of *HST* and *Vindija 33.19*.
Table S52. Predictions of the mitochondrial TMRCA given different split times between the *Vindija 33.19* population and a hypothetical isolated Neandertal population.
Table S53. Predictions of the mitochondrial TMRCA as done for table S51 but using either the upper or the lower estimates of the Neandertal population size.
Fig. S1. Length distribution of unique DNA fragments aligned to the human reference genome hg19 with a mapping quality of 25 or above (average length = 33 bp for *HST* and 25 bp for *Scladina I-4A*) and mapping uniquely (alignability track, map35_L100).
Fig. S2. Proportion of spurious alignment for different sequence lengths in the three libraries of *HST* that represent ~80% of the generated sequences for this specimen.

# Note S1. Ancient DNA recovery and treatment.

## *Sampling, decontamination procedures and DNA extraction*

**Hohlenstein-Stadel Neandertal (*HST*):** Using a dentistry drill, a total of 315 mg of bone powder was removed from the *HST* femur, after having removed the external surface of the bone from the sampling site. **Table S1** presents an outline of the laboratory procedures performed on the bone powder collected from this specimen and the negative controls carried along the sample.

In an initial experiment (set 1 in **table S1**), we applied three different decontamination strategies, each on ~30 mg of bone powder. Four 2.8 mm ceramic beads (Precellys ceramic kit, Peqlab, Erlangen, Germany) were added to each bone powder to assist in the resuspension steps (*17*).

(I) Pre-digestion and re-extraction of the bone pellet (*38*, *39*): 0.5 ml of lysis buffer (0.45 M EDTA, pH 8.0; 0.25 mg/ml Proteinase K; 0.05% Tween-20) was added to the bone powder and rotated for 5 minutes at 37°C. The bone powder was pelleted using a bench centrifuge and the supernatant, constituting the 'pre-digestion' fraction, was transferred to a fresh tube and stored at -20°C until the next day. 0.5 mL of lysis buffer was then added to the bone pellet and rotated overnight at 37°C ('re-extraction' fraction).

(II) Washing with 0.5% sodium hypochlorite solution (*17*): The bone powder was incubated in 1 mL of 0.5% sodium hypochlorite solution for 15 minutes at room temperature with rotation. After pelleting the bone powder, three consecutive washes with 1 mL water were carried out for 3 minutes each at room temperature. The bone pellet was then resuspended in 0.5 mL of lysis buffer and rotated overnight at 37°C.

(III) Washing with sodium phosphate solution (*17*): The bone powder was incubated three times in 1 ml of sodium phosphate buffer (0.5 M sodium phosphate, pH 7.0; 0.1% Tween-20) for 15 minutes at room temperature, each time removing the supernatant after pelleting the bone powder using a bench centrifuge prior to the next incubation step. Residual sodium phosphate buffer was removed by re-suspending the bone pellet using 1 mL of TT buffer (10 mM Tris-HCl, pH 8.0; 0.1% Tween-20). As above, the bone pellet was incubated with rotation in 0.5 mL of lysis buffer overnight at 37°C.

In all procedures, following the overnight incubation in lysis buffer, DNA was bound to silica columns, purified and eluted for a total volume of 50 µL as described in (*14*) with modifications in (*17*). As the incubation with 0.5% sodium hypochlorite solution reduced the microbial and present-day human DNA contamination most efficiently (see **tables S3** and **S6**), three additional bone powder samples from *HST* were treated and extracted using this procedure on two separate occasions (sets 2 and 3 in **table S1**).

***Scladina I4-A*:** We removed in total 50.7 mg of bone powder from the Scladina maxillary fragment (*Scla 4A-2*), 56.2 mg of the dentine of its *in situ* unerupted right permanent upper second premolar (*Scla 4A-2/P*$^4$), and 45.4 mg of dentine from its isolated right deciduous lower second molar (*Scla 4A-13*) using a sterile dentistry drill. The obtained powder from each specimen was evenly split in two separate "aliquots". In an initial screening, one powder aliquot was extracted using a silica-based method (*14*) as implemented in (*17*) with no prior pre-treatment of the powder (**table S2**). The second powder aliquot of each specimen was treated

with 0.5% sodium hypochlorite solution prior to DNA extraction, as described above, in an attempt to remove present-day human and microbial DNA contamination from the specimens (*17*).

## *DNA library preparation*

Aliquots of 10 or 15 µL of the DNA extracts were used to generate single-stranded DNA libraries, either manually using the protocol in (*16*) with the modifications as described in (*17*); or on an automated liquid handling platform (Bravo NGS workstation B, Agilent Technologies) using the implementation of the protocol in (*15*) described in (*33*). The number of DNA molecules in each library, as well as the number of control oligonucleotides spiked-in to monitor the efficiency of library preparation (*40*), were quantified by quantitative PCR (qPCR) (*16, 40*) or digital droplet PCR (ddPCR) (QX200 system, Bio-Rad) (*41*). Each library was labelled with two unique indexes and amplified into plateau using AccuPrime Pfx DNA polymerase (Life Technologies) (*42*) following the procedure of (*32*) as modified in (*17*). PCR products were purified using the MinElute PCR purification kit (Qiagen); or using SPRI beads (*43*) on the automated liquid handling platform (*33*). DNA concentration of the purified DNA libraries was determined using a NanoDrop Spectrophotometer ND-1000 (NanoDrop Technologies).

## *Enrichment for human mitochondrial DNA*

An aliquot of each DNA library, containing ~1 µg of DNA, was enriched for human mitochondrial (mt) DNA fragments using a hybridization capture method (*44*) as modified in (*33*). Probes spanning the full mitochondrial genome included in the human reference genome version hg19 (*45*) or the revised Cambridge Reference Sequence (rCRS) (*33*) were used as baits. The hybridization capture was carried out in one or two rounds, either manually or using the automated liquid handling platform as described in (*33*).

## *Sequencing*

The amplified libraries were pooled along with libraries from other experiments. Each pool underwent a single-cycle PCR amplification by Herculase II Fusion DNA polymerase (Agilent Technologies) (*42*) with primers IS5 and IS6 (*46*) to remove heteroduplices. Sequencing was carried out on Ilumina MiSeq and HiSeq 2500 in 76-cycle paired-end runs (*32*).

**Table S1. Overview of DNA extracts and libraries prepared from the *HST* femur.** Data are shown per DNA extraction set, with negative controls indicated in gray. (*) – quantification was carried out by quantitative PCR. Extraction Negative Control (ENC), Library Negative Control (LNC).

| Set | Extract ID | Amount powder [mg] | Decontamination method | Input in library [µl] | Library preparation protocol (reference) | Number of molecules | Number of control oligonucleotide | Indexed library ID | Captured library ID |
|---|---|---|---|---|---|---|---|---|---|
| 1 | E2899 | 30.4 | Pre-digested fraction | 15 | (*16*) | 5.02E+09 | 9.00E+05 | L5262 | L5289 |
| | E2900 | | Re-extraction | 15 | (*16*) | 2.80E+09 | 7.85E+05 | L5263 | L5290 |
| | E2901 | 29.4 | Sodium hypochlorite | 15 | (*16*) | 3.80E+08 | 7.40E+05 | L5264 | L5291 |
| | E2902 | 30.1 | Phosphate buffer | 15 | (*16*) | 6.45E+08 | 3.05E+05 | L5265 | L5292 |
| | ENC | - | - | 15 | (*16*) | 6.10E+07 | 5.65E+05 | L5266 | L5293 |
| | ENC | - | Sodium hypochlorite | 15 | (*16*) | 6.35E+07 | 3.95E+05 | L5267 | L5294 |
| | ENC | - | Phosphate buffer | 15 | (*16*) | 3.39E+08 | 7.70E+05 | L5268 | L5295 |
| | LNC | - | - | 15 | (*16*) | 2.86E+07 | 5.70E+05 | L5270 | L5296 |
| 2 | E3035 | 31.8 | Sodium hypochlorite | 15 | (*16*) | 2.58E+08 | 2.55E+05 | L5386 | L5408 |
| | | | | 10 | (*15*) | 2.94E+07 (*) | 5.98E+05 (*) | F7016 | F4166 |
| | | | | 10 | (*15*) | 2.94E+07 (*) | 7.30E+05 (*) | F7017 | F4167 |
| | ENC | - | Sodium hypochlorite | 15 | (*16*) | 7.05E+07 | 9.15E+05 | L5389 | L5411 |
| | LNC | - | - | 15 | (*16*) | 2.87E+07 | 2.35E+05 | L5400 | L5413 |
| | LNC | - | - | 10 | (*15*) | 1.62E+07 (*) | 1.20E+06 (*) | F3995 | F4146 |
| 3 | E3656 | 34.6 | Sodium hypochlorite | 10 | (*16*) | 4.24E+07 (*) | 4.39E+04 (*) | R5784 | R4294 |
| | E3657 | 32.1 | Sodium hypochlorite | 10 | (*16*) | 4.03E+07 (*) | 5.35E+04 (*) | R5785 | R4295 |
| | ENC | - | Sodium hypochlorite | 10 | (*16*) | 1.83E+06 (*) | 3.69E+04 (*) | R5791 | R4301 |
| | LNC | - | - | 10 | (*16*) | 2.54E+06 (*) | 5.92E+04 (*) | R5792 | R4302 |

**Table S2. Overview of DNA extracts and libraries prepared for *Scladina I-4A*.** Negative controls are indicated in gray. All quantifications were carried out by quantitative PCR, rather than digital droplet PCR. Extraction Negative Control (ENC), Library Negative Control (LNC).

| Specimen | Extract ID | Amount powder [mg] | Decontamination method | Input in library [µl] | Library preparation protocol (reference) | Number of molecules | Number of control oligonucleotide | Indexed library ID | Captured library ID |
|---|---|---|---|---|---|---|---|---|---|
| **Scladina maxillary fragment** | E5322 | 26.2 | - | 10 | (*15*) | 2.35E+09 | 1.43E+06 | F3297 | D8925 |
| | E5846 | 24.5 | Sodium hypochlorite | 10 | (*15*) | 9.40E+07 | 3.79E+05 | F7490 | F4687 |
| | | | | 10 | (*15*) | 1.46E+08 | 4.18E+05 | G2159 | G3380 |
| | | | | 10 | (*15*) | 1.35E+08 | 4.52E+05 | G2160 | G3381 |
| | | | | 10 | (*15*) | 1.42E+08 | 4.49E+05 | G2161 | G3382 |
| **Scladina tooth in the maxilla** | E5323 | 24.9 | - | 10 | (*15*) | 6.51E+09 | 1.36E+06 | F3298 | D8926 |
| | E5847 | 31.3 | Sodium hypochlorite | 10 | (*15*) | 4.37E+08 | 5.63E+05 | F7491 | F4688 |
| **Scladina deciduous tooth** | E5324 | 17.3 | - | 10 | (*15*) | 6.25E+09 | 1.25E+06 | F3299 | D8927 |
| | E5849 | 28.1 | Sodium hypochlorite | 10 | (*15*) | 7.29E+07 | 7.85E+05 | F7493 | F4690 |
| **ENC** | E5331 | - | - | 10 | (*15*) | 6.16E+08 | 1.39E+06 | F3307 | D8934 |
| **ENC** | E5852 | - | Sodium hypochlorite | 10 | (*15*) | 1.31E+07 | 5.50E+05 | F7499 | F4693 |
| **LNC** | - | - | - | 10 | (*15*) | 4.49E+08 | 7.93E+05 | F3269 | D8904 |
| **LNC** | - | - | - | 10 | (*15*) | 5.31E+08 | 9.35E+05 | F3292 | D8923 |
| **LNC** | - | - | - | 10 | (*15*) | 1.24E+07 | 5.99E+05 | F7470 | F4675 |
| **LNC** | - | - | - | 10 | (*15*) | 6.71E+07 | 5.73E+05 | G2162 | G3383 |

# Note S2. Decontamination methods and initial screening.

For a cost-effective data production, we evaluated the decontamination strategies described in the previous section to select the most efficient method at increasing the proportion of endogenous sequences to contaminant sequences. The proportion of usable sequences was defined as the number of sequences that successfully mapped to the human reference genome over the total number of sequences generated (**tables S3**, **S4**, and **S5**). We further determined by qPCR or ddPCR the number of DNA molecules in each library, allowing us to estimate the number of usable sequences that would be generated from each library if the sequencing was performed to exhaustion (**tables S3**, **S4**, and **S5**) (*40*). We note that this calculation does not take into account any present-day human DNA contamination and therefore represents an upper estimate of the Neandertal DNA content. Therefore, we also estimated the proportion of present-day human DNA contamination by computing the proportion of molecules that carry the allele seen in modern humans at positions known to differ between the mitochondrial genomes of modern humans and Neandertals (as described in Supplementary Note 5).

For *HST*, of the three decontamination methods, the 0.5% sodium hypochlorite treatment yielded the highest proportion of human DNA sequences (**table S3**) and the lowest proportion of present-day human DNA contamination (**table S6**). We applied this treatment to three additional bone powder aliquots from *HST* and generated five single-stranded DNA libraries from these DNA extracts (**table S1**, see **table S4** for a summary of the human DNA content of these libraries).

For *Scladina I-4A*, an initial screening of DNA preservation in the different skeletal elements revealed high proportions of present-day human DNA contamination (83% to 99%, **Table S7**; see also **table S5** for a summary of their content of human DNA). We therefore applied the 0.5% sodium hypochlorite treatment to the bone/tooth powder, which led to an appreciable decrease of present-day human DNA contamination only in the maxillary bone (7% compared to 95% in the two other samples, **table S7**). Three additional single-stranded DNA libraries from this extract were generated and sequenced (**table S2**).

**Table S3. DNA content in the libraries prepared from *HST* extracts prepared following different decontamination methods (set 1 in table S1).** The usable fraction was calculated as the proportion of generated sequences that were longer than 35bp and mapped to the human reference genome with a mapping quality of at least 25. The average length was also computed from the molecules that are longer than 35bp and with a mapping quality of at least 25. The reported average genomic coverage corresponds to an estimate if the library was sequenced to exhaustion (based on a genome length of $3x10^9$bp, the expected number of usable sequences in the library and their average length, (*40*)).

| Extract ID | Treatment | Library ID | Number of molecules in the library | Usable fraction | Average sequence length | Estimated genomic coverage (library) | Estimated genomic coverage (extract) |
|---|---|---|---|---|---|---|---|
| E2899 | Pre-digested fraction | L5262 | 5.02E+09 | 0.0012 | 51.9 | 0.104 | 0.347 |
| E2900 | Re-extraction | L5263 | 2.80E+09 | 0.0017 | 54.6 | 0.087 | 0.288 |
| E2901 | Sodium hypochlorite | L5264 | 3.80E+08 | 0.0104 | 45.9 | 0.060 | 0.201 |
| E2902 | Phosphate buffer | L5265 | 6.45E+08 | 0.0052 | 47.7 | 0.053 | 0.178 |

**Table S4. DNA content in the libraries prepared from the bone powder treated with sodium hypochlorite.** Labelling as in **Table S3**.

| Neandertal | Extract ID | Library ID | Number of molecules in the library | Usable fraction | Average sequence length | Estimated genomic coverage (library) | Estimated genomic coverage (extract) |
|---|---|---|---|---|---|---|---|
| *Scladina I-4A* | E5846 | F7490 | 9.40E+07 | 0.0032 | 52.7 | 0.0053 | 0.0265 |
| *Scladina I-4A* | E5847 | F7491 | 4.37E+08 | 0.0925 | 52.8 | 0.7603 | 3.8015 |
| *Scladina I-4A* | E5849 | F7493 | 7.29E+07 | 0.0240 | 61.7 | 0.0359 | 0.1794 |
| *Scladina I-4A* | E5846 | G2159 | 1.46E+08 | 0.0018 | 54.9 | 0.0048 | 0.0240 |
| *Scladina I-4A* | E5846 | G2160 | 1.35E+08 | 0.0017 | 54.6 | 0.0042 | 0.0209 |
| *Scladina I-4A* | E5846 | G2161 | 1.42E+08 | 0.0018 | 54.5 | 0.0046 | 0.0232 |
| *HST* | E2901 | L5264 | 3.80E+08 | 0.0104 | 45.9 | 0.060 | 0.201 |
| *HST* | E3035 | L5386 | 2.58E+08 | 0.0313 | 47.2 | 0.127 | 0.423 |
| *HST* | E3656 | R5784 | 4.24E+07 | 0.0390 | 48.0 | 0.026 | 0.132 |
| *HST* | E3657 | R5785 | 4.03E+07 | 0.0414 | 47.0 | 0.026 | 0.131 |
| *HST* | E3035 | F7016 | 2.94E+07 | 0.0176 | 47.8 | 0.008 | 0.041 |
| *HST* | E3035 | F7017 | 2.94E+07 | 0.0148 | 47.6 | 0.007 | 0.035 |

**Table S5. DNA content in the initial libraries prepared from the untreated extracts from *Scladina I-4A*.** Labelling as in **Table S3**.

| Neandertal | Extract ID | Library ID | Number of molecules in the library | Usable fraction | Average sequence length | Average genomic coverage (library) | Average genomic coverage (extract) |
|---|---|---|---|---|---|---|---|
| *Scladina I-4A* | E5322 | F3297 | 2.35E+09 | 0.0054 | 64.8 | 0.274 | 1.371 |
| *Scladina I-4A* | E5323 | F3298 | 6.51E+09 | 0.1583 | 58.4 | 20.061 | 100.305 |
| *Scladina I-4A* | E5324 | F3299 | 6.25E+09 | 0.0488 | 68.1 | 6.924 | 34.618 |

**Table S6. Present-day human DNA contamination estimates after three decontamination methods applied to bone powder from the *HST* femur.** Numbers in brackets correspond to sequences with C-to-T substitutions within the three last positions of either ends. Informative positions used in this analysis correspond to a set of 77 sites that differ between the *HST* consensus sequence (*10*) and 312 modern human mitochondrial genomes (*63*) (including the revised Cambridge Reference Sequence, rCRS, (*34*)). Sequences are considered conflicting when overlapping multiple informative positions and carrying both *HST* and modern human alleles. We disregarded sequences in the forward orientation if one allele of the polymorphism was a C and in the reverse orientation if one allele was a G. **See table S20 for contamination estimates for all generated libraries.**

| Library ID | Treatment | *HST* state | Human state | Conflicting | Contamination estimate (%) | Binomial 95% Confidence Intervals |
|---|---|---|---|---|---|---|
| L5289 | Pre-digested fraction | 3,111 [1,012] | 162 [3] | 1 [0] | 4.95 [0.30] | 4.23 - 5.75 |
| L5290 | Re-extraction | 803 [267] | 282 [6] | 0 [0] | 25.99 [2.20] | 23.40 - 28.71 |
| L5291 | Sodium hypochlorite | 1,372 [554] | 61 [2] | 1 [0] | 4.25 [0.36] | 3.27 - 5.43 |
| L5292 | Phosphate buffer | 787 [333] | 43 [2] | 1 [0] | 5.17 [0.60] | 3.77 - 6.91 |

**Table S7. Present-day human DNA contamination estimates from *Scladina I-4A* mtDNA based on differences between Neandertals and modern humans.** Numbers in brackets correspond to the number of DNA sequences with C-to-T substitutions within the three last positions of either ends. DNA sequences were separated based on the carried allele at the 52 positions that differ between all available Neandertal mitochondrial genomes (including *HST*, (*8*, *10*)) and 312 modern human genomes (*34*, *63*).

| Library ID | Treatment | Archaic state | Modern state | Conflicting | Contamination estimate (%) | Binomial 95% CI |
|---|---|---|---|---|---|---|
| D8925 | - | 557 [138] | 2,783 [48] | 1 [0] | 83.30 [25.81] | 82.02-84.57 |
| F4687 | Sodium Hypochlorite | 357 [93] | 27 [1] | 0 [0] | 7.03 [1.06] | 4.68-10.07 |
| D8926 | - | 767 [192] | 14,823 [388] | 1 [0] | 95.07 [66.90] | 94.73-95.41 |
| F4688 | Sodium Hypochlorite | 354 [97] | 7,110 [205] | 0 | 95.26 [67.88] | 94.73-95.73 |
| D8927 | - | 99 [7] | 13,272 [221] | 1 [1] | 99.25 [96.51] | 99.10-99.40 |
| F4690 | Sodium Hypochlorite | 17 [4] | 328 [7] | 0 [0] | 95.07 [63.64] | 92.23-97.10 |

# Note S3. Data generation and data processing.

All libraries prepared from *HST* extracts were sequenced on an Illumina MiSeq except for libraries from extract E3035 that were further sequenced on a HiSeq 2500 platform as they yielded a substantially higher proportion of endogenous DNA (**table S8**). For *Scladina I-4A*, we selected the extract with the lowest level of present-day human DNA contamination (E5846, Supplementary Note 5) and sequenced the libraries prepared from it on a HiSeq 2500.

Base calling was performed using Bustard (*47*). Adapter sequences were removed and overlapping forward and reverse reads were merged using leeHom (*48*). Sequences with the expected barcode combinations were identified with Jivebunny, a probabilistic demultiplexer for double-indexed Illumina sequencing runs able to detect and remove contamination from unexpected libraries (https://bitbucket.org/ustenzel/jivebunny) (*6*).

Sequences were aligned to the human reference genome (hg19) with a Burrows-Wheeler Aligner (BWA) (*49*) using parameters for ancient DNA "-n 0.01 -o 2 -l 16500" (*19*). Sequences with a minimum mapping quality cutoff of 25 and mapping uniquely (alignability track, map35_L100, (*8*)) were kept for further analyses (*6, 20*). Short microbial sequences can align spuriously (see peak in the length distributions of **fig. S1**) which can be overcome by applying a minimum length cutoff. Using the approach from (*50*), we determined that sequences at least 30bp long have a spurious alignment rate of less than 1% and used this cutoff for all downstream analyses (**figs. S2** and **S3**). After mapping, sequences starting and ending at identical coordinates (representing PCR duplicates) were collapsed into a single sequence using bam-rmdup (https://bitbucket.org/ustenzel/biohazard). Data generated on different sequencing runs were merged using samtools 1.3.1 (*51*).

We summarize the sequencing statistics after each filtering step in **tables S9** and **S11** for *HST* and *Scladina I-4A*, respectively, and in **tables S12** and **S13** for the negative controls. We report in **table S8** and **S10** values for a length cutoff of 35 bp to allow easy comparison to previous datasets that employed this cutoff. We computed the average depth of coverage, i.e. the average number of times that a base in the reference genome is covered by an aligned read, and the breadth of coverage, i.e. the number of bases that are covered at least once (**tables S16**, **S17**, **S18**, and **S19**).

Mitochondrial DNA capture data were processed in the same way, except that they were aligned to the revised Cambridge Reference Sequence (rCRS) (*34*) and the *Altai Neandertal* mtDNA (*8*). We report the number of mitochondrial sequences generated from each library in **tables S14** and **S15**.

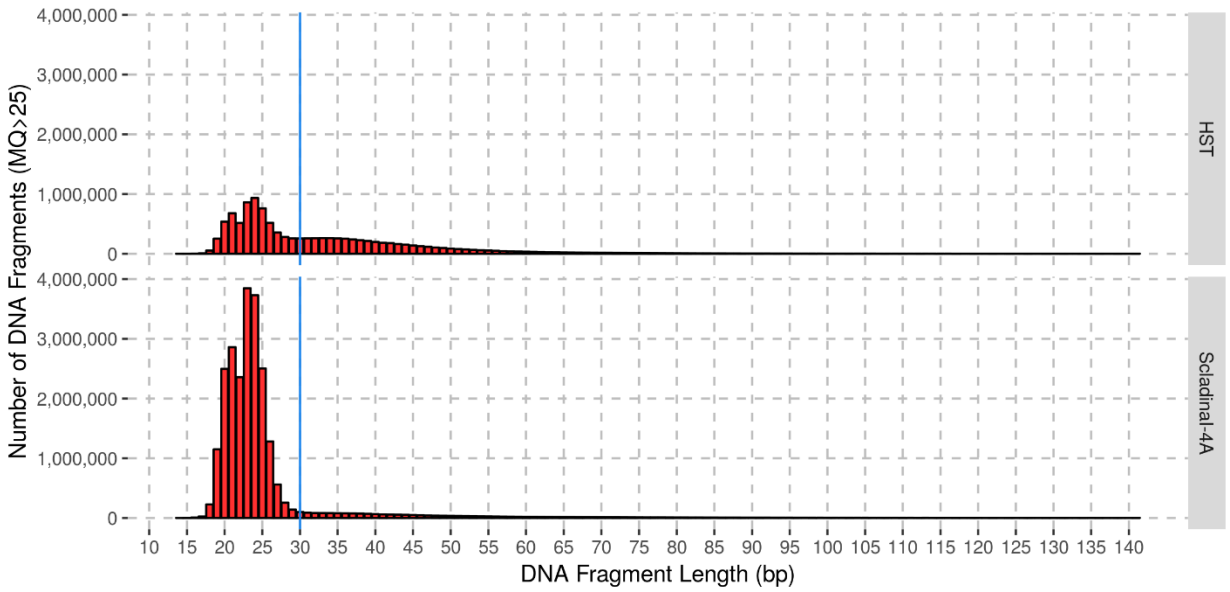


**Fig. S1. Length distribution of unique DNA fragments aligned to the human reference genome hg19 with a mapping quality of 25 or above (average length = 33 bp for *HST* and 25 bp for *Scladina I-4A*) and mapping uniquely (alignability track, map35_L100, (*8*)).** The blue lines represent the minimal length cutoff used for the analyses (length ≥ 30 bp).

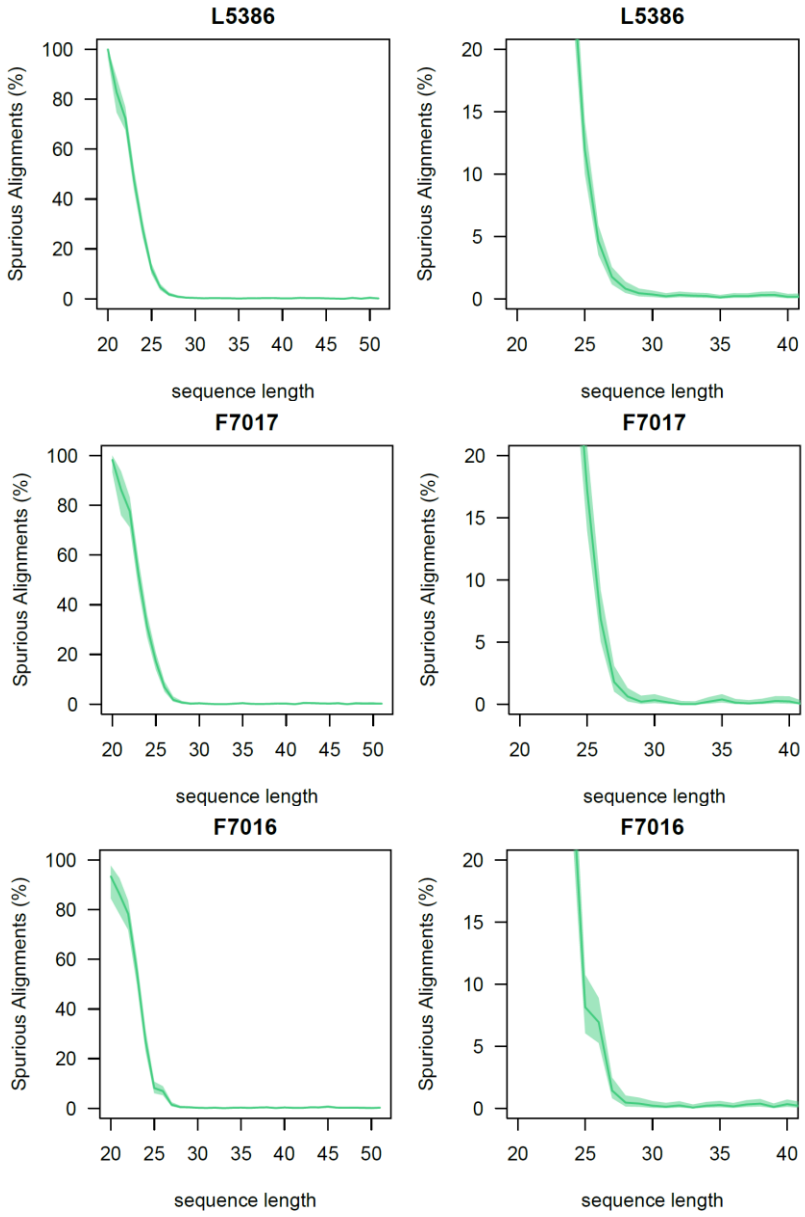


**Fig. S2. Proportion of spurious alignment for different sequence lengths in the three libraries of *HST* that represent ~80% of the generated sequences for this specimen.** The right panels correspond to enlargements of the left panels (see scale differences). 95% binomial confidence intervals are represented by a shaded area around the curves.

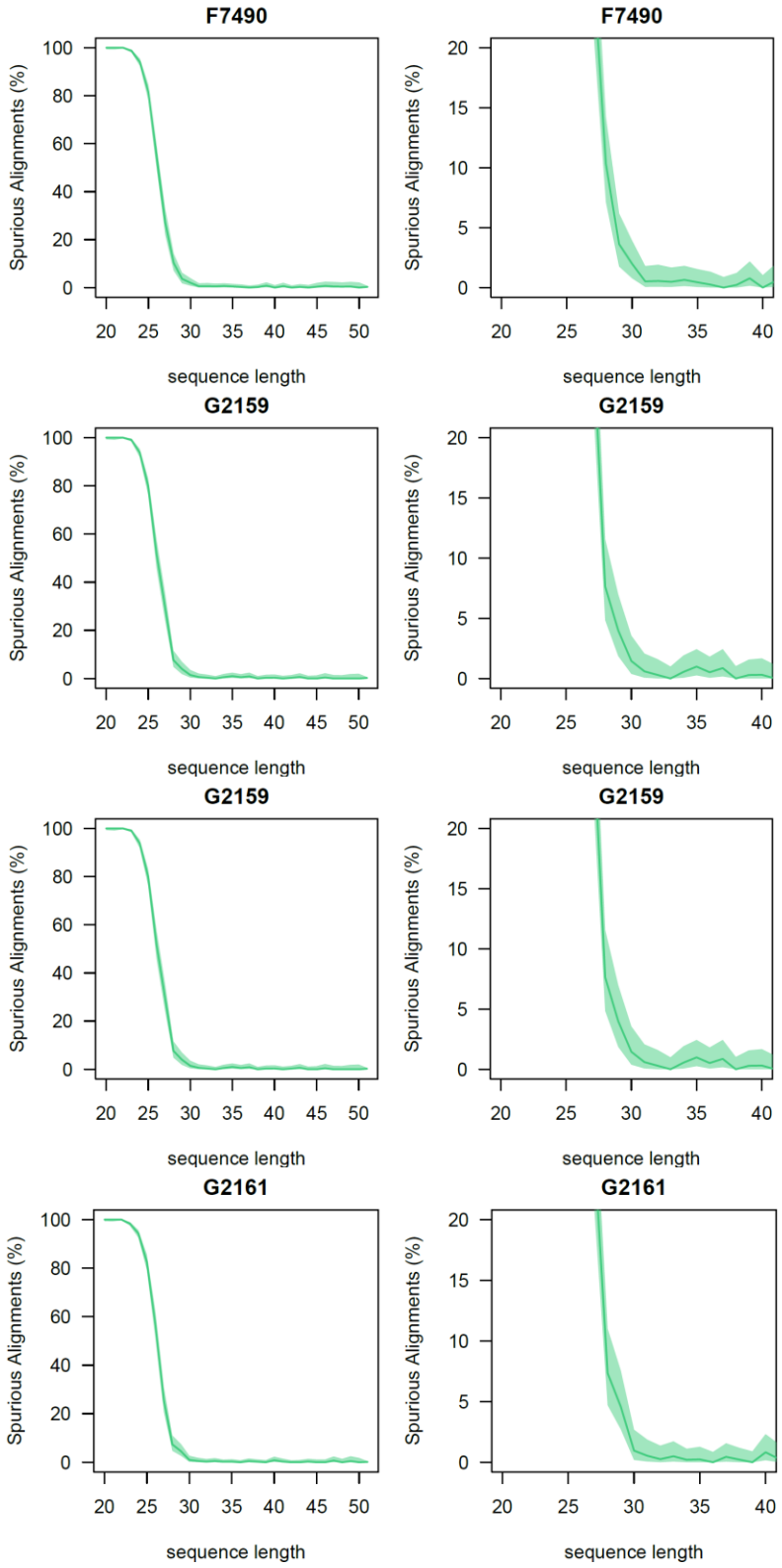


**Fig. S3. Proportion of spurious alignment in the libraries of *Scladina I-4A* (same as for *HST* in fig. S2).**

**Table S8. Sequencing summary statistics for *HST* with the following filters: length (≥35 bp) and mapping quality (≥25).**

| Library ID | Raw number of molecules | nº molecules (L≥35bp) | Mapped molecules (L≥35bp, MQ≥25) | % mapped (L≥35, MQ≥25) | unique | deaminated (first or last 3 positions) |
|---|---|---|---|---|---|---|
| L5262 | 6,600,285 | 4,422,896 | 8076 | 0.183 | 7,270 | 1,670 |
| L5263 | 15,591,196 | 10,211,480 | 26,740 | 0.262 | 23,694 | 1,833 |
| L5264 | 17,489,861 | 8,407,976 | 181,890 | 2.163 | 156,595 | 53,640 |
| L5265 | 17,717,192 | 8,237,193 | 91,899 | 1.116 | 82,476 | 18,216 |
| L5386 | 99,372,306 | 19,119,717 | 3,105,489 | 16.242 | 1,340,820 | 416,492 |
| R5784 | 2,506,618 | 1,246,570 | 97,816 | 7.847 | 87,828 | 24,034 |
| R5785 | 3,581,740 | 1,733,087 | 148,221 | 8.552 | 132,298 | 36,802 |
| F7016 | 96,042,050 | 12,459,524 | 1,685,834 | 13.530 | 1,011,463 | 297,283 |
| F7017 | 95,421,547 | 11,820,053 | 1,410,200 | 11.931 | 868,113 | 244,373 |
| **TOTAL** | **354,322,795** | **77,658,496** | **6,756,165** | **8.7** | **3,710,557** | **1,094,343** |

**Table S9. Sequencing summary statistics for *HST* with the following filters: length (≥30 bp) and mapping quality (≥25).**

| Library ID | Raw number of sequences | nº sequences (L≥30bp) | Mapped sequences (L≥30bp, MQ≥25) | % mapped (L≥30, MQ≥25) | unique | deaminated (first or last 3 positions) |
|---|---|---|---|---|---|---|
| L5262 | 6,600,285 | 5,008,101 | 11,288 | 0.225 | 10,228 | 2,358 |
| L5263 | 15,591,196 | 11,374,451 | 34,028 | 0.299 | 30,435 | 2,527 |
| L5264 | 17,489,861 | 10,229,789 | 262,104 | 2.562 | 227,824 | 76,878 |
| L5265 | 17,717,192 | 10,233,576 | 130,540 | 1.276 | 117,990 | 26,690 |
| L5386 | 99,372,306 | 25,280,238 | 4,228,360 | 16.726 | 1,832,672 | 566,296 |
| R5784 | 2,506,618 | 1,544,315 | 134,423 | 8.704 | 121,963 | 34,101 |
| R5785 | 3,581,740 | 2,169,947 | 205,559 | 9.473 | 185,297 | 51,885 |
| F7016 | 96,042,050 | 16,011,900 | 2,201,855 | 13.751 | 1,331,412 | 391,030 |
| F7017 | 95,421,547 | 15,385,516 | 1,855,645 | 12.061 | 1,151,260 | 323,561 |
| **TOTAL** | **354,322,795** | **97,237,833** | **9,063,802** | **9.321** | **5,009,081** | **1,475,326** |

**Table S10. Sequencing summary statistics for *Scladina I-4A* with the following filters: length (≥35 bp) and mapping quality (≥25).**

| Library ID | Raw number of molecules | nº molecules (L≥35bp) | Mapped molecules (L≥35bp, MQ≥25) | % mapped (L≥35, MQ≥25) | unique | deaminated (first or last 3 positions) |
|---|---|---|---|---|---|---|
| G2159 | 263,741,289 | 41,355,441 | 493,324 | 1.193 | 363,680 | 56,913 |
| G2160 | 330,298,115 | 50,820,654 | 601,539 | 1.184 | 422,233 | 66,285 |
| G2161 | 304,661,159 | 48,884,400 | 577,476 | 1.181 | 413,533 | 64,872 |
| F7490 | 153,666,638 | 41,387,303 | 491,301 | 1.187 | 355,991 | 59,930 |
| **TOTAL** | **1,052,367,201** | **182,447,798** | **2,163,640** | **1.186** | **1,555,437** | **248,000** |

**Table S11. Sequencing summary statistics for *Scladina I-4A* with the following filters: length (≥30 bp) and mapping quality (≥25).**

| Library ID | Raw number of molecules | nº molecules (L≥30bp) | Mapped molecules (L≥30bp, MQ≥25) | % mapped (L≥30, MQ≥25) | unique | deaminated (first or last 3 positions) |
|---|---|---|---|---|---|---|
| G2159 | 263,741,289 | 57,656,119 | 620,656 | 1.076 | 460,677 | 76,928 |
| G2160 | 330,298,115 | 70,691,425 | 757,560 | 1.072 | 534,713 | 89,612 |
| G2161 | 304,661,159 | 68,441,834 | 731,150 | 1.068 | 527,038 | 87,980 |
| F7490 | 153,666,638 | 60,107,427 | 635,773 | 1.058 | 463,524 | 82,769 |
| **TOTAL** | **1,052,367,201** | **256,896,805** | **2,745,139** | **1.069** | **1,985,952** | **337,289** |

**Table S12. Sequencing statistics of the negative controls for *HST* (see table S1).** Labelling as in **table S9**.

| Library ID | Raw number of sequences | nº sequences (L≥30bp) | Mapped sequences (L≥30bp, MQ≥25) | % mapped (L≥30, MQ≥25) | unique | deaminated (first or last 3 positions) |
|---|---|---|---|---|---|---|
| L5266 | 1,195,059 | 563,085 | 5,739 | 1.019 | 5,055 | 46 |
| L5267 | 30,220 | 13,505 | 108 | 0.800 | 100 | 2 |
| L5268 | 46,922 | 8,640 | 136 | 1.574 | 122 | 5 |
| L5270 | 306,370 | 59,604 | 1,710 | 2.869 | 1,412 | 30 |
| L5389 | 776,380 | 309,412 | 4,007 | 1.295 | 3,598 | 56 |
| L5400 | 649,043 | 37,872 | 1,589 | 4.196 | 1,405 | 18 |
| R5791 | 35,112 | 6,043 | 742 | 12.279 | 662 | 12 |
| R5792 | 34,519 | 3,954 | 111 | 2.807 | 95 | 3 |
| F3995 | 1,173,710 | 38,568 | 217 | 0.563 | 187 | 1 |

**Table S13. Sequencing statistics of the negative controls for *Scladina I-4A* (see table S2).** Labelling as in **table S11**.

| Library ID | Raw number of sequences | nº sequences (L≥30bp) | Mapped sequences (L≥30bp, MQ≥25) | % mapped (L≥30, MQ≥25) | unique | deaminated (first or last 3 positions) |
|---|---|---|---|---|---|---|
| F3307 | 207,836 | 997 | 61 | 6.118 | 53 | 0 |
| F3269 | 232,737 | 857 | 14 | 1.634 | 9 | 0 |
| F3292 | 261,268 | 998 | 4 | 0.401 | 3 | 0 |
| F7499 | 280,039 | 15,194 | 627 | 4.127 | 567 | 3 |
| F7470 | 240,963 | 9,328 | 40 | 0.429 | 37 | 0 |
| G2162 | 1,383,269 | 17,141 | 27 | 0.158 | 24 | 1 |

**Table S14. Summary of *HST* mtDNA sequencing.**

| Library ID | Raw number of sequences | nº sequences with L≥35bp | Mapped sequences (L≥35bp, MQ≥25) | % mapped (L≥35, MQ≥25) | unique | deaminated (first or last 3 positions) |
|---|---|---|---|---|---|---|
| L5289 | 2,835,359 | 1,888,102 | 289,730 | 15.114 | 39,295 | 13,842 |
| L5290 | 2,211,856 | 1,483,183 | 168,193 | 11.256 | 12,230 | 3,839 |
| L5291 | 2,854,268 | 1,580,699 | 636,233 | 39.481 | 17,563 | 7,045 |
| L5292 | 3,160,299 | 1,490,326 | 296,309 | 19.478 | 12,752 | 5,378 |
| L5408 | 7,940,845 | 3,351,885 | 2,016,381 | 59.464 | 16,981 | 6,722 |
| R4294 | 882,376 | 487,890 | 214,633 | 43.527 | 21,207 | 8,101 |
| R4295 | 1,148,041 | 568,103 | 253,656 | 44.162 | 21,433 | 8,131 |
| F4166 | 320,158 | 205,246 | 173,889 | 83.757 | 8,910 | 3,435 |
| F4167 | 310,283 | 193,779 | 164,732 | 84.060 | 8,530 | 3,387 |
| **TOTAL** | **21,663,485** | **11,249,213** | **4,213,756** | **37.458** | **158,901** | **59,880** |

**Table S15. Summary of *Scladina I-4A* mtDNA sequencing.** Only the libraries generated from the best extract (E5846, see **table S2**) are shown.

| Library ID | Raw number of sequences | nº sequences with L≥35bp | Mapped sequences (L≥35bp, MQ≥25) | % mapped (L≥35, MQ≥25) | unique | deaminated (first or last 3 positions) |
|---|---|---|---|---|---|---|
| F4687 | 495,464 | 305,529 | 247,339 | 80.954 | 7,063 | 2,234 |
| G3380 | 880,362 | 500,728 | 420,082 | 83.894 | 8,680 | 2,744 |
| G3381 | 888,852 | 505,697 | 431,244 | 85.277 | 8,536 | 2,760 |
| G3382 | 802,711 | 434,817 | 365,422 | 84.040 | 8,306 | 2,728 |
| **TOTAL** | **3,067,389** | **1,746,771** | **1,464,087** | **83.817** | **32,585** | **10,466** |

**Table S16. Coverage statistics for all sequences from *HST* within the alignability track, map35_L100 (*8*).**

| Chromosomes | Mapping Criteria | Average depth of coverage | Breadth of coverage (bp) |
|---|---|---|---|
| Autosomes | L≥35bp, MQ≥25 | 0.0804 | 132,139,286 |
| Autosomes | L≥30bp, MQ≥25 | 0.1006 | 162,737,990 |
| X Chromosome | L≥35bp, MQ≥25 | 0.0459 | 3,739,725 |
| X Chromosome | L≥30bp, MQ≥25 | 0.0567 | 4,561,944 |
| Y Chromosome | L≥35bp, MQ≥25 | 0.0366 | 171,073 |
| Y Chromosome | L≥30bp, MQ≥25 | 0.0463 | 214,359 |

**Table S17. Coverage statistics for *HST* sequences with a C-to-T substitution within the three first or last positions of either ends.** We only considered regions in the alignability track, map35_L100 (*8*).

| Chromosomes | Mapping Criteria | Average depth of coverage | Breadth of coverage (bp) |
|---|---|---|---|
| Autosomes | L≥35bp, MQ≥25 | 0.0228 | 39,297,015 |
| Autosomes | L≥30bp, MQ≥25 | 0.0288 | 49,468,234 |
| X Chromosome | L≥35bp, MQ≥25 | 0.0118 | 1,000,312 |
| X Chromosome | L≥30bp, MQ≥25 | 0.0148 | 1,245,060 |
| Y Chromosome | L≥35bp, MQ≥25 | 0.0111 | 54,153 |
| Y Chromosome | L≥30bp, MQ≥25 | 0.0139 | 67,539 |

**Table S18. Coverage statistics for all sequences from *Scladina I-4A* within the alignability track, map35_L100 (*8*).**

| Chromosomes | Mapping Criteria | Average depth of coverage | Breadth of coverage (bp) |
|---|---|---|---|
| Autosomes | L≥35bp, MQ≥25 | 0.0380 | 64,785,412 |
| Autosomes | L≥30bp, MQ≥25 | 0.0446 | 75,274,514 |
| X Chromosome | L≥35bp, MQ≥25 | 0.0271 | 2,259,579 |
| X Chromosome | L≥30bp, MQ≥25 | 0.0326 | 2,696,045 |
| Y Chromosome | L≥35bp, MQ≥25 | 0.0121 | 58,444 |
| Y Chromosome | L≥30bp, MQ≥25 | 0.0135 | 65,192 |

**Table S19. Coverage statistics for *Scladina I-4A* sequences with a C-to-T substitution within the three first or last positions of either ends.** We only considered regions in the alignability track, map35_L100 (*8*).

| Chromosomes | Mapping Criteria | Average depth of coverage | Breadth of coverage (bp) |
|---|---|---|---|
| Autosomes | L≥35bp, MQ≥25 | 0.0050 | 8,782,501 |
| Autosomes | L≥30bp, MQ≥25 | 0.0064 | 11,168,981 |
| X Chromosome | L≥35bp, MQ≥25 | 0.0050 | 425,442 |
| X Chromosome | L≥30bp, MQ≥25 | 0.0063 | 534,402 |
| Y Chromosome | L≥35bp, MQ≥25 | 0.0001 | 538 |
| Y Chromosome | L≥30bp, MQ≥25 | 0.0001 | 675 |

# Note S4. Sex determination.

## *Sex estimation based on morphometric features*

### Hohlenstein-Stadel Neandertal

The Hohlenstein-Stadel (*HST*) specimen was identified as the shaft of a right femur, attributed to a Neandertal (based on its morphology and stratigraphic position), and assigned to an adult (*9*). The individual was estimated to be male based on the robusticity of the bone in comparison with other Neandertal femora, and its stature was estimated to be ~1.60 m (*9*).

### Scladina I-4A

The *Scladina I-4A* juvenile comprises a mandible, a partial maxilla and a series of *in situ* and isolated deciduous and permanent teeth (*13*). Based on the incremental growth lines preserved in its permanent teeth, *Scladina I-4A* was estimated to have died at 8 years of age (*52*). Although all the diagnostic features are not yet fully expressed in a juvenile, concordant morphological and metrical evidence allowed assigning *Scladina I-4A* to a Neandertal (*13*).

The determination of the sex of a juvenile fossil specimen is always difficult due to the fact that the extent of sexual dimorphism is often not known in extinct taxa, and that sexually dimorphic features are fully expressed only after the growth spurt of adolescence. Yet, Toussaint (*13*) had discussed morphometric features in the light of sex assignment for *Scladina I-4A*. Crown sizes (mesio-distal and bucco-lingual diameters) of the permanent teeth of *Scladina I-4A* either fall in the upper range of variation of the Neandertals described as females or as undetermined ((*13*), after (*53*)). Tooth root length has been suggested to show a greater sexual dimorphism than crown diameters in recent modern humans (*54, 55*), with males having longer roots than females (*56*). Interestingly, clinical studies on genetic disorders tend to support the influence of sex chromosomes on root length (*57-59*). The noticeably short root dimensions (exempt of any root resorption) of the permanent teeth of *Scladina I-A4* would argue in favor of a female individual (**figs. S4** and **S5**). Along the same line of evidence, their large pulp cavities would also point to a female individual (**fig. S6**), males having thicker radicular dentine (*60*). However, as reminded by Zilberman and Smith (*61*), the combination of sexual dimorphism and ageing would affect the progressive closing of the pulp cavity throughout life, by deposition of secondary dentine. One should keep in mind the age of the Scladina child, which could mostly account for the large pulp volumes. Indeed secondary dentine would not have yet been deposited significantly on the walls of the pulp chambers by the time of *Scladina I-4A*'s death (*13*). Toussaint (*13*) further describes several mandibular features of *Scladina I-4A*. These include metrical observations such as the small dimensions of its mandibular corpus, the relatively small height and thickness of its mandibular symphysis, the relatively small corpus thickness at the level of the canine, the first and second premolars and the first molars. Toussaint (*13*) last suggests that the *incisura submentalis* is weakly expressed, which could be a female trait according to Loth and Henneberg (*62*). In comparison with other immature Neandertals of the same age group and for which a sex estimation has been proposed, all observations tend to portray *Scladina I-4A* as a young female individual.

## *Sex determination based on sequence coverage of the sex chromosomes*

To determine the sex of the individuals, we counted the number of sequences that align to the X chromosome and compared it to the number of sequences that align to the whole genome. We only used sequences equal or longer than 30 base pairs with a mapping quality of at least 25 in the uniquely mappable regions defined by (*8*) and that exhibit an apparent deamination within the last three positions at either of their ends as indicated by a C-to-T substitution compared to the human reference genome. The expected proportion for a female or a male was calculated by computing the length of the mappable regions on the X ($L_X$) and the rest of the genome ($L_{AUTOSOMES}$ and $L_Y$). For a female, the expected proportion is $\frac{2\times L_X}{2\times L_X+2\times L_{AUTOSOMES}}$ while for a male it is $\frac{L_X}{L_X+L_Y+2\times L_{AUTOSOMES}}$. By comparing these to the observed proportions (**fig. S7**), we concluded that *HST* was a male and *Scladina I-4A* a female. However, both proportions slightly deviate from the expectation. For *HST*, the deviation could be explained by female contamination, but contamination cannot account for the difference seen for *Scladina I-4A*. We additionally note that the sequence coverage on the Y chromosome support these sex determinations, with a negligible number of sequences mapping to the Y chromosome for *Scladina I-4A* contrasting with the elevated Y chromosome sequence coverage of *HST* (**fig. S8**).

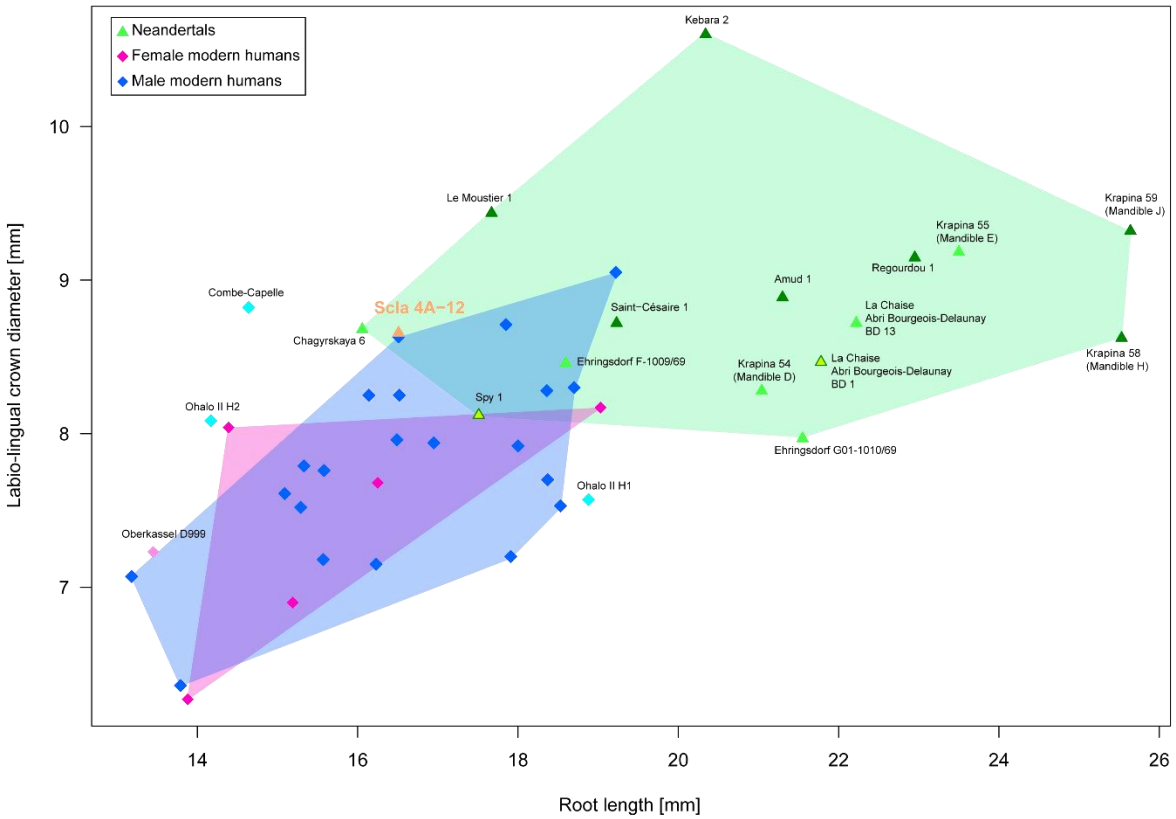


**Fig. S4. Bivariate plot of root length against labio-lingual crown diameter (in millimeter) for the permanent mandibular canine.** Although the differences are not significant in the present sample, female modern humans tend to have shorter roots than males. The *Scladina I-4A* incisor (orange) shows amongst the smallest dimensions of root and crown within the Neandertal variation (green). Sex estimation has been tentatively conducted for only a few Neandertals, and this information is represented only for illustrative purpose, as its reliability is questionable. The following specimens were estimated to be males (in darker green): *Le Moustier 1* (*102*), *Regourdou 1* (*103*), *Saint-Césaire 1* (*104*), *Kebara 2* (*105*) and *Amud 1* (*106*), while *BD 1* (*107*) and *Spy 1* (*108, 109*) (green-yellow) were proposed as females. Upper-/Epi-paleolithic and Mesolithic modern humans are plotted for information and were all estimated to be males: *Combe-Capelle* (*110*), *Ohalo II H1* (*111*), *Ohalo II H2* (*112*), only *Oberkassel D999* was estimated to be female (*113*). Recent modern humans are clinically extracted teeth with known sex information from the patients, and a couple of archeological teeth with associated skull or postcranial remains on which were based the sex estimation with good reliability (*114*).

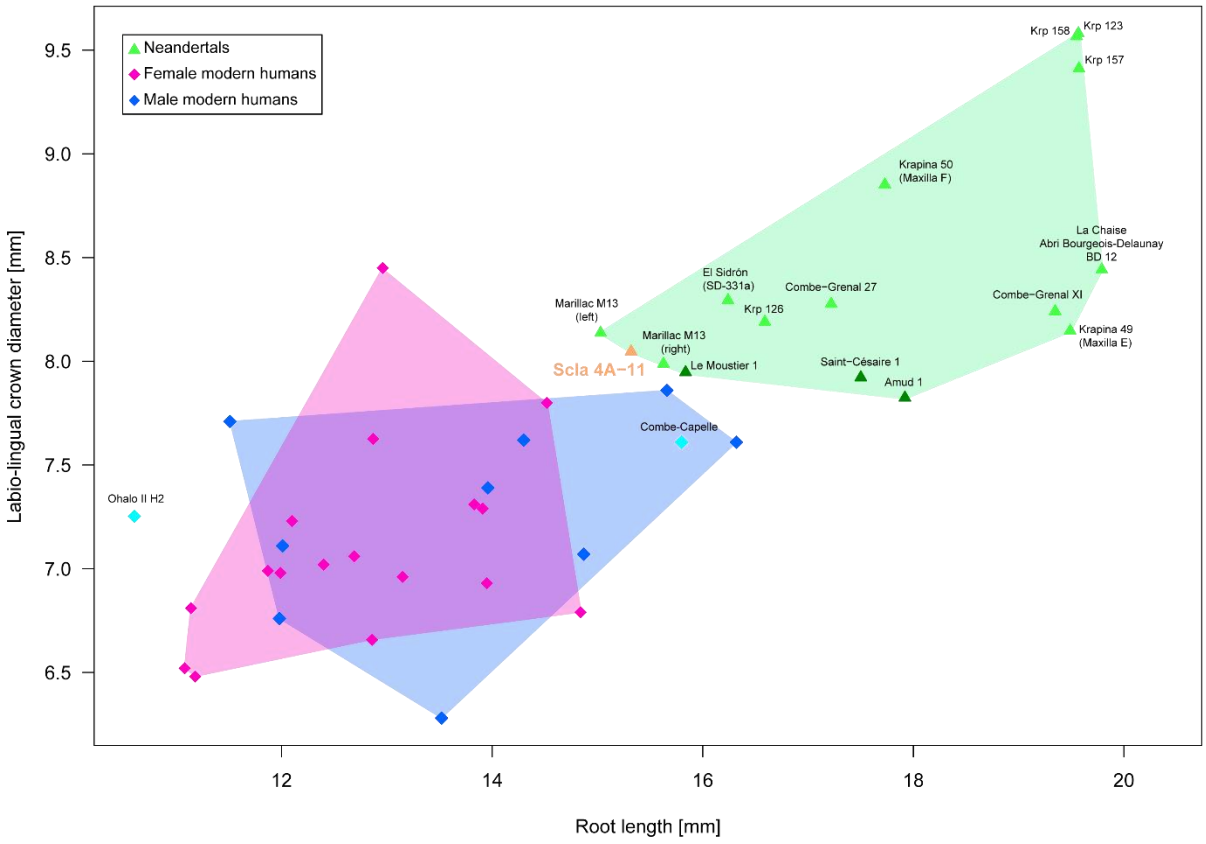


**Fig. S5. Bivariate plot of root length against labio-lingual crown diameter (in millimeter) for the permanent maxillary central incisor.** Although the differences are not significant in the present sample, female modern humans tend to have shorter roots than males. The *Scladina I-4A* incisor (orange) shows amongst the smallest dimensions of root and crown within the Neandertal variation. See **fig. S4** for the sexed Neandertals.

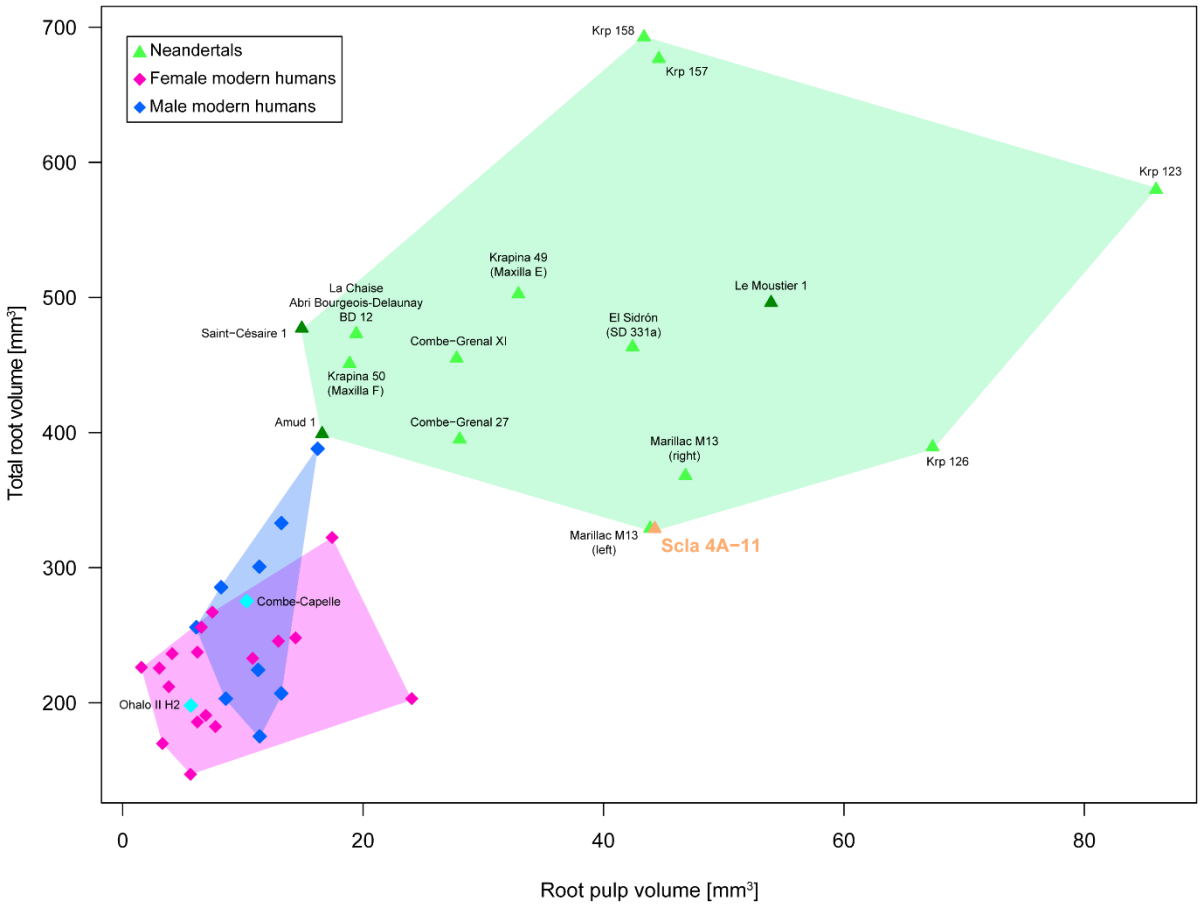


**Fig. S6. Bivariate plot of root pulp volume against total root volume (in cubic millimeter) for the permanent maxillary central incisor.** Although the differences are not significant in the present sample, female modern humans tend to have larger pulp cavities and overall less robust roots than males. The *Scladina I-4A* incisor (orange) shows amongst the smallest dimensions in root volume within the Neandertal variation, and a moderately high pulp cavity volume. *Amud 1* and *Saint-Césaire 1* tend to show small pulp cavities yet this might be mainly related with their advanced age, while *Le Moustier 1* in spite of being estimated to be male, would still retain large pulp cavities due to its young age. See **fig. S4** for the sexed Neandertals.

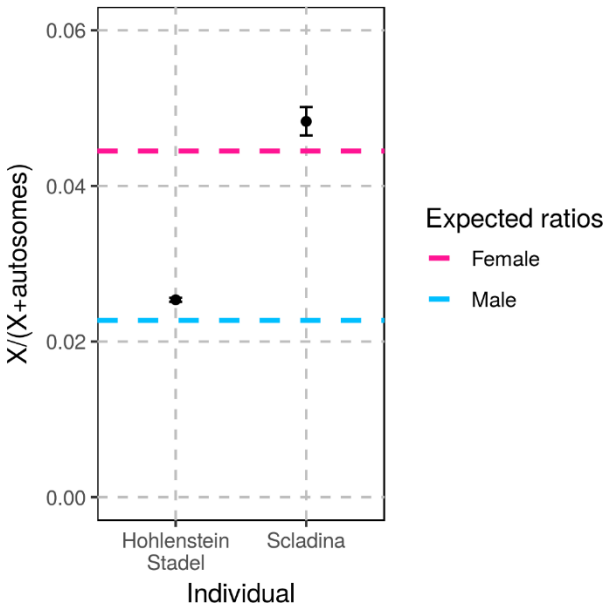


**Fig. S7. Ratio of sequences aligning to the X chromosome and autosomes.** Only sequences with terminal C-to-T substitutions (within the last 3bp), at least 30bp long and with a mapping quality of at least 25 were considered. Dashed lines correspond to the expected ratios for a male and a female. The bars represent the 95% binomial confidence intervals.

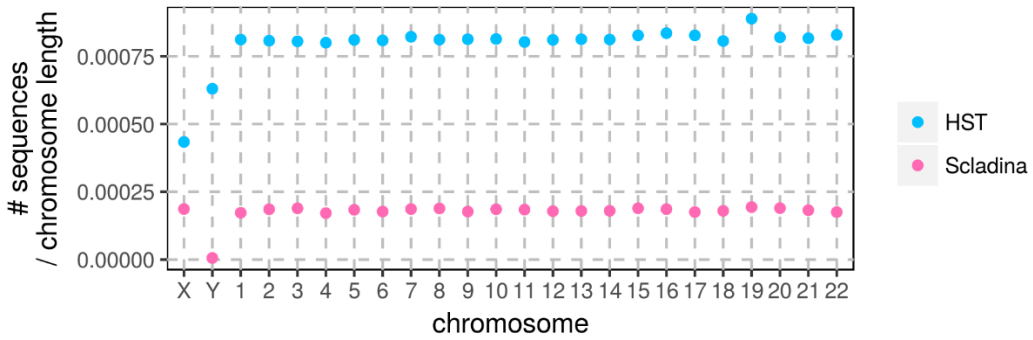


**Fig. S8. Number of sequences mapping to each chromosome normalized by chromosome length.** Only sequences with terminal C-to-T substitutions (within the last 3bp), at least 30bp long and with a mapping quality of at least 25 were considered.

# Note S5. Mitochondrial contamination estimates.

We estimated the proportion of present-day human DNA contamination in *HST* mitochondrial data leveraging positions that differ between the previously reconstructed consensus sequence of *HST* (*10*) and 312 present-day human mitochondrial genomes (*63*) (including rCRS, (*34*)). We aligned these consensus sequences using MAFFT (*64*) and identified 77 such positions. We then computed the proportion of mtDNA sequences that carry the modern human allele among all sequences from *HST* that align to these positions (**table S20**). To avoid errors stemming from cytosine deamination, we restricted our analysis to sequences that were sequenced in the reverse orientation if one of the diagnostic alleles was a C and the forward orientation if one of the diagnostic alleles was a G (*1, 20*). The mitochondrial contamination estimate was 9.0% [95% confidence interval (CI): 8.5–9.5%] for the merged dataset (for estimates per captured library see **table S20**).

For *Scladina I-4A*, as the mitochondrial consensus sequence was unknown, we originally estimated the proportion of present-day human DNA contamination at a different set of diagnostic positions. We identified 52 positions where all available Neandertal mitochondrial genomes (including *HST*) (*6, 8, 10, 63, 65-69*) differ from those of 312 present-day humans (*63*) (including rCRS, (*34*)). To avoid misidentification of the alleles because of deamination, we again restricted our analysis to the relevant sequenced strands for each diagnostic position as described above. The mitochondrial contamination estimate was 8.6% [CI: 7.3-9.9%] for the merged dataset (see **table S21** for estimates per captured library). As the majority of DNA fragments supported *Scladina I-4A* having an mtDNA of the Neandertal type, we reconstructed her consensus sequence (see Supplementary Note 6) and compared it to the sequence of 312 present-day human mitochondrial genomes. We identified 71 differences between them that were then used to estimate levels of present-day human DNA contamination in *Scladina I-4A* as it was done for *HST*. The resulting contamination estimate was 10.5% [CI: 9.4-11.9%] for the merged dataset (results per captured library are in **table S22**).

To monitor if any contamination was introduced in the laboratory, we carried out the same analysis on the negative controls and report the results in **tables S23** and **S24**. We also report the deamination patterns observed in the mtDNA fragments either stemming from DNA contamination or coming from the Neandertal mitochondrial genome in **fig. S9**.

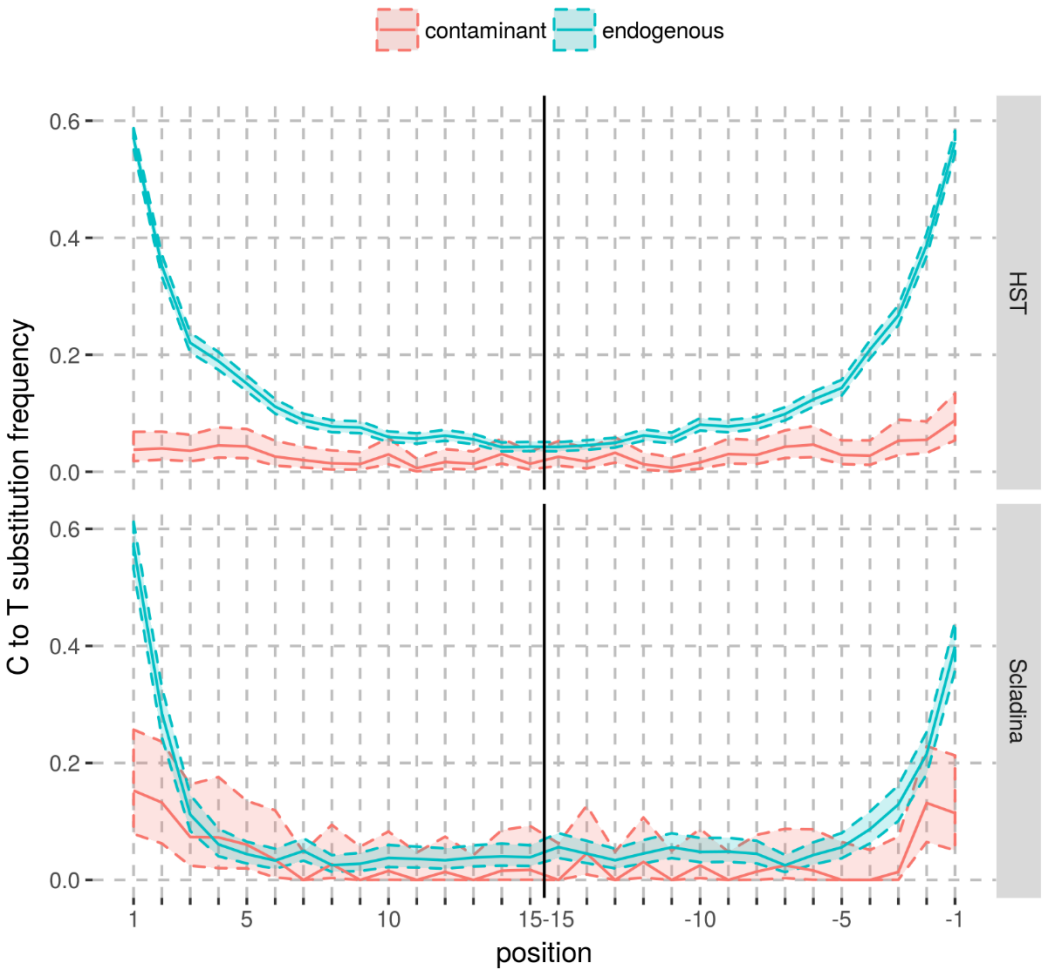


**Fig. S9. Deamination patterns from the mtDNA.** At positions where the Neandertal (either *HST* or *Scladina I-4A*) and 312 present-day humans differ, we separated molecules into "endogenous" (blue) or "contaminant" (pink) based on the carried allele. At C/T (G/A) polymorphisms, we discarded sequences obtained in the forward (reverse) orientation. We further removed sequences that covered multiple informative positions with conflicting alleles (both the Neandertal and modern human alleles).

**Table S20. Present-day human DNA contamination estimates from *HST* mtDNA.** Numbers in brackets correspond to DNA sequences with C-to-T substitutions within the three last positions of either end. Informative positions used in this analysis correspond to a set of 77 sites that differ between the *HST* consensus sequence (*10*) and 312 modern human mitochondrial genomes (*63*) (including the rCRS, (*34*)). Sequences are considered conflicting when overlapping multiple informative positions and carrying both *HST* and modern human alleles. We further discarded sequences obtained in the forward (reverse) orientation at C/T (G/A) polymorphisms or sequences carrying a third allele.

| Library ID | *HST* state | Modern state | Conflicting | Contamination estimate (%) | Binomial 95% Confidence Intervals |
|---|---|---|---|---|---|
| L5289 | 3,111 [1,012] | 162 [3] | 1 [0] | 4.95 [0.30] | 4.23 - 5.75 |
| L5290 | 803 [267] | 282 [6] | 0 [0] | 25.99 [2.20] | 23.40 - 28.71 |
| L5291 | 1,372 [554] | 61 [2] | 1 [0] | 4.25 [0.36] | 3.27 - 5.43 |
| L5292 | 787 [333] | 43 [2] | 1 [0] | 5.17 [0.60] | 3.77 - 6.91 |
| L5408 | 1,193 [510] | 173 [25] | 8 [1] | 12.59 [4.66] | 10.88 - 14.46 |
| R4294 | 1,385 [548] | 151 [7] | 1 [1] | 9.82 [1.26] | 8.38 - 11.42 |
| R4295 | 1,457 [547] | 98 [10] | 1 [0] | 6.30 [1.80] | 5.14 - 7.62 |
| F4166 | 623 [232] | 73 [3] | 1 [0] | 10.47 [1.28] | 8.30 - 12.99 |
| F4167 | 561 [228] | 77 [4] | 1 [0] | 12.05 [1.72] | 9.63 - 14.83 |
| **TOTAL** | **11,292 [4,231]** | **1,120 [62]** | **15 [2]** | **9.02 [1.44]** | **8.53 - 9.54** |

**Table S21. Present-day human DNA contamination estimates from *Scladina I-4A* mtDNA based on differences between Neandertals and modern humans.** Numbers in brackets correspond to DNA fragments deaminated at the last position on either end. Informative positions used in this analysis correspond to a set of 52 sites that differ between all available Neandertal mitochondrial genomes (*6, 8, 10, 63, 65-69*) and 312 modern human mitochondrial genomes (*63*) (including the rCRS, (*34*)). Sequences are considered conflicting when overlapping multiple informative positions and carrying both archaic and modern human alleles. We further discarded sequences obtained in the forward (reverse) orientation at C/T (G/A) polymorphisms or sequences carrying a third allele.

| Library ID | Archaic state | Modern state | Conflicting | Contamination estimate (%) | Binomial 95% Confidence Intervals |
|---|---|---|---|---|---|
| F4687 | 357 [93] | 27 [1] | 0 [0] | 7.03 [1.06] | 4.68-10.07 |
| G2159 | 476 [156] | 40 [0] | 3 [0] | 7.71 [0.00] | 5.60-10.41 |
| G2160 | 419 [120] | 47 [2] | 1 [0] | 10.06 [1.64] | 7.51-13.19 |
| G2161 | 394 [119] | 40 [6] | 0 [0] | 9.22 [4.80] | 6.67-12.34 |
| **TOTAL** | **1,646 [488]** | **154 [9]** | **4 [0]** | **8.56 [1.81]** | **7.30-9.94** |

**Table S22. Present-day human DNA contamination estimates from *Scladina I-4A* mtDNA based on differences between *Scladina I-4A* and modern humans.** Numbers in brackets correspond to DNA fragments deaminated within the three last positions on either end. Informative positions used in this analysis correspond to a set of 71 sites that differ between *Scladina I-4A* and 312 modern human mitochondrial genomes (*63*) (including the rCRS, (*34*)). Sequences are considered conflicting when overlapping multiple informative positions and carrying both *Scladina I-4A* and modern human alleles. We further discarded sequences obtained in the forward (reverse) orientation at C/T (G/A) polymorphisms or sequences carrying a third allele.

| Library ID | *Scladina I-4A* state | Modern state | Conflicting | Contamination estimate (%) | Binomial 95% Confidence Intervals |
|---|---|---|---|---|---|
| F4687 | 441 [123] | 42 [3] | 0 [0] | 8.70 [2.38] | 6.34-11.57 |
| G2159 | 647 [202] | 71 [7] | 3 [0] | 9.85 [3.35] | 7.80-12.31 |
| G2160 | 543 [164] | 73 [5] | 1 [0] | 11.83 [2.96] | 9.41-14.67 |
| G2161 | 503 [153] | 66 [10] | 0 [0] | 11.60 [6.13] | 9.09-14.52 |
| **TOTAL** | **2,134 [642]** | **252 [25]** | **4 [0]** | **10.54 [3.89]** | **9.36-11.86** |

**Table S23. Present-day human DNA contamination estimates on mtDNA in the blank libraries of *HST* based on differences between *HST* and modern humans.** Same processing as for **table S20.**

| Library ID | Raw number of sequences | Mapped (L≥35, MQ≥25) and unique | Deaminated | *HST* state | Human state | Conflicting | Binomial 95% Confidence Intervals |
|---|---|---|---|---|---|---|---|
| L5293 | 325,575 | 183 | 2 | 5 [1] | 12 [0] | 0 | 44.0-89.7 |
| L5294 | 299,493 | 151 | 0 | 0 [0] | 22 [1] | 0 | 84.6-100.0 |
| L5295 | 538,382 | 318 | 2 | 1 [0] | 35 [1] | 0 | 85.5-99.9 |
| L5296 | 372,733 | 170 | 1 | 1 [0] | 18 [1] | 0 | 74.0-99.9 |
| L5411 | 742,590 | 244 | 1 | 2 [0] | 17 [0] | 0 | 66.9-98.7 |
| L5413 | 698,261 | 101 | 7 | 2 [1] | 9 [0] | 0 | 48.2-97.7 |
| R4301 | 154,898 | 62 | 1 | 0 [0] | 5 [0] | 0 | 47.8-100.0 |
| R4302 | 162,274 | 19 | 1 | 0 [0] | 2 [0] | 0 | 15.8-100.0 |
| F4146 | 25,441 | 36 | 1 | 0 [0] | 4 [0] | 0 | 39.8-100.0 |

**Table S24. Present-day human DNA contamination estimates on mtDNA in the blank libraries of *Scladina I-4A* based on differences between Neandertals and modern humans.** Same processing as for **table S21**.

| Library ID | Raw number of sequences | Mapped (L≥35, MQ≥25) and unique | Deaminated | Archaic state | Modern state | Conflicting | Binomial 95% Confidence Intervals |
|---|---|---|---|---|---|---|---|
| D8934 | 42,632 | 413 | 8 | 2 [1] | 38 [0] | 0 | 83.1-99.4 |
| F4693 | 40,262 | 217 | 3 | 0 [0] | 16 [0] | 0 | 79.4-100.0 |
| D8904 | 42,632 | 92 | 9 | 0 [0] | 7 [0] | 0 | 59.0-100.0 |
| D8923 | 35,961 | 46 | 3 | 0 [0] | 2 [0] | 0 | 15.8-100.0 |
| F4675 | 44,159 | 113 | 5 | 0 [0] | 2 [0] | 0 | 15.8-100.0 |
| G3383 | 700,428 | 83 | 6 | 0 [0] | 4 [0] | 0 | 39.8-100.0 |

# Note S6. Reconstruction of the mitochondrial genomes.

## *Scladina I-4A*

To reconstruct the mtDNA genome of *Scladina I-4A* we aligned the DNA sequences to the *Altai Neandertal* mitochondrial genome sequence (*8*). Because the mitochondrial DNA is circular and the reference is linear, sequences will not successfully align to the beginning and end of the reference. To get a uniform coverage, we duplicated the beginning of the reference at its end (1,000 bp). We removed PCR duplicates with *bam-rmdup* (version 0.6.3; https://bitbucket.org/ustenzel/biohazard) and only retained sequences longer than 35 bp and with a mapping quality of at least 25. This filtering results in an average depth of coverage of 107-fold, representing 33,374 sequences.

We then called a consensus base by a majority vote at every position with at least three overlapping sequences and at least two-thirds of the sequences carrying the same base (as done previously, (*6*)). Terminal Ts and As at the three last positions were masked (converted into Ns) to avoid introduction of deaminated bases into the consensus. Only three positions did not pass our criteria: position 304 in the Altai sequence (reference: C; coverage: 61; consensus support: 62.3%), positions 8,286 and 8,287 (reference: TA; coverage: 43 and 52 respectively; consensus support: 51.16 and 50% respectively). While a visual inspection of positions 8,286 and 8,287 revealed a gap of 2bp, position 304 lies in a poly-C stretch that is difficult to resolve. For resolving this position, we focused only on DNA sequences spanning the complete stretch and sequenced in a reverse orientation to avoid C to T substitutions resulting from deamination. Among 14 such DNA sequences, 13 support a stretch of 7 Cs + 1 T + 6 Cs and one had an extra C (7 Cs + 1 T + 7 Cs) corresponding to 7% of the DNA fragments, which is compatible with the contamination estimate on the mtDNA based on diagnostic positions (Supplementary Note 5). We therefore included a stretch of 7 Cs + 1 T + 6 Cs in our reconstruction of the mitochondrial genome.

We also made sure the poly-CA stretch (517-522) was accurately reconstructed. Among 50 sequences spanning the CA repeats (including the two previous and two following bases of the stretch), 44 had 3 CAs (including 3 sequences with a C to T substitution compatible with ancient DNA damage, as these 3 molecules were sequenced in the forward orientation), 3 sequences had 5 CAs and an additional 3 sequences had 4 CAs. We concluded that the Neandertal endogenous sequence had 3 CA repeats.

## *Hohlenstein-Stadel*

The mitochondrial genome of *HST* was reconstructed in previous work from Posth et al. (*10*) with a ~35-fold average mtDNA coverage. However, bases remained uncalled at 59 positions in troublesome regions like the poly-C (pos. 303–318 in the *Altai Neandertal* sequence) and poly-CA (517–522) stretches. Our higher mtDNA depth of coverage of 413-fold (139,773 sequences at least 35 bp long and with a mapping quality of at least 25) allowed us to resolve these regions and reconstruct the complete mtDNA of *HST*. We note that at all the positions called by Posth et al., our consensus sequence matches perfectly the previous reconstruction of the *HST* mtDNA.

To resolve the poly-C stretch, we aligned the sequences to the *Altai Neandertal* mitochondrial genome. Out of 79 sequences spanning the C stretch and sequenced in the reverse orientation, 62

had a chain of 8 Cs followed by a T and 6 Cs (the support for these terminal 6 Cs was even higher with 76 out of 79 sequences).

To identify the number of CA repeats in the poly-CA stretch, we relied on the neighboring position (546 in our reference coordinates) that harbors a fixed difference between modern humans and Neandertals (shared with *HST* according to the published reference, and confirmed here by a consensus call). By separating sequences that carry the human and the Neandertal alleles, we found better support for 6 repeats for the putative Neandertal sequences and 4 repeats for the modern human contaminant. We realigned sequences to a reference with 6 repeats (edited from the Altai sequence), restricting to sequences in the reverse orientation that span the full poly-CA stretch (87 sequences), and counted how many exhibit 7 repeats (6 sequences), 6 repeats (68 sequences), 5 repeats (6 sequences) and 4 repeats (7 sequences). This supports 6 repeats for the endogenous Neandertal DNA. Only the sequences with 6 CA repeats showed signs of deamination at the last 3 positions of the sequences.

The other missing positions were resolved by calling a consensus base at positions in the same way we reconstructed the mtDNA genome of *Scladina I-4A* (i.e., covered by at least three sequences with at least two-thirds of the sequences carrying the same base and masking the terminal Ts and As at the three last positions). The consensus call failed only at position 207 (reference: G; coverage: 72; consensus support: 63.89 %). Sequences carrying both the *HST*-specific deletion of one of the three As of positions 247, 248 or 249 and the allele G at position 240 were also associated with an A at position 207 (sequenced in forward orientation). We therefore included an A at position 207 in the *HST* consensus sequence.

# Note S7. Phylogenetic analysis of the mitochondrial genomes.

## *Maximum parsimony tree*

While the full mitochondrial genome of *HST* has been described previously (*10*) and represent a deeply divergent lineage among Neandertals, the relationship of the mitochondrial genome of *Scladina I-4A* was previously assessed from 123 bp of its hypervariable region (*12*). Analysis of this small region suggested a close relationship to the mitochondrial genome of the *Altai Neandertal* (*10*) but the fully reconstructed mitochondrial genome described here allows us to reconstruct the phylogeny with more confidence. We therefore built a maximum parsimony tree using a multiple sequence alignment (made using MAFFT v7.271 (*64*)) of the mitochondrial genome sequences from 322 modern humans (including the rCRS and 10 ancient modern human genomes (*46, 70-74*)), 23 Neandertals (*6, 8, 10, 63, 65-69*) including *HST* and *Scladina I-4A*, 4 Denisovans (*4, 75-77*), one hominin from Sima de los Huesos (*78*) and one chimpanzee (*79*) (we refer to Table S5.3 from (*6*) for details about the samples used here). The tree was obtained using the Subtree-Pruning-Regrafting algorithm (p.126 in (*80*)) in MEGA6 (*81*). All positions containing gaps and missing data were removed (a total of 15,771 positions were used in the analysis). This tree supports the close relationship of *Scladina I-4A* to the *Altai Neandertal* mitochondrial genome (**fig. S10**).

## *Bayesian analysis*

We used Beast2 (version 2.4.8, (*82*)) to estimate the divergence time of *Scladina I-4A* from other available Neandertal mitochondrial genomes and to estimate a molecular date for this Neandertal that has been previously dated based on uranium and thorium isotopic ratios measured by gamma spectrometry to 127kya (95-173kya, (*13*)), with a minimum age of 80 or 87kya based on the geological context (*13, 83*).

As above, we used the full sequence of 23 Neandertal mitochondrial genomes (*6, 8, 10, 63, 65-69*), including *HST* and *Scladina I-4A*, as well as the genomes from 312 present-day humans (*63*), 10 ancient humans (*46, 70-74*), 4 Denisovans (*4, 75-77*), a hominin from Sima de los Huesos (*78*) and a chimpanzee as outgroup (isolate *Jenny*, (*79*)). As the D-loop is the most variable region of the mitochondrial genome, concerns have been raised previously that a poorly covered D-loop in some available Neandertal genomes concomitant with the use of a mutation rate estimated from the whole molecule would accelerate the mutation rate of the coding region and lead to biased estimates (*10*). For consistency with previous work, we therefore repeated the analysis restraining to the mtDNA coding region (577-16,023 in rCRS coordinates, (*73*)).

For both datasets, the best fitting substitution model was Tamura-Nei 1993 (TN93) (*84*) with a fraction of invariable sites and gamma distributed rate variation among sites, according to the model selection measures computed from jModelTest 2.1.10 (*85*) (Bayesian Information Criterion, a performance measure based on Decision Theory and the corrected Akaike Information Criterion; **table S25**).

In order to choose the best fitting clock model (strict clock or uncorrelated lognormal clock) and tree model (constant population size or Bayesian Skyline), we performed a marginal likelihood estimation analysis using the path sampling approach implemented in the MODEL_SELECTION package from BEAST2 (*82*). For each model combination, we used 40

path steps and a chain length of 25,000,000 iterations, with a parameter alpha of 0.3 for the Beta distribution used to space out steps, a pre-burn-in of 75,000 iterations followed by a burn-in representing 80% of the chain. We used a mutation rate of $2.53\times10^{-8}$ substitution per site per year for the whole genome and of $1.57\times10^{-8}$ for the coding region, corresponding to direct estimates of the mitochondrial substitution rate in modern humans obtained by comparing present-day and directly radiocarbon dated ancient modern humans (*73*). For the uncorrelated lognormal clock model, we fixed the mean to the human mutation rate and used a gamma distributed standard deviation. The date of modern samples was set to 0 while uniform priors were used for the ancient samples, using either a range spanning the 95% confidence intervals for the dated Neandertals (see the supplementary information of Posth et al. (*10*) for these calibrated radiocarbon dates, with the exception of *El Sidrón 1253* for which we used the most recent estimates from (*86*)) or a range from 30,000 to 200,000 for the undated Neandertals (initial value of 50,000 years ago) and 30,000 to 300,000 for the Denisovans (with the exception of *Denisova 3*, for whom we used a narrower range from 30,000 to 100,000 to reflect prior knowledge from the analysis of the nuclear genome, (*20*)). For the age of the Sima de los Huesos hominin, we used a uniform prior spanning the confidence intervals of the most recent dates (*2*) from 260,000 to 780,000 years ago. Finally, we constrained modern humans and Neandertals as two monophyletic groups and estimated their respective TMRCAs (uniform priors from 50,000 to infinity for modern humans and from 100,000 to infinity for Neandertals).

The best fitting model combination was a relaxed clock and a constant population size for the whole genome ($\log_{10}$ BF>11, **table S27**) whereas this model combination was not fitting significantly better for the coding region than the simpler model of a fixed clock and a constant population size ($\log_{10}$ BF=0.23; **table S26**). We therefore used these two model combinations for inferring the date of *Scladina I-4A* and the divergence to the *Altai Neandertal*. For both datasets (i.e. coding region or whole genome), we performed three MCMC runs of 75,000,000 iterations, sampling parameter values and trees every 2,000 iterations, with a burn-in of 10,000,000 iterations. We then merged the results using the program logcombiner (*82*). All estimates with their 95% HPD interval are reported in **table S28**. Both individuals are estimated to have lived 120kya (95% HPD: 76-168kya and 55-185kya for *Scladina I-4A* and *HST*, respectively), similar to previous results for *HST* (*10*) and in agreement with both the direct date of the skeletal remains and the date obtained from the geological context for *Scladina I-4A* (*13*, *83*). The generated tree (**fig. S11**) support the tree built by maximum parsimony (**fig. S10**) with a close relationship of *Scladina I-4A* to the *Altai Neandertal* mitochondrial genome. The mtDNA MRCA of *Scladina I-4A* and the *Altai Neandertal* is estimated to 163kya (95% HPD: 126-203kya), while the date for the MRCA of *HST* and the *Altai Neandertal* is estimated to 286kya (95% HPD: 238-335kya; coinciding with a previous estimate of 270kya, 219-316kya in (*10*)). In the main text of this manuscript, we report these estimates restrained to the coding region for consistency with previous work (*10*) and because of higher ESS values (Effective Sample Size), which is a measure of the correlation between sampled states in the Markov chain and is higher for more precise estimates. However, we note that the mitochondrial mutation rate for Neandertals and Denisovans is not known and assumed here to be identical to that of modern humans.

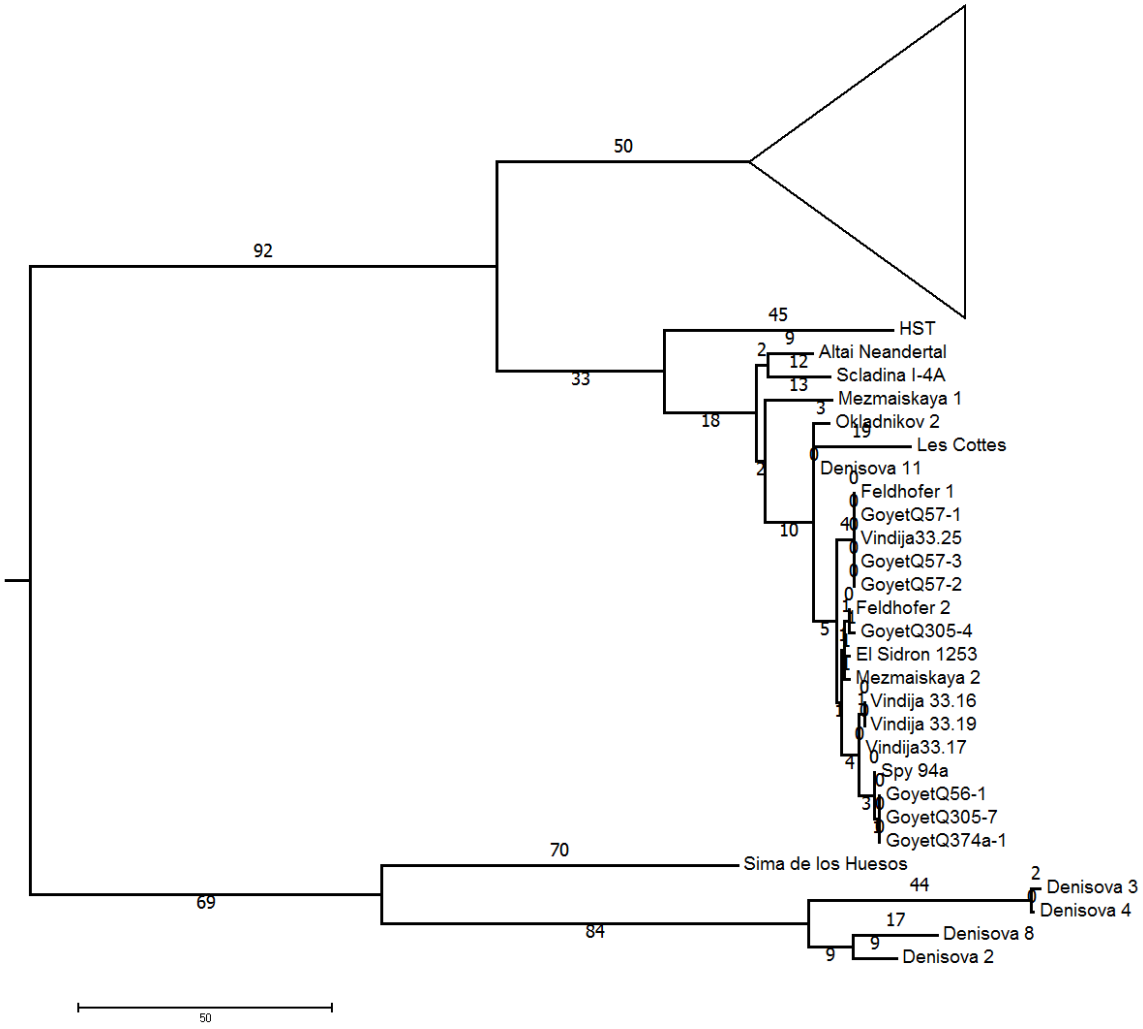


**Fig. S10. Maximum parsimony tree built with MEGA6 (Molecular Evolutionary Genetics Analysis, program version 6).** The branch representing the mtDNA of a chimpanzee used to root the tree is not shown and the branches corresponding to the 322 modern human mtDNAs were collapsed (triangle on the upper branch). The numbers correspond to the branch length measured in number of mutations.

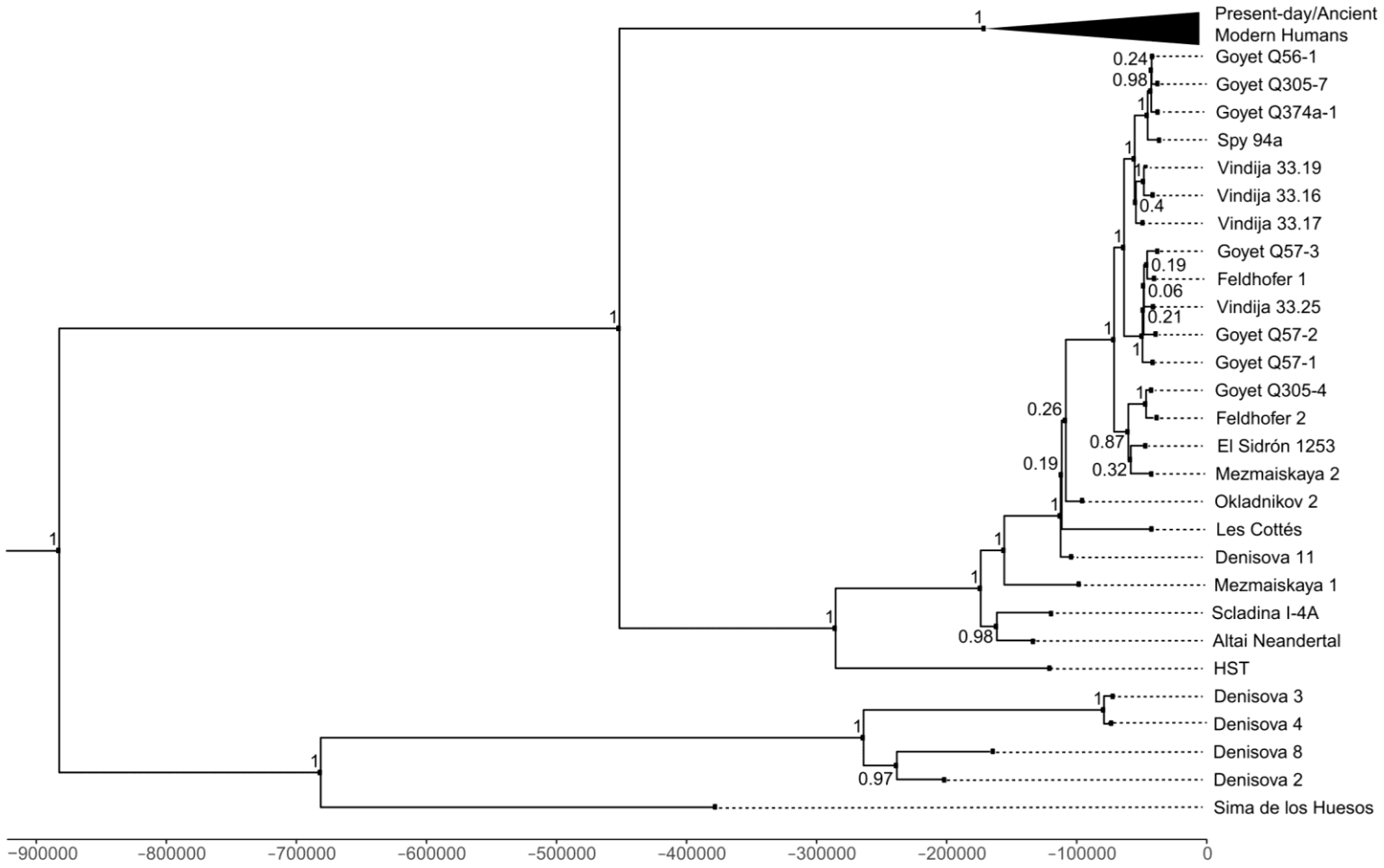


**Fig. S11. Phylogenetic relationship of currently available archaic human mitochondrial genomes reconstructed from a Bayesian analysis with BEAST 2 (Bayesian Evolutionary Analysis Sampling Trees, program version 2).** The branch representing the mtDNA of a chimpanzee used to root the tree is not shown and the branches corresponding to the 322 modern human mtDNAs were collapsed. The x-axis represents time in years and the numbers at the nodes correspond to posterior probabilities of the depicted branching orders.

**Table S25. Best substitution models according to the three model selection measures computed by jModelTest 2.1.10.** BIC = Bayesian Information Criterion, DT = Decision Theory and AICc = corrected Akaike Information Criterion.

| Dataset | Measure | Model | Rank | Log-likelihood | Measure value |
|---|---|---|---|---|---|
| **Coding only** | **AICc** | **GTR+I+G** | **1** | **-46,579.94087** | **94,648.270279** |
| Coding only | AICc | TrN+I+G | 2 | -46,583.33931 | 94,648.477076 |
| Coding only | AICc | TrN+G | 3 | -46,659.96264 | 94,799.527637 |
| **Coding only** | **BIC** | **TrN+I+G** | **1** | **-46,583.33931** | **99,987.048568** |
| Coding only | BIC | GTR+I+G | 2 | -46,579.94087 | 100,009.192437 |
| Coding only | BIC | TrN+G | 3 | -46,659.96087 | 100,130.648311 |
| **Coding only** | **DT** | **TrN+I+G** | **1** | **-46,583.33931** | **0.000000** |
| Coding only | DT | GTR+I+G | 2 | -46,579.94087 | 0.000278 |
| Coding only | DT | TrN+I | 3 | -46,661.77621 | 0.011456 |
| **Whole genome** | **AICc** | **TrN+I+G** | **1** | **-56,432.87071** | **114,342.759927** |
| Whole genome | AICc | GTR+I+G | 2 | -56,430.66449 | 114,344.895057 |
| Whole genome | AICc | HKY+I+G | 3 | -56,469.80541 | 114,414.447353 |
| **Whole genome** | **BIC** | **TrN+I+G** | **1** | **-56,432.87071** | **119,735.516519** |
| Whole genome | BIC | GTR+I+G | 2 | -56,430.66449 | 119,760.254469 |
| Whole genome | BIC | HKY+I+G | 3 | -56,469.80541 | 119,799.669123 |
| **Whole genome** | **DT** | **TrN+I+G** | **1** | **-56,432.87071** | **0.000000** |
| Whole genome | DT | GTR+I+G | 2 | -56,430.66449 | 0.007475 |
| Whole genome | DT | TPM1uf+I+G | 3 | -56,469.15619 | 0.010884 |

**Table S26. Marginal likelihoods of the different tested clock and tree models obtained from a path sampling approach using only the coding region of the mitochondrial sequences.** The two equally good best models are marked in bold.

| Clock model | Tree model | Marginal log-likelihood |
|---|---|---|
| **Strict** | **Coalescent with constant population size** | **-49,014.8621** |
| **Relaxed (uncorrelated lognormal)** | **Coalescent with constant population size** | **-49,014.3345** |
| Strict | Bayesian Skyline | -49,544.8279 |
| Relaxed (uncorrelated lognormal) | Bayesian Skyline | -49,437.8623 |

**Table S27. Marginal likelihoods of the different tested clock and tree models obtained from a path sampling approach using the full mitochondrial genome sequences.** The best-supported model is marked in bold.

| Clock model | Tree model | Marginal log-likelihood |
|---|---|---|
| Strict | Coalescent with constant population size | -59,388.2449 |
| **Relaxed (uncorrelated lognormal)** | **Coalescent with constant population size** | **-59,361.5080** |
| Strict | Bayesian Skyline | -59,874.1802 |
| Relaxed (uncorrelated lognormal) | Bayesian Skyline | -59,758.7983 |

**Table S28. Estimates of molecular age and divergence times.** For both the analysis based on the full mitochondrial genome and the coding region only, estimates were obtained from three MCMC runs of 75,000,000 iterations (sampling parameter values and trees every 2,000 iterations, with a burn-in of 10,000,000 iterations). At the exception of the mutation rate and the clock model used (see **tables S26** and **S27**), all parameters were the same for both analyses.

| Parameter | Mitochondrial data | Mean | 95% HPD lower | 95% HPD upper | ESS |
|---|---|---|---|---|---|
| Human-Chimpanzee TMRCA | Whole genome | 3,764,300 | 2,646,800 | 4,990,300 | 1,072 |
| | Coding region | 5,643,200 | 5,071,300 | 6,213,500 | 9,487 |
| Archaic and Modern Human TMRCA | Whole genome | 680,590 | 560,250 | 809,930 | 211 |
| | Coding region | 880,130 | 798,410 | 964,280 | 682 |
| Neandertal-Modern Human TMRCA | Whole genome | 363,970 | 295,020 | 441,010 | 551 |
| | Coding region | 452,120 | 397,930 | 507,050 | 1,944 |
| Modern Human TMRCA | Whole genome | 142,820 | 121,080 | 166,680 | 1,228 |
| | Coding region | 173,040 | 150,620 | 196,230 | 2,508 |
| Neandertal TMRCA | Whole genome | 233,250 | 182,970 | 287,410 | 458 |
| | Coding region | 286,190 | 238,110 | 335,300 | 1,146 |
| *Altai Neandertal* and *Scladina I-4A* TMRCA | Whole genome | 143,040 | 108,230 | 179,540 | 278 |
| | Coding region | 162,780 | 125,900 | 203,120 | 602 |
| *Scladina I-4A* age | Whole genome | 100,570 | 54,322 | 144,600 | 485 |
| | Coding region | 120,450 | 75,630 | 167,590 | 865 |
| *HST* age | Whole genome | 104,750 | 35,932 | 171,270 | 1,245 |
| | Coding region | 119,620 | 54,673 | 185,480 | 2,489 |
| Altai age | Whole genome | 112,980 | 70,788 | 156,330 | 391 |
| | Coding region | 133,430 | 88,708 | 177,140 | 776 |
| Vindija 33.17 age | Whole genome | 50,165 | 42,228 | 57,507 | 3,012 |
| | Coding region | 52,247 | 41,292 | 62,985 | 4,836 |
| Vindija 33.19 age | Whole genome | 47,821 | 45,580 | 51,317 | 4,380 |
| | Coding region | 48,646 | 45,580 | 53,809 | 6,296 |
| Vindija 33.25 age | Whole genome | 43,978 | 36,174 | 51,620 | 4,389 |
| | Coding region | 44,264 | 32,568 | 56,576 | 4,188 |
| Mezmaiskaya 1 age | Whole genome | 99,316 | 56,180 | 141,160 | 481 |
| | Coding region | 98,946 | 55,091 | 141,570 | 1,089 |
| Okladnikov 2 age | Whole genome | 80,404 | 53,592 | 108,270 | 410 |
| | Coding region | 96,751 | 69,820 | 125,240 | 673 |
| Goyet Q305-7 age | Whole genome | 40,359 | 33,518 | 45,813 | 6,123 |
| | Coding region | 39,691 | 31,380 | 46,222 | 10,147 |
| Goyet Q374a-1 age | Whole genome | 40,360 | 33,389 | 45,574 | 6,256 |
| | Coding region | 39,686 | 31,201 | 46,038 | 10,216 |
| Goyet Q57-1 age | Whole genome | 42,999 | 34,853 | 51,001 | 3,803 |
| | Coding region | 44,239 | 32,512 | 56,683 | 3,189 |
| Denisova 11 age | Whole genome | 96,172 | 74,905 | 120,320 | 267 |

| | | | | | |
|---|---|---|---|---|---|
| | Coding region | 105,070 | 80,501 | 131,110 | 532 |
| Denisova 3 age | Whole genome | 68,470 | 35,950 | 100,000 | 57 |
| | Coding region | 72,357 | 40,256 | 100,000 | 141 |
| Denisova 4 age | Whole genome | 73,799 | 36,181 | 107,220 | 55 |
| | Coding region | 76,451 | 40,490 | 108,690 | 135 |
| Denisova 8 age | Whole genome | 154,620 | 64,587 | 253,260 | 180 |
| | Coding region | 166,160 | 87,953 | 244,070 | 405 |
| Denisova 2 age | Whole genome | 184,220 | 102,170 | 282,820 | 159 |
| | Coding region | 202,600 | 131,230 | 277,220 | 348 |
| Sima de los Huesos age | Whole genome | 381,480 | 260,000 | 524,700 | 289 |
| | Coding region | 375,550 | 260,030 | 483,900 | 873 |

# Note S8. Characterization of present-day human DNA contamination in the nuclear genome.

Ancient DNA is characterized by elevated frequencies of apparent C to T substitutions that accumulate at the end of DNA fragments over time due to the deamination of cytosines (*18, 72, 87, 88*). Because this chemical modification is a slow process, this feature can be used to differentiate between ancient DNA and present-day human contaminant DNA. Considering sequences in which the base at the 5' or 3' ends aligns to a C in the human reference genome, 46.0% of the 5' and 43.4% of the 3' ends, respectively, of *HST* DNA sequences include Ts, while 29.8% and 22.7% of the *Scladina I-4A* DNA sequences do so (**fig. S12**). The latter frequencies are lower than typically observed in specimens of this age (*6, 28*), suggesting that the libraries are contaminated with present-day human DNA (*1*), which tend to be much less affected by cytosine deamination (*87*). In addition, when we select ancient DNA sequences that exhibit a C-to-T substitution at one end, C-to-T substitution frequencies computed at the opposite end are significantly higher compared to all sequences (**fig. S12**). This confirms the presence of a population of molecules that were not affected by cytosine deamination and likely represent present-day human contaminant DNA. To circumvent the presence of contamination, we performed all subsequent analyses using sequences that exhibit at least one C-to-T substitution within 3bp of either ends, assuming the absence of C-to-T substitutions in contaminant sequences. In this section, we explore whether that assumption is valid and describe levels of present-day human contamination in the *HST* and *Scladina I-4A* datasets.

## *Deamination patterns on contaminant molecules*

While the Neandertal remains from Scladina Cave were discovered in 1993 (*11*), the femur of *HST* was found in 1937 (*9*). Deamination of cytosines typical of ancient DNA may have already accumulated on the modern human contaminant molecules, if introduced early after the discovery, violating our assumption that deamination would be a signal specific of the Neandertal sequences. To test this possibility, for each Neandertal, we identified a set of sequences that carry modern human derived alleles found in the genomes of present-day Luhya and Yoruba individuals from Africa (*89*) but that are absent in the available high-coverage Neandertal and Denisovan genomes (*8, 19, 20*) (the derived allele was identified by comparing to the genomes of several Great Apes as done in other analyses; see Material and Methods). These sets of sequences should be mostly composed of present-day human contamination. However, we note that a Neandertal origin for such sequences cannot be completely excluded, as some ancestral polymorphisms may have been shared. This sharing is dependent on the frequency of the derived alleles in modern humans as higher frequency variants are likely older and more often shared with the archaics. Indeed, when we compute the proportion of alleles that are derived in the *Altai Neandertal* but ancestral in the *Vindija 33.19* Neandertal and the Denisovan genomes stratified by the allele frequency in the Luhya and Yoruba populations of the 1000 Genomes dataset (*89*), up to 4.5% of the sites with derived alleles that are near fixation in these modern human populations are shared with the *Altai Neandertal* (**fig. S13**). In contrast, low frequency variants were rarely shared (**fig. S13**). We therefore examined the proportion of terminal C-to-T substitutions in *HST* and *Scladina I-4A* sequences that carry the modern human-like derived allele and stratified the results by the allele frequency observed in Luhya and

Yoruba (**figs. S14** and **S15**). Focusing on low frequency variants that most often represent recent mutations in modern humans, we found a low level of terminal deamination on the putatively contaminant sequences from *Scladina I-4A* (up to ~2%), while a high-proportion of fragments from *HST* carried terminal deaminations with up to ~8% and ~5% of C-to-T substitutions on the 5' and 3' ends of the fragments, respectively. These deamination frequencies represent upper estimates as it is unclear how many Neandertal sequences remain after this filtering. Relatively high rates of C-to-T substitutions in the data generated from *HST* suggest that some cytosines in the contaminating DNA fragments are deaminated.

## *Lower estimates of present-day human DNA contamination based on deamination patterns*

To estimate the levels of nuclear DNA contamination from modern human sequences, we first relied on the presence of C-to-T substitutions that accumulate at the ends of ancient DNA molecules over time due to cytosine deamination (*18, 87, 88*). Assuming the absence of this damage on DNA fragments stemming from present-day human contamination, we can use the frequency of deamination to evaluate the excess of molecules that do not exhibit C-to-T substitutions and are thus more likely to represent contamination. Note that this assumption is violated in the dataset from *HST* (see previous section), and we can therefore only infer the minimal level of contamination with this approach. More accurate estimates are given later based on the genetic relationships to other modern and archaic humans.

Restraining our analysis to molecules that align on both ends to Cs or Gs in the reference sequence (depending on the sequenced strand), we counted the proportion of molecules with a deamination at both ends, noted **α**, at only the 5' or 3' end of the sequenced strand, noted **β** and **γ** respectively, and without deamination, noted **δ**. Assuming that the frequencies of deamination at the 5' and 3' ends (noted $f_5$ and $f_3$) are independent, we can derive the following linear system of equations

$$\alpha = (1-p) \times f_5 \times f_3,$$
$$\beta = (1-p) \times f_5 \times (1-f_3),$$
$$\gamma = (1-p) \times f_3 \times (1-f_5),$$
$$\delta = (1-p) \times (1-f_5) \times (1-f_3) + p$$

with $p$ representing the proportion of contaminant molecules. A rearrangement of the last equation leads to: $p = \delta - \frac{\beta \times \gamma}{\alpha}$.

In addition to the assumption of absence of deamination on the contaminant sequences, we caution that this approach makes other assumptions that may be violated, such as the independence of deamination at both ends of the sequences. The estimates are therefore approximate at best. This said, we estimated that at least 11% and 52% of sequences (L≥30, MQ≥25) for *HST* and *Scladina I-4A* originate from modern human DNA contamination, respectively (see **tables S29** and **S30** for estimates per library). For *HST*, the estimates varied with the length of the sequences (with higher estimates for longer sequences, **table S31**), suggesting that contaminating modern human sequences in this specimen tend to be longer than

endogenous sequences (as observed before in other samples, (*72*)). This characteristic of the contaminant is relevant because of the design of our analyses, most of which are based on the prior identification of informative sites. Longer sequences are statistically more likely to overlap such sites, leading to a higher proportion of modern human contaminant sequences detected in our analyses. Therefore, a distinction should be made between the former contamination estimates per molecule and contamination estimates per base pair, which are more adequate for analyses based on specific informative sites. We estimated the contamination rate per base pair by looking at molecules overlapping a random set of 4,000 and 2,000 positions (any position in the genome) for *HST* and *Scladina I-4A*, respectively. While estimates remained stable for *Scladina I-4A* (52%), the level of per-base contamination for *HST* increased to 16%.

## *Contamination estimates based on the genetic relationship to a modern human*

We additionally estimated contamination based on the proportion of sequences carrying the human allele at sites where a modern human (Mbuti, HGDP00456, (*19*)) genome differs from the genomes of four Great Apes (*21-24*), *Denisova 3* (*19*) and the *Altai Neandertal* (*8*). As reported in the Material and Methods, we used a simple equation to model these proportions ($p$) as a linear combination of the expected allele sharing of a modern human contaminant ($p_c$) and a Neandertal ($p_e$) with the Mbuti genome: $p = c \times p_c + (1 - c) \times p_e$, with c being the contamination rate. Values of $p_c$ and $p_e$ were obtained by computing the proportion of derived alleles in the Mbuti genome that are shared with a modern human from Eurasia (same result for a European, HGDP00521 (*19*), or an Asian, HGDP00775 (*8*)) and *Vindija 33.19*, respectively. We report in **table S32** the results obtained by solving this equation for both deaminated and all sequences from *HST* and *Scladina I-4A*. For the datasets of deaminated sequences that we used in most of the analyses, the contamination estimates are 2.0% and 5.5% [CI: 1.2-2.9% and 3.5-7.9%] for *HST* and *Scladina I-4A*, respectively, whereas the contamination estimates for the full datasets (i.e. including the sequences without signs of deamination) are 22.9% and 64.8% [CI: 22.1-23.8% and 63.0-66.7%], respectively. We note that similar estimates can be obtained if we use instead *Vindija 33.19* to ascertain positions and the *Altai Neandertal* to compute $p_e$.

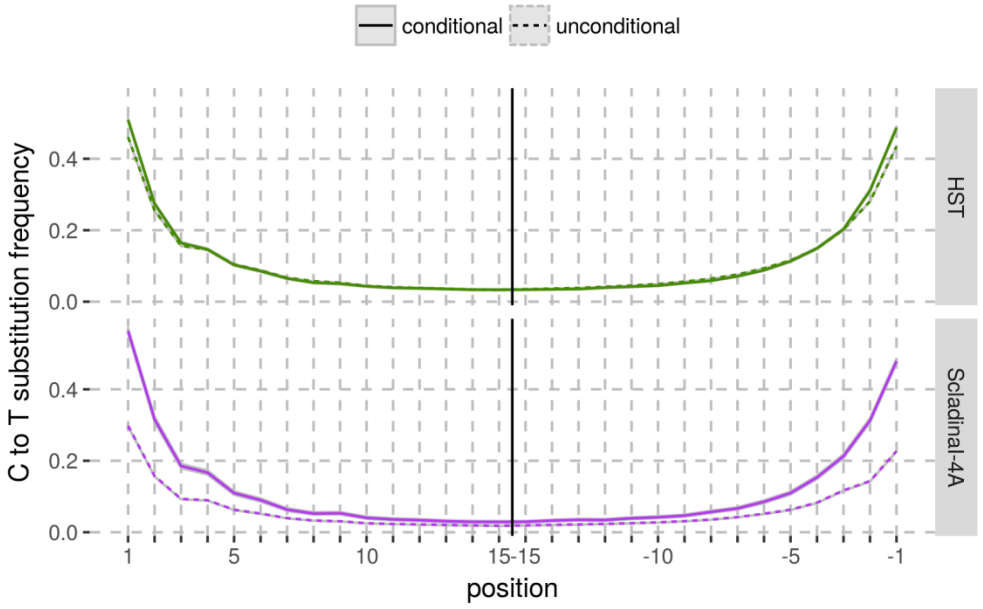


**Fig. S12. C-to-T substitution frequencies at the end of nuclear DNA sequences (dashed lines), including frequencies conditioned on a C-to-T substitution at the other end (solid lines).**

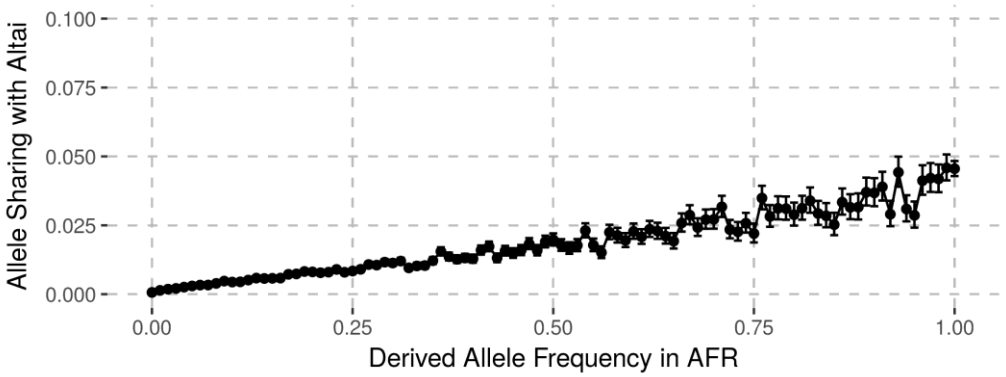


**Fig. S13. Proportion of alleles that are derived in the Altai Neandertal but ancestral in the *Vindija 33.19* Neandertal and Denisovan genomes stratified by the allele frequency in the Luhya and Yoruba populations (AFR) of the 1000 genomes dataset (*80*).** Bars represent 95% binomial confidence intervals.

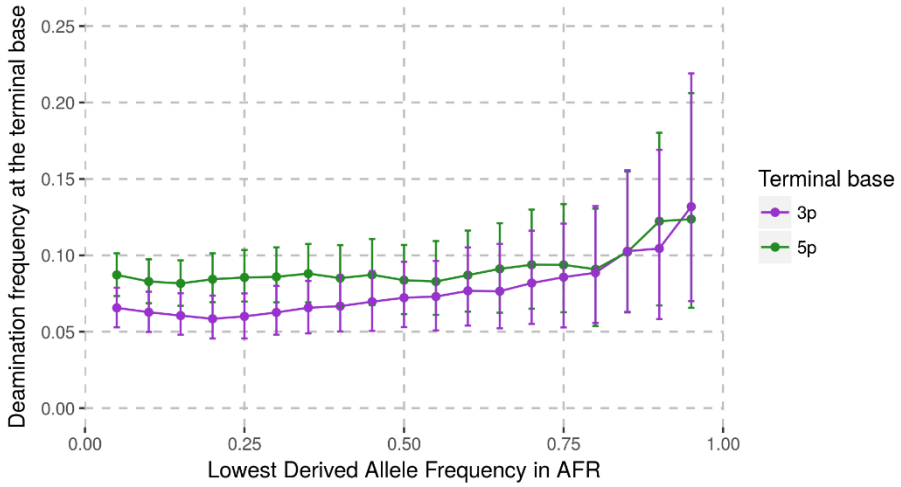


**Fig. S14. Deamination frequencies on sequences from *HST* that carry a modern human allele absent from the currently available Neandertal genomes.** This set of sequences should therefore be mostly composed of present-day human DNA contaminant sequences. Each dot represents the frequency of terminal C-to-T substitutions on sequences that carry a modern human allele with a derived allele frequency higher than or equal to the frequency reported on the X-axis. The results for the 3' ("3p") and 5' ("5p") ends are reported in purple and green, respectively. Bars represent 95% binomial confidence intervals.

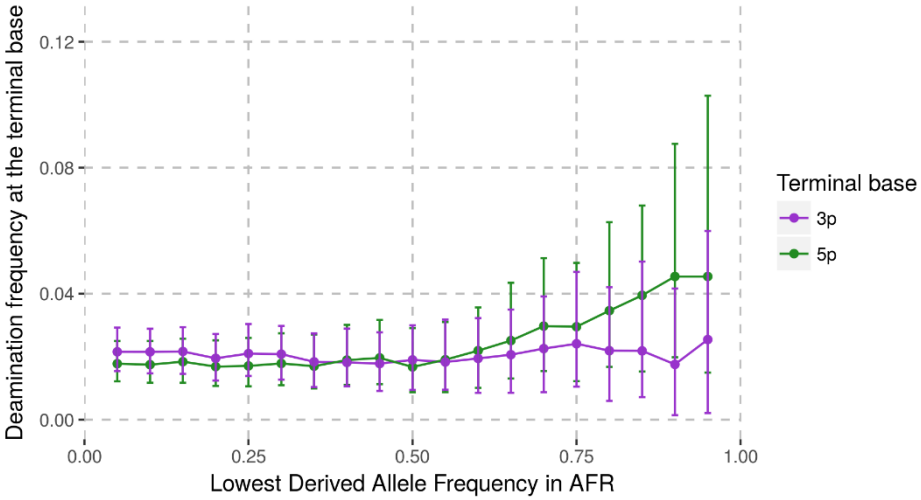


**Fig. S15. Deamination frequencies on sequences from *Scladina I-4A* that carry a modern human allele absent from the currently available Neandertal genomes.** This set of sequences should therefore be mostly composed of present-day human DNA contaminant sequences. Each dot represents the frequency of terminal C-to-T substitutions on sequences that carry a modern human allele with a derived allele frequency higher than or equal to the frequency reported on the X-axis. The results for the 3' ("3p") and 5' ("5p") ends are reported in purple and green, respectively. Bars represent 95% binomial confidence intervals.

**Table S29. Present-day human DNA contamination estimates for *HST* nuclear DNA based on deamination rates on the last positions of the molecules.** These numbers are computed only from the sequences that align on both ends to Cs or Gs in the reference sequence, depending on the sequenced strand (forward or reverse, respectively).

| Library ID | Not deaminated | Deaminated only in 3' | Deaminated only in 5' | Deaminated in 3' and 5' | Contamination estimate |
|---|---|---|---|---|---|
| L5262 | 249 | 96 | 78 | 81 | 31.06 |
| L5263 | 798 | 75 | 59 | 74 | 73.38 |
| L5264 | 3,021 | 2,829 | 2,488 | 2,722 | 3.93 |
| L5265 | 2,012 | 993 | 721 | 995 | 27.38 |
| L5386 | 23,433 | 20,037 | 17,154 | 20,081 | 7.83 |
| R5784 | 2,046 | 1,204 | 1,219 | 1,156 | 13.80 |
| R5785 | 3,226 | 1,864 | 1,788 | 1,761 | 15.43 |
| F7016 | 21,726 | 11,119 | 17,483 | 13,805 | 11.92 |
| F7017 | 22,742 | 11,682 | 13,492 | 10,983 | 14.25 |
| **TOTAL** | **79,253** | **49,899** | **54,482** | **51,658** | **11.32** |

**Table S30. Present-day human DNA contamination estimates for *Scladina I-4A* nuclear DNA based on deamination rates on the last positions of the molecules.** These numbers are computed only from the sequences that align on both ends to Cs or Gs in the reference sequence, depending on the sequenced strand (forward or reverse, respectively).

| Library ID | Not deaminated | Deaminated only in 3' | Deaminated only in 5' | Deaminated in 3' and 5' | Contamination estimate |
|---|---|---|---|---|---|
| F7490 | 14,652 | 2,322 | 3,469 | 3,075 | 51.16 |
| G2159 | 12,859 | 2,207 | 2,953 | 2,719 | 50.45 |
| G2160 | 14,631 | 2,436 | 2,488 | 3,419 | 50.75 |
| G2161 | 14,478 | 2,453 | 3,392 | 3,171 | 50.67 |
| **TOTAL** | **56,620** | **9,418** | **12,302** | **12,384** | **52.10** |

**Table S31. Relationship between sequence length and present-day human DNA contamination estimate based on deamination rates in *HST* nuclear DNA sequences.**

| Sequence length | Not deaminated | Deaminated only in 3′ | Deaminated only in 5′ | Deaminated in 3′ and 5′ | Contamination rate |
|---|---|---|---|---|---|
| 30 | 4952 | 2907 | 3359 | 2398 | 0.0646312 |
| 31 | 4653 | 3072 | 3397 | 2646 | 0.0515028 |
| 32 | 4278 | 3039 | 3319 | 2798 | 0.0501061 |
| 33 | 4244 | 3017 | 3400 | 2646 | 0.0276005 |
| 34 | 4101 | 2984 | 3259 | 2865 | 0.0534965 |
| 35 | 3753 | 2892 | 3150 | 2699 | 0.0302345 |
| 36 | 3640 | 2748 | 3054 | 2674 | 0.0413902 |
| 37 | 3489 | 2567 | 2734 | 2407 | 0.0511979 |
| 38 | 3207 | 2434 | 2630 | 2309 | 0.0410796 |
| 39 | 2963 | 2206 | 2449 | 2221 | 0.0539221 |
| 40 | 2709 | 2038 | 2296 | 2036 | 0.0452412 |
| 41 | 2576 | 1857 | 2082 | 1910 | 0.0654923 |
| 42 | 2312 | 1907 | 2104 | 2323 | 0.0676361 |
| 43 | 2248 | 1717 | 1857 | 2148 | 0.0958106 |
| 44 | 2062 | 1522 | 1542 | 1914 | 0.118723 |
| 45 | 1856 | 1332 | 1521 | 1790 | 0.111428 |
| 46 | 1745 | 1259 | 1308 | 1568 | 0.118157 |
| 47 | 1586 | 1171 | 1167 | 1381 | 0.112433 |
| 48 | 1414 | 927 | 993 | 1239 | 0.146742 |
| 49 | 1346 | 966 | 927 | 1099 | 0.122449 |
| 50 | 1164 | 789 | 895 | 946 | 0.110052 |
| 51 | 1157 | 668 | 736 | 808 | 0.162815 |
| 52 | 1068 | 641 | 637 | 797 | 0.1768 |
| 53 | 989 | 549 | 556 | 704 | 0.198504 |
| 54 | 886 | 517 | 559 | 564 | 0.147895 |
| 55 | 864 | 440 | 474 | 539 | 0.205896 |

**Table S32. Present-day human DNA contamination estimates based on the sharing of derived alleles with a modern human** (Mbuti, HGDP00456, (*19*); see Supplementary Note 8 or Material and Methods for a description of the site ascertainment scheme). $p_c$and $p_e$ represent the proportion of derived alleles in the Mbuti genome that are shared with a modern human from Eurasia (same result for a European, HGDP00521 (*19*), or an Asian, HGDP00775 (*8*)) and *Vindija 33.19*, respectively. Sequences were considered deaminated if they exhibit at least one C-to-T substitution within the last three positions of either ends.

| Individual | Filter | Proportion of human alleles (*p*) | $p_c$ | $p_e$ | Contamination estimate | 95% Binomial CI |
|---|---|---|---|---|---|---|
| *HST* | Deaminated | 260/12,149 (2.1%) | 0.332 | 0.015 | 2.0% | 1.2-2.9% |
| *HST* | No filter | 3,781/43,157 (8.8%) | 0.332 | 0.015 | 22.9% | 22.1-23.8% |
| *Scladina I-4A* | Deaminated | 89/2,736 (3.3%) | 0.332 | 0.015 | 5.5% | 3.5-7.9% |
| *Scladina I-4A* | No filter | 4,239/19,251 (22.0%) | 0.332 | 0.015 | 64.8% | 63.0-66.7% |

# Note S9. Genetic relationships and effect of present-day human DNA contamination, sequencing errors, and reference bias.

## *Assignment to an archaic lineage*

To investigate the relationship of *HST* and *Scladina I-4A* to modern and archaic humans, we first applied an analysis introduced in the study of the Sima de los Huesos hominins (*1*) that relies on the proportion of sequences that match the derived alleles seen in a present-day human (Mbuti, HGDP00456, (*19*)), a Denisovan (*Denisova 3*, (*19*)) and/or a Neandertal genome (*Vindija 33.19*, (*20*)). We described in the Material and Methods our strategy to ascertain informative sites, identify the ancestral alleles and filter out potential errors. Using alignments with a mapping quality of 25 or above, we found that the allele sharing of *HST* and *Scladina I-4A* was highest with the Neandertal genome (69% and 64% for *HST* and *Scladina I-4A*, respectively, compared to 2-3% with the Denisovan and modern human genomes), confirming that both *HST* and *Scladina I-4A* are Neandertals. However, this allele sharing is much lower than what has previously been observed for other Neandertal genomes, particularly for Neandertals dated to 40-45kya (78-83%, **fig. S16**) (*6*), consistent with the older ages of *HST* and *Scladina I-4A*.

## *Closer relationship to Vindija 33.19 than to the Altai Neandertal*

At sites where either *Vindija 33.19* or the *Altai Neandertal* genome carries a derived allele (but the Mbuti and the Denisovan genome carry the ancestral allele), *HST* sequences with terminal C-to-T substitutions (within the last three bases) carry Vindija-like alleles more often than Altai-like alleles (531 vs. 466; two-sided binomial test : p=0.018; **table S33**). In contrast, *Scladina I-4A* sequences with terminal C-to-T substitutions do not share more often *Vindija 33.19* alleles than *Altai Neandertal* alleles (110 against 106, two-sided binomial test: p=0.367). As this may be due to the limited amount of data available, we repeated by including all sequences generated from the two Neandertals, and found that both exhibit significantly more *Vindija 33.19* derived alleles than *Altai Neandertal* derived alleles (1676 vs. 1326 for *HST* and 443 vs. 321 for *Scladina I-4A*; two-sided binomial tests: $p<10^{-4}$). This suggests that both *HST* and *Scladina I-4A* have a closer relationship to *Vindija 33.19* than to the *Altai Neandertal*.

However, it is not clear for *Scladina I-4A* whether this signal is driven by the contaminant sequences, as introgressing Neandertal populations that contributed ancestry to non-Africans were more closely related to *Vindija 33.19* than to the *Altai Neandertal* (*20*). We therefore estimated how many of the alleles shared with *Vindija 33.19* could come from Neandertal haplotypes present in the modern human contaminant. Among the 3,756 and 2,836 sites that are covered by sequences from *Scladina I-4A* and are derived in the *Vindija 33.19* and *Altai Neandertal* genomes, respectively, with a contamination rate per base pair of 64.8% for *Scladina I-4A* (63.0-66.7%, estimates in **table S32**), we expect 2,434 (2,366-2,505) and 1,838 (1,787-1,892) alleles from contaminant sequences. Given that a present-day European would carry the *Vindija 33.19* allele and the *Altai Neandertal* allele at 3.77% and 3.68% of these positions, respectively (as computed using genotypes from a French genome, HGDP00521 (*19*)), we expect the contaminant to contribute 92 (89-94) and 68 (66-70) derived alleles that are shared uniquely with the *Vindija 33.19* genome or the *Altai Neandertal* genome, respectively. This expected excess of 24 alleles matching the *Vindija 33.19* genome over the *Altai Neandertal* genome represents only 20% of the observed difference (*Scladina I-4A* shares 122 more alleles with

*Vindija 33.19* than with the *Altai Neandertal* genome). This suggests that contamination is not sufficient to explain the higher sharing of alleles observed between *Scladina I-4A* and *Vindija 33.19* and that *Scladina I-4A* is truly more closely related to *Vindija 33.19* than to the *Altai Neandertal*.

## *Excess of ancestral alleles in the original alignments*

*HST* and *Scladina I-4A* belonged to a population more closely related to *Vindija 33.19* than to the *Altai Neandertal*. Assuming that their ancestors did not receive gene flow from other sources, predictions can be made about the frequency with which derived alleles are shared among these Neandertal genomes. We present in **fig. S17** these expectations:

- We expect more positions in the genomes of *HST* and *Scladina I-4A* to support the topology that is concordant with their population history, i.e. a closer relationship to *Vindija 33.19* than to the *Altai Neandertal*.
- Positions that support the two other possible topologies are the result of "incomplete lineage sorting", i.e. they represent ancestral polymorphisms that were randomly distributed when the ancestral population split. These should be less represented in the genomes of *HST* and *Scladina I-4A* and should support both discordant topologies equally.

To evaluate the support for the three tree topologies, we looked at positions where either *Vindija 33.19* or the *Altai Neandertal* or both carry a derived allele that is absent from the genomes of an Mbuti, a Denisovan and several great apes (see Materials and Methods). Depending on the allele carried by *HST* or *Scladina I-4A* at these positions, we then identified the ones that are informative about the underlying tree topology (see **fig. S17** for the corresponding allelic configurations). When multiple sequences from *HST* or *Scladina I-4A* covered the same position, we chose one sequence randomly.

Contrary to the predictions, the most supported tree topology is the one where *HST* and *Scladina I-4A* represent outgroups, with an overrepresentation of positions where *Vindija 33.19* and the *Altai Neandertal* share a derived allele but *HST* or *Scladina I-4A* carry the ancestral allele seen in the Mbuti, Denisovan and several great ape genomes (**table S33**). This discrepancy may either suggest additional ancestry from a divergent population that would have re-introduced ancestral alleles or might be the result of present-day human contamination and technical biases that we describe in the following sections.

## *Effect of present-day human DNA contamination*

Present-day human DNA contamination that persists despite restriction to putatively deaminated sequences is a plausible explanation for observing more ancestral alleles in *HST* and *Scladina I-4A* sequences than expected. We estimated the level of contamination required to make these Neandertals appear ancestral when they are truly more closely related to *Vindija 33.19*. If the *HST* and Scladina Neandertals had split off the *Vindija 33.19* population, one would expect them and the Vindija Neandertal to be equally related to the *Altai Neandertal* (**fig. S17**). We therefore estimated the level of contamination required to make *HST* and *Scladina I-4A* carry more ancestral alleles than *Vindija 33.19* at positions where the *Altai Neandertal* is derived (i.e.

positions with alleles that are not observed in the genomes of an African, *Denisova 3* and the four Great Apes). We observe that *Vindija 33.19* shares 76.3% ($p_e$) of the Altai-derived alleles, while *HST* and *Scladina I-4A* share 71.6% (binomial CI: 70.5-72.6%) and 68.7% (CI: 66.3-71.1%) of the Altai-derived alleles ($p$), respectively. Modern human contamination would add alleles that are derived only at 9.1% of the sites ($p_c$) where the *Altai Neandertal* carries a derived variant (according to the observed sharing between a European genome, HGDP00521, and the *Altai Neandertal* genome). By solving the equation $c \times p_c + (1 - c) \times p_e = p$, with $c$ being the contamination rate, one can then estimate the contamination required to account for the observed number of ancestral alleles in *HST* and *Scladina I-4A* sequences. We estimated that the lower sharing of Altai-like alleles of *HST* and *Scladina I-4A* compared to *Vindija 33.19* would translate into 7.0 and 11.3% of contamination (95% binomial CI: 5.5-8.6% and 7.8-14.9%) that would be required to explain these results. These estimates are much higher than the present-day human DNA contamination estimates of 2.0% [1.2-2.9%] and 5.5% [3.5-7.9%] reported in Supplementary Note 8 based on the allele sharing with a Mbuti individual, suggesting that the level of present-day human contamination alone is not sufficient to explain the excess of ancestral alleles seen for both *Scladina I-4A* and *HST*.

## *Effect of sequencing errors*

Sequencing errors could also lead to an excess of ancestral alleles by changing bases at many positions where all Neandertals are derived (for instance, about 445,000 positions are shared derived between *Vindija 33.19* and the *Altai Neandertal* but absent from the Mbuti and Denisovan genomes). To test whether errors can account for the remaining ancestral alleles that cannot be explained by present-day human DNA contamination, we first determined the expected sharing of derived alleles with the *Altai Neandertal* assuming contamination levels of 2.0 and 5.5% for *HST* and *Scladina I-4A* (Supplementary Note 8), respectively, and assuming that both diverged from the *Vindija 33.19* population after the split from the *Altai Neandertal* population. As mentioned above, *Vindija 33.19* shares 76.3% of the derived alleles seen in the *Altai Neandertal* genome, while a present-day European individual shares 9.1%. The expected extent of sharing derived alleles with the *Altai Neandertal* genome for the *HST* data including contamination is thus $0.02 \times 0.091 + (1 - 0.02) \times 0.763 \approx 0.749$, and 0.725 for *Scladina I-4A*. When compared to the observed allele sharing with the *Altai Neandertal* (71.6 and 68.7% for *HST* and *Scladina I-4A*), there remains an excess of ancestral alleles of 3.3 and 3.8% (229 and 57 erroneous ancestral variants over erroneous derived variants for *HST* and *Scladina I-4A*, respectively, out of 6,927 and 1,500 positions). Since more alleles that are shared are derived rather than ancestral, errors would be expected to increase the proportion of ancestral alleles as long as errors leading to ancestral variants are equally probable as errors leading to derived variants. If errors were to explain the remaining 3.3% excess of ancestral alleles in *HST*, the error rate $e$ should be equal to 6.6% (calculated from $0.749 \times e - (1 - 0.749) \times e = 0.033$)), and 8.4% for *Scladina I-4A*. These estimates are higher than the error rates of less than 1% typically observed with Illumina sequencing (*90, 91*). A contribution of substitutions due to ancient DNA damage to these error rates can be ruled out since these C-to-T substitutions were removed from the analysis by using a filter based on the alignment orientation (see Material and Methods). Thus, the ancestral placement of both *HST* and *Scladina I-4A* could not be explained by a combination of sequencing error and present-day human DNA contamination.

## *Effect of the reference bias*

An alignment bias to the reference genome (*92, 93*) could represent a potential explanation for the excess of ancestral alleles we observe in *HST* and *Scladina I-4A* sequences at sites that are derived in other Neandertal genomes. Neandertal sequences that carry non-reference alleles are less likely to align to the human reference genome, making the Neandertal appear more often ancestral. Since the human reference genome often carries the ancestral allele at positions where Neandertals carry a derived allele, a sequenced fragment with the derived allele will contain an additional mismatch to the reference when compared to a fragment carrying the ancestral allele. Further, we restrict analyses to sequences carrying signs of cytosine deamination on at least one of their terminal bases, which implies at least one additional mismatch to the human reference. The alignment criteria applied here allow for up to three mismatches in the sequences of length of 30 to 42bp. We note that aligning such short damaged sequences to a reference with higher divergence is expected to exacerbate the bias towards ancestral alleles; when aligning to the chimpanzee genome (panTro4) we find that *HST* sequences show even more ancestral alleles compared to the alignments to the human reference genome (**table S34**).

Compared to *Vindija 33.19*, the low-coverage genomes of five late Neandertals (*6*) also exhibit a significant excess of ancestral alleles in their human alignments, from 0.72% to 3.24%, at sites derived in the *Altai Neandertal* (**table S35**). These Neandertals were shown to be descendants of the same ancestral population that split from the *Altai Neandertal* population 130-145kya and should therefore all exhibit the same genetic relationship to the *Altai Neandertal* (*6*). The observed increase of ancestral alleles after filtering for sequences that exhibit terminal C-to-T substitutions allows us to exclude present-day human DNA contamination as a plausible explanation and supports the presence of a reference bias (**table S35**). The additional observation that *Vindija 87* shares less alleles with the *Altai Neandertal* than *Vindija 33.19* does (**table S35**), although both Vindija specimens were shown to come from the same individual (*6*), confirmed that our observations are the result of a technical issue.

Allowing more mismatches when aligning the sequences would be a straightforward solution to limit the effects of a reference bias but may also increase spurious alignments of microbial sequences. We therefore relied on a different strategy that consists of aligning the sequences to two reference genomes: the original human reference genome and a modified version of this genome that includes Neandertal alleles ("Neandertalized" reference, see Material and Methods for details). Thus, sequences are given the same chance to align, regardless of the carried allele.

We tested the effects of this alignment procedure on two late Neandertals, *Vindija 87* and *Goyet Q56-1*. We chose *Vindija 87* because *Vindija 33.19* is a high-coverage version of the same genome, and *Goyet Q56-1* because it showed the lowest excess of ancestral alleles and we expect minor differences between the two alignment strategies. For convenience, we only used sequences from one library for each Neandertal (A9228 for *Vindija 87*, and A9349 for *Goyet Q56-1*), which nonetheless represent 7-10x more sequences than the *HST* dataset. We processed these libraries following the same steps applied to *HST* and *Scladina I-4A* (mapping quality $\geqslant$ 25, length $\geqslant$ 30, alignments in the mappability track, C-to-T substitutions in the last three positions of either ends). By aligning to the Neandertalized reference, the allele sharing with the *Altai Neandertal* for both Neandertals increased to match the observed allele sharing of *Vindija 33.19* with the *Altai Neandertal*, increasing by 2.8% for *Vindija 87* and by 1.0% for *Goyet Q56-1* (**table S36**). This correction of the allele sharing for these two Neandertals supports our

hypothesis that a reference bias was responsible for the previously observed excess of ancestral alleles.

We further tested the effect of the alignments by computing the proportion of alternative alleles in the genome of *Vindija 87* at positions where the high-coverage *Vindija 33.19* genome is heterozygous (**table S37**). Given that both genomes originate from the same individual (*6*), *Vindija 87* should carry the alternative allele at 50% of these positions. We found that *Vindija 87* carried the alternative allele at 48.79% of the heterozygous positions compared to only 42.62% in the original alignments, demonstrating again an improvement over standard alignments to hg19.

We also looked at positions that are homozygous different in the *Vindija 33.19* and the *Altai Neandertal* genomes and estimated the proportion of these sites where *Vindija 87* carries the allele seen in the *Altai Neandertal* genome, which should represent sequencing errors or misalignments (**table S38**). We compared the error rate from the original alignments to the modified alignments, separating the cases when the alternative allele introduced in the reference was the *Altai Neandertal* allele or the *Vindija 33.19* allele (**table S38**). When the alternative allele in the Neandertalized reference was from *Vindija 33.19*, the modified alignment strategy allowed us to recover sequences carrying that allele at 4,300 additional sites in the *Vindija 87* genome without introducing more errors (in fact, there were 3 errors less). At positions where *Vindija 33.19* is homozygous for the allele seen in hg19 but the *Altai Neandertal* is homozygous for an alternative allele, introducing the alternative allele in the reference genome lead to an increase of errors (140 more errors among 20,538 sites), still below 1% and lower than the error rate seen with the original alignments at positions where *Vindija 33.19* is homozygous for an alternative allele (**table S38**). We conclude that aligning to the two references introduces a few more errors at sites where the studied Neandertal carries the original reference allele, an observation that is marginal compared to the overall gain in accuracy at other positions.

We therefore carried on with this modified alignment strategy and applied it to *HST* and *Scladina I-4A* sequences (see **table S39** for a summary of the sequences that align to these references). The allele sharing with the *Altai Neandertal* increased to 74.73% and 71.58% for *HST* and *Scladina I-4A*, respectively, much closer to the sharing of *Vindija 33.19* with the *Altai Neandertal* (76.3%) (**table S40**) (see also the higher sharing of derived alleles with *Vindija 33.19* in **fig. S18**). This result does not change if we focus on longer sequences (at least 35bp, **table S40**).

Finally, we estimated the level of contamination required to make *HST* and *Scladina I-4A* carry more ancestral alleles than *Vindija 33.19* at positions where the *Altai Neandertal* is derived. As described above, solving equation $c \times p_c + (1 - c) \times p_e = p$, we estimated that 2.3% (CI: 0.9-3.8%) and 7.0% (3.9-10.3%) contamination would be sufficient to account for the lower allele sharing of *HST* and *Scladina I-4A* (74.58% and 71.58%, respectively) than expected for a Neandertal from the Vindija population (76.3%). These estimates are now compatible with our observed contamination estimates (2.0% [1.2-2.9%] and 5.5% [3.5-7.9%] reported in Supplementary Note 8). We conclude that the excess of ancestral alleles observed in *HST* and *Scladina I-4A* sequences can be explained by the combination of reference bias and present-day human contamination.

## *Tree support correction*

To illustrate the effect of confounding biases, in **Fig. 2** of the main text, we presented corrected counts of positions that support the different tree topologies relating *Vindija 33.19*, the *Altai Neandertal* and *HST* or *Scladina I-4A*. To correct for the effect of the reference bias, we computed the tree support from the re-aligned sequences as described above. We then applied a correction to remove the contribution of present-day human DNA to these observed counts. We describe here this correction and show results for the full datasets including sequences without signs of ancient DNA damage.

At the positions informative about the underlying tree topologies (see number of positions covered in **table S41**), sequences from the *HST* or *Scladina I-4A* datasets come either from the Neandertal genome or from present-day human DNA contamination, following the proportion estimated in Supplementary Note 8 (we used here the contamination estimates based on the relationship with an Mbuti genome, **table S32**). Any Eurasian living today will carry the derived allele seen only in the *Altai Neandertal* genome, only in the *Vindija 33.19* genome, or in both, at 3.68%, 3.77% and 10.80% of the positions, respectively, as computed using genotypes from a French genome (HGDP00521 (*19*); sampling a random allele at heterozygous positions). For a Han Chinese genome (HGDP00775 (*8*)), these numbers are 3.77%, 3.83% and 10.70%. We are therefore able to estimate how many of the contaminant sequences carry the derived or ancestral alleles, which we can use to correct the counts supporting each tree topology. For instance, there are 5,817 positions covered by deaminated sequences from the *HST* dataset where both *Vindija 33.19* and the *Altai Neandertal* carry a derived allele. Assuming a contamination of 2.0% for the *HST* deaminated sequences (Supplementary Note 8), we expect to see the contaminant sequences at 116 positions, among which 89.2% will carry the ancestral allele (as 10.8% will carry the derived allele). Therefore, among the 655 positions where both *Vindija 33.19* and the *Altai Neandertal* carry a derived allele absent from *HST*, supporting an ancestral placement of *HST*, we expect that 104 ancestral alleles come from contaminant sequences and 551 from the Neandertal sequences. We report in **table S42** these corrected counts for both *HST* and *Scladina I-4A*, using either the sequences with signs of ancient DNA damage or all sequences. Consistent with observations from the previous section, in all datasets, the most supported tree topology suggests a closer relationship to the Vindija Neandertal. Interestingly, the *HST* dataset including all sequences is the only dataset that does not exhibit equal support for the two alternative topologies, as expected if *HST* and *Scladina I-4A* are early representatives of the Vindija Neandertal population and did not receive gene flow from other sources. Assuming a contamination of 22.9% (CI: 22.1-23.8%; **table S32**), the full dataset of *HST* still exhibits a higher support for the tree where *HST* is an out-group to both *Vindija 33.19* and *Altai Neandertal* compared to the tree where *HST* is closer to the *Altai Neandertal* (1,690 vs. 1,388 positions; two-sided binomial test p-value $< 10^{-7}$; see **table S42**). This result holds true if we use the upper contamination estimate to correct the counts: using a contamination of 23.8%, the difference in support becomes 1546 vs. 1386 positions (two-sided binomial test p-value = 0.003). Although, this result seems unaffected to the contamination estimate uncertainty, we note that the corrected counts for the two topologies match a contamination estimate of 24.6%. Given that *HST* has a deeply divergent mitochondrial DNA, it is tempting to speculate that this excess of ancestral alleles reflects some ancestry from a divergent population, but we do not see this signal in the smaller but less contaminated set of deaminated sequences. The high level of contamination and

the low amount of sequences currently available preclude a definitive conclusion regarding this observation.

## *Effective number of independent positions*

Given that only a few megabases of the nuclear genomes of *HST* and *Scladina I-4A* are available, we assumed independence between the positions that support the different tree topologies relating *Vindija 33.19*, the *Altai Neandertal* and *HST* or *Scladina I-4A*. Here we test the validity of this assumption. We present in **tables S43** and **S44** summary statistics about the distance between informative positions covered by all sequences or deaminated sequences for *HST* and *Scladina I-4A*, respectively. We also estimated the effective number of independent positions that support a closer relationship to *Vindija 33.19*, the *Altai Neandertal* or an ancestral relationship to both. To achieve this, we estimated the probability that at least one recombination happened between two consecutive informative positions and computed the expected number of independent pairs of positions (**table S45**).

We first assumed that recombination events follow a Poisson process, so that the distance from one position to the next recombination follows an exponential distribution with parameter $L^{-1}$, L being the expected length between two recombination events. Therefore, the probability that a recombination event happened between two positions is $1 - e^{\frac{d}{L}}$, with *d* the physical distance (bp) between the positions. For simplicity, we assume that the population sizes (Ne) and the generation time are constant (Ne=2,000 and a generation is 29 years). We made the computation for two scenarios: *HST*/*Scladina I-4A* are either dated to 100kya (t = 3,448 generations ago) and direct ancestors of the *Vindija 33.19* population, or dated to 140kya (t = 4,828 generations ago) at the time of the population split between the *Vindija 33.19* and the *Altai Neandertal* populations ($t_{anc}$= 4,828 generations ago). In both scenarios, *Vindija 33.19* and the *Altai Neandertal* are dated to 50,000kya ($t_v$ = 1,724 generations ago) and 120,000kya ($t_a$ = 4,138 generations ago), respectively.

The expected length of the three types of regions (closer to the *Altai Neandertal*, to *Vindija 33.19* or ancestral to both) depends on the cumulative branch length (in generations) of the two lineages involved in the first coalescence and the recombination rate per base pair per generation. If the first coalescence involves *HST*/*Scladina I-4A* and the *Altai Neandertal*, this expected branch length is $t_{anc} - t + \frac{2}{3}Ne + t_{anc} - t_a + \frac{2}{3}Ne$ with $\frac{2}{3}Ne$ the expected time to the first coalescence for a sample of three lineages (*94*). If *HST*/*Scladina I-4A* are ancestral to both the *Altai Neandertal* and *Vindija 33.19*, i.e. the *Altai Neandertal* and *Vindija 33.19* coalesce first; the expected branch length is then $t_{anc} - t_v + \frac{2}{3}Ne + t_{anc} - t_a + \frac{2}{3}Ne$. For the last type of region, when the first coalescence involves *HST*/*Scladina I-4A* and *Vindija 33.19*, in the scenario when *HST*/*Scladina I-4A* are dated to the split between the populations of *Vindija 33.19* and the *Altai Neandertal*, we can replace $t_a$ by *t* in the previous formula. Whereas, in the other scenario, the coalescence can either happen during the shared ancestral population of *HST*/*Scladina I-4A* and *Vindija 33.19* between $t_{anc}$ and *t* with probability $1 - e^{\frac{-(t_{anc}-t)}{2Ne}}$ or in the shared population by all three Neandertals with probability $e^{\frac{-(t_{anc}-t)}{2Ne}}$. In the first case, the expected branch length is $t - t_v + 2 \times \left( 2Ne - \frac{(t_{anc}-t)e^{\frac{-(t_{anc}-t)}{2Ne}}}{1-e^{\frac{-(t_{anc}-t)}{2Ne}}} \right)$ and the second case it is again $t_{anc} - t_v + \frac{2}{3}Ne + t_{anc} - t + \frac{2}{3}Ne$. To get

the expected length of the regions, we then multiplied these expected branch lengths by the average recombination rate of $1.2 \times 10^{-8}$ Morgan/bp.

For both deaminated sequences and all sequences, we estimated that more than 98% and 94% of the positions are independent, respectively (**table S45**). Less than 11 positions are expected to be linked for the analysis using deaminated sequences. The set of positions supporting an ancestral relationship of *HST*/*Scladina I-4A* to both the *Altai Neandertal* and *Vindija 33.19* for all sequences is the only set with a larger number of linked positions (248 positions among 5,796 for *HST* and 229 positions among 5,714 for *Scladina I-4A*), where a large proportion of the data represents present-day human DNA contamination. We assumed a haploid genome but, in reality, alleles could come from two chromosomes or even the contaminant genome, therefore the expected number of independent pairs represent conservative estimates. We concluded that the sequences are distributed sparsely enough in the genome so that positions can be considered independent regarding our interpretation that *HST* and *Scladina I-4A* are more closely related to *Vindija 33.19* than to the *Altai Neandertal*. For the estimates of population split time (Supplementary Note 10), we however opted for a block jackknife resampling approach to take into account the uncertainty associated with a potential linkage of the positions analyzed.

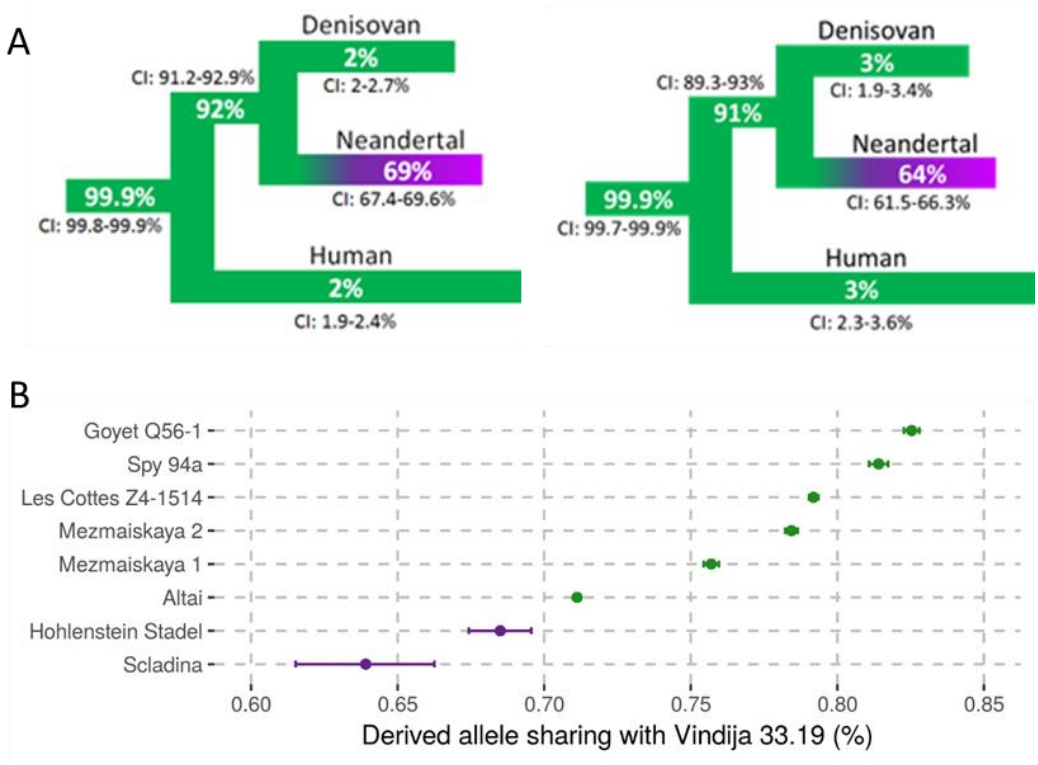


**Fig. S16. Lineage assignment before correcting for the reference bias** (A) using deaminated fragments from *HST* (left) and *Scladina I-4A* (right) (the Neandertal used as reference is *Vindija 33.19*) and (B) in comparison to other Neandertals in terms of allele sharing with *Vindija 33.19*. 95% binomial confidence intervals are shown. See **fig. S18** for the lineage assignment corrected for the reference bias.

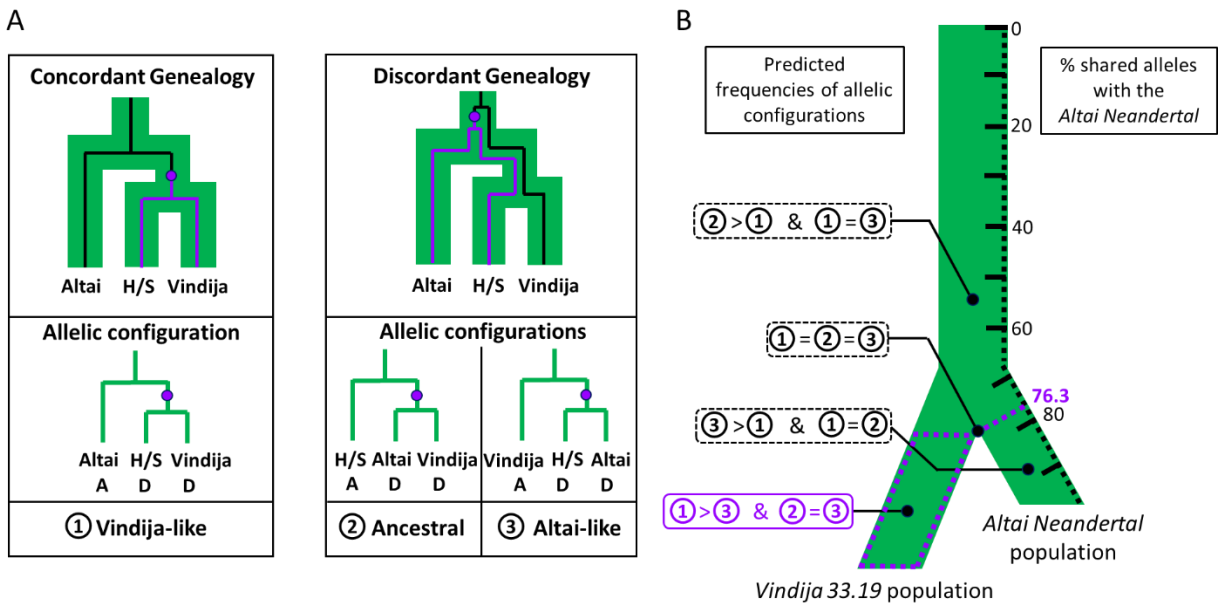


**Fig. S17. Expectations for the genetic relationship of *HST* and *Scladina I-4A* to *Vindija 33.19* and the Altai Neandertal.** (A) Three possible tree topologies relating these Neandertals (H/S for *HST* or *Scladina I-4A*) with corresponding allelic configurations that are informative about the underlying topology (A: ancestral; D: derived). Allelic configuration 1 ("Vindija-like") is concordant with the population relationship while the two other allelic configurations (2 "Ancestral" and 3 "Altai-like") are discordant. Discordance only occurs if lineages find a common ancestor in the ancestral population of all three Neandertals (see schematic on top), when the three topologies are then equally likely. Informative mutations (purple dots) arise in the branch between the two common ancestors. (B) Predictions of allele sharing depending on the placement of a Neandertal along the branches leading to the *Vindija 33.19* and *Altai Neandertal* populations. Different hypothetical origins are represented by black dots. Numbers in the boxes correspond to the allelic configurations depicted in (A) and the purple box with solid lines represents the prediction for *HST* and *Scladina I-4A*. The scale on the right side represents the expected proportion of derived alleles shared with the *Altai Neandertal* for different splits from that branch. The expected allele sharing for a Neandertal belonging to the *Vindija 33.19* population is 76.3% (part highlighted by the purple dashed lines).

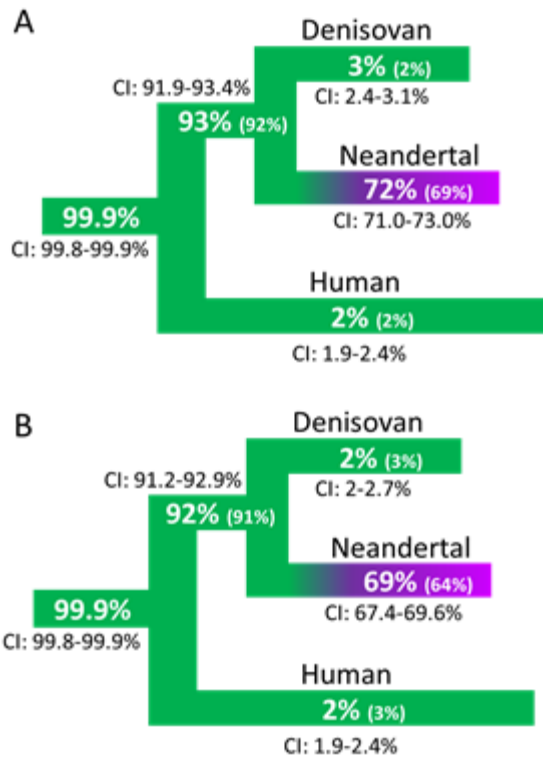


**Fig. S18. Lineage assignment after correcting for the reference bias.** We used sequences with signs of potential terminal deamination from *HST* (A) and *Scladina I-4A* (B). As in **Figure S16**, the percentage for the Neandertal branch corresponds to the derived allele sharing with *Vindija 33.19*. Binomial 95% confidence intervals (CI) are presented next to the corresponding branches. Percentages in parentheses show results before correcting for reference bias. The terminal branch with the highest support is highlighted in purple.

**Table S33. Genome-wide counts of the three possible allelic configurations informative about the underlying topologies relating *Vindija 33.19* and the Altai Neandertal to *HST* and *Scladina I-4A* before correcting for reference bias or contamination (see tables S40 and S41 for corrected results and fig. S17 for a description of these allelic configurations).** Numbers in parentheses correspond to the total number of positions covered (for instance, for the Vindija-like category, all covered positions where *Vindija 33.19* is derived but the *Altai Neandertal* is ancestral). If a position was covered by multiple sequences, each allele was counted only once.

| Neandertal | Dataset | Vindija-like | Ancestral | Altai-like |
|---|---|---|---|---|
| *HST* | Deaminated | 531 (2,172) | 647 (5,074) | 466 (1,757) |
| *HST* | All sequences | 1,676 (8,046) | 5,797 (19,033) | 1,326 (6,175) |
| *Scladina I-4A* | Deaminated | 110 (504) | 191 (1,109) | 106 (382) |
| *Scladina I-4A* | All sequences | 443 (3,638) | 5,708 (9,065) | 321 (2,761) |

**Table S34. Comparison of alignments to hg19 and panTro4.** The reported proportion of derived alleles was computed at sites where both *Vindija 33.19* and the *Altai Neandertal* genomes share a derived allele that is ancestral in the genomes of an Mbuti (HGDP00456) and a Denisovan (*Denisova 3*).

| | **hg19** | **panTro4** |
|---|---|---|
| **Number of mapped sequences (L5386):** | 1,832,672 | 1,336,163 |
| **Proportion of sequences with the derived allele [95% binomial CI]:** | 72% [70.6-72.7%] | 67% [65.5-68.2%] |

**Table S35. Excess of ancestral alleles in Late Neandertals compared to *Vindija 33.19* at sites that are derived in the Altai Neandertal genome but ancestral in the genomes of an Mbuti and a Denisovan.** The expected derived allele sharing at these sites for a Neandertal from the Vindija population is 76.3%. Deaminated sequences correspond to sequences with a C-to-T substitution at the last position of either end. Note that *Vindija 87* is the same individual as *Vindija 33.19*. With the exception of *Spy 94a*, the increase of ancestral alleles in the damage-restricted data would be compatible with a reference bias due to too many mismatches to the reference genome. The decrease of ancestral alleles in the damage-restricted data of *Spy 94a* potentially represents the removal of present-day human contamination (which is highest in this sample, with estimates varying from 1.75% to 4.1%, (*6*)).

| Neandertal | Sequences | Number of Derived alleles | Number of Ancestral alleles | Proportion of Derived alleles (%) | Excess of Ancestral alleles (%) [95% binomial CI] |
|---|---|---|---|---|---|
| *Goyet Q56-1* | All | 345,684 | 457,425 | 75.57 | **0.72 [0.60-0.85]** |
| *Goyet Q56-1* | Deaminated | 41,297 | 54,672 | 75.54 | **0.76 [0.40-1.13]** |
| *Les Cottés Z4-1514* | All | 395,217 | 527,824 | 74.88 | **1.42 [1.31-1.54]** |
| *Les Cottés Z4-1514* | Deaminated | 128,934 | 173,939 | 74.13 | **2.17 [1.97-2.38]** |
| *Spy 94a* | All | 143,022 | 195,755 | 73.06 | **3.24 [3.04-3.44]** |
| *Spy 94a* | Deaminated | 29,389 | 39,447 | 74.50 | **1.80 [1.37-2.23]** |
| *Mezmaiskaya 2* | All | 258,458 | 346,466 | 74.60 | **1.70 [1.56-1.85]** |
| *Mezmaiskaya 2* | Deaminated | 75,342 | 102,706 | 73.36 | **2.94 [2.67-3.21]** |
| *Vindija 87* | All | 185,698 | 250,186 | 74.22 | **2.08 [1.90-2.25]** |
| *Vindija 87* | Deaminated | 65,990 | 89,540 | 73.70 | **2.60 [2.31-2.89]** |

**Table S36. Effect of the modified alignment procedure on the allele sharing with the Altai Neandertal.** Sites considered are derived in the *Altai Neandertal* but ancestral in a Mbuti (HGDP00456, (*19*)) and *Denisova 3*. We only report results for sequences with terminal C-to-T substitutions within the last 3 bp of either ends. (*) These were calculated in the previous section (Effect of sequencing errors) and represent the expected allele sharing with the *Altai Neandertal* given the estimated level of contamination if these Neandertals belonged to the Vindija population (Supplementary Note 8).

| | Derived allele sharing with the Altai Neandertal (%) | | |
|---|---|---|---|
| **Neandertal (library)** | **Original (hg19)** | **Modified** | **Expected** |
| *Vindija 87* (A9228) | 73.70 [73.41-73.99] | 76.51 [76.25-76.77] | 76.3 |
| *Goyet Q56-1* (A9349) | 75.54 [75.17-75.90] | 76.53 [76.04-77.02] | 76.3 |
| *HST* (All) | 71.58 [70.50-72.64] | 74.73 [73.75-75.69] | 74.9**(*)** |
| *Scladina I-4A* (All) | 68.73 [66.32-71.07] | 71.58 [69.38-73.70] | 72.5**(*)** |

**Table S37. Alleles seen in *Vindija 87* at positions that are heterozygous in *Vindija 33.19*.**

| Alignment procedure | N° of sites with the hg19 allele | N° of sites with the alternative allele | Proportion of sites with the alternative allele (%) [binomial CI] |
|---|---|---|---|
| Original (hg19) | 31,037 | 23,053 | 42.62 [42.20-43.04] |
| Modified | 30,892 | 29,428 | 48.79 [48.39-49.19] |

**Table S38. Sequencing and alignment errors of *Vindija 87* sequences at positions where *Vindija 33.19* is homozygous different from the Altai Neandertal, comparing the original alignments to hg19 with our modified alignment procedure.** We only used sequences with terminal C-to-T substitutions (at the last 3 positions of either ends) and in the sequenced orientation that do not lead to ambiguities from deaminations (forward sequences if one allele is a G, reverse if one allele is a C). We only used sequences from one arbitrarily chosen library from the *Vindija 87* dataset (A9228).

| Alignment procedure | Neandertal with the alternative allele | N° of sites with the *Vindija 33.19* allele | N° of sites with the *Altai Neandertal* allele | Error rate (%) |
|---|---|---|---|---|
| Original (hg19) | *Altai Neandertal* | 20,367 | 58 | 0.28 [0.22-0.37] |
| Original (hg19) | *Vindija 33.19* | 20,452 | 253 | 1.22 [1.08-1.38] |
| Modified | *Altai Neandertal* | 20,340 | 198 | 0.96 [0.83-1.11] |
| Modified | *Vindija 33.19* | 24,752 | 250 | 1.00 [0.88-1.13] |

**Table S39. Summary of the alignments to the two references.** (*) These alignments were excluded. In the parentheses, we report the number of sequences that overlap sites that differ between the two reference genomes.

| Neandertal: | *HST* | *Scladina I-4A* |
|---|---|---|
| Alignments specific to the original reference (hg19): | 6,809 (6,119) | 4,719 (4,272) |
| Alignments specific to the "Neandertalized" reference: | 18,783 (18,495) | 9,804 (9,530) |
| Alignments to both references at the same position: | 5,001,750 (267,141) | 1,980,901 (121,597) |
| Alignments to both references at different positions(*): | 522(*) | 332(*) |

**Table S40. Applying different sequence lengths cutoffs does not affect the allele sharing with the Altai Neandertal after realignments.** We only report results from sequences with C-to-T substitutions in the last three positions of either end. The derived allele sharing is computed from *HST* and *Scladina I-4A* sequences overlapping sites that are derived in the *Altai Neandertal* but ancestral in an Mbuti and a Denisovan genome.

| | Derived allele sharing with the Altai Neandertal (%) | |
|---|---|---|
| **Neandertal** | **Sequences longer than 29bp** | **Sequences longer than 34bp** |
| *HST* | 74.73 [73.75-75.69] | 74.64 [73.54-75.73] |
| Scladina | 71.58 [69.38-73.70] | 71.44 [68.92-73.86] |

**Table S41. Genome-wide counts of the three possible allelic configurations informative about the underlying topologies relating *Vindija 33.19* and the Altai Neandertal to *HST* and *Scladina I-4A* after correcting for reference bias (see table S33 to compare with uncorrected results and table S42 for results corrected for contamination).** Numbers in parentheses correspond to the total number of positions covered (i.e. all covered positions where *Vindija 33.19* is derived but the *Altai Neandertal* is ancestral for the Vindija-like category for instance). If a position was covered by multiple sequences, each allele was counted only once.

| Neandertal | Dataset | Vindija-like | Ancestral | Altai-like |
|---|---|---|---|---|
| *HST* | Deaminated | 640 (2,282) | 655 (5,871) | 544 (1,839) |
| *HST* | All sequences | 1,847 (8,215) | 5,796 (20,103) | 1,441 (6,286) |
| *Scladina I-4A* | Deaminated | 156 (561) | 200 (1,285) | 127 (412) |
| *Scladina I-4A* | All sequences | 527 (3,730) | 5,714 (9,377) | 370 (2,810) |

**Table S42. Counts of the three possible allelic configurations informative about the underlying topologies relating *Vindija 33.19* and the Altai Neandertal to *HST* and *Scladina I-4A* after correcting for both reference bias and contamination.** Labelling as in **Table S41**.

| Neandertal | Dataset | Vindija-like | Ancestral | Altai-like |
|---|---|---|---|---|
| *HST* | Deaminated | 638 [637.5-639.0] | 550 [503.1-592.2] | 542 [542.0-543.2] |
| *HST* | All sequences | 1,776 [1,773-1,778] | 1,690 [1,528-1,833] | 1,388 [1,386-1,390] |
| *Scladina I-4A* | Deaminated | 155 [154.3-155.3] | 137 [109.5-159.9] | 126 [125.8-126.5] |
| *Scladina I-4A* | All sequences | 436 [433-438] | 294 [135-444] | 303 [301-305] |

**Table S43. Summary statistics about the physical distance between the positions used to infer the genetic relationship of *HST* to *Vindija 33.19* and the Altai Neandertal.**

| | All sequences | | | Deaminated sequences | | |
|---|---|---|---|---|---|---|
| | Vindija-like | Altai-like | Ancestral | Vindija-like | Altai-like | Ancestral |
| Average distance | 1,568,792 | 1,996,011 | 504,298 | 4,454,862 | 5,160,985 | 4,363,011 |
| 20-quantiles of distances: | | | | | | |
| 0 | 15 | 1 | 7 | 458 | 1,047 | 1,170 |
| 0.05 | 13,039 | 22,084 | 14,522 | 55,893 | 75,681 | 106,425 |
| 0.1 | 35,951 | 56,760 | 35,231 | 200,390 | 262,248 | 279,397 |
| 0.15 | 87,115 | 119,150 | 56,523 | 448,933 | 451,285 | 468,314 |
| 0.2 | 154,980 | 239,214 | 80,530 | 616,738 | 821,242 | 740,546 |
| 0.25 | 240,749 | 333,141 | 108,519 | 900,094 | 1,202,169 | 992,476 |
| 0.3 | 332,768 | 442,923 | 137,042 | 1,093,443 | 1,455,684 | 1,257,041 |
| 0.35 | 437,853 | 577,382 | 170,564 | 1,442,208 | 1,752,452 | 1,632,141 |
| 0.4 | 548,996 | 714,705 | 209,305 | 1,869,600 | 2,243,409 | 1,881,212 |
| 0.45 | 674,240 | 891,524 | 250,582 | 2,303,518 | 2,594,063 | 2,212,799 |
| 0.5 | 839,956 | 1,091,555 | 298,623 | 2,721,979 | 2,989,633 | 2,668,333 |
| 0.55 | 995,609 | 1,303,375 | 347,098 | 3,199,279 | 3,554,897 | 3,203,832 |
| 0.6 | 1,207,529 | 1,577,564 | 402,367 | 3,605,501 | 4,178,927 | 3,739,015 |
| 0.65 | 1,426,188 | 1,916,022 | 467,059 | 4,049,940 | 4,909,830 | 4,215,989 |
| 0.7 | 1,656,088 | 2,194,764 | 538,777 | 4,799,721 | 5,661,841 | 4,705,388 |
| 0.75 | 2,035,196 | 2,612,077 | 635,285 | 5,496,434 | 6,772,027 | 5,688,294 |
| 0.8 | 2,399,100 | 3,107,225 | 750,497 | 6,789,838 | 8,141,534 | 6,630,632 |
| 0.85 | 3,003,852 | 3,775,844 | 919,022 | 8,611,851 | 9,738,578 | 8,075,378 |
| 0.9 | 3,870,805 | 4,917,755 | 1,167,914 | 10,846,444 | 12,498,740 | 9,486,136 |
| 0.95 | 5,379,118 | 6,769,614 | 1,661,184 | 15,022,930 | 17,057,069 | 12,623,052 |
| 1 | 38,054,416 | 38,155,847 | 32,337,366 | 44,069,378 | 55,574,824 | 81,410,948 |

**Table S44. Summary statistics about the physical distance between the positions used to infer the genetic relationship of *Scladina I-4A* to *Vindija 33.19* and the Altai Neandertal.**

| | All sequences | | | Deaminated sequences | | |
|---|---|---|---|---|---|---|
| | Vindija-like | Altai-like | Ancestral | Vindija-like | Altai-like | Ancestral |
| Average distance | 5,381,676 | 7,188,825 | 512,308 | 16,962,339 | 18,503,653 | 13,085,932 |
| 20-quantiles of distances: | | | | | | |
| 0 | 21 | 3,216 | 4 | 28,142 | 18,902 | 18,394 |
| 0.05 | 118,664 | 157,189 | 15,429 | 1,150,006 | 421,255 | 600,766 |
| 0.1 | 295,512 | 444,638 | 34,916 | 2,305,475 | 1,086,023 | 1,502,231 |
| 0.15 | 562,303 | 730,940 | 58,187 | 2,711,318 | 1,616,857 | 2,298,019 |
| 0.2 | 856,342 | 1,040,636 | 83,363 | 3,822,368 | 2,239,792 | 2,630,257 |
| 0.25 | 1,148,826 | 1,438,775 | 111,370 | 4,429,599 | 3,107,699 | 3,389,747 |
| 0.3 | 1,517,232 | 2,054,528 | 141,204 | 5,203,809 | 4,060,297 | 4,264,188 |
| 0.35 | 1,815,090 | 2,597,449 | 171,685 | 6,091,760 | 6,169,289 | 5,316,830 |
| 0.4 | 2,302,618 | 3,125,824 | 205,929 | 7,109,035 | 9,106,140 | 6,262,976 |
| 0.45 | 2,717,966 | 3,517,815 | 248,647 | 8,380,323 | 10,692,643 | 7,055,834 |
| 0.5 | 3,133,213 | 4,348,687 | 297,272 | 10,275,561 | 11,808,414 | 8,582,481 |
| 0.55 | 3,614,502 | 5,130,699 | 351,877 | 12,293,073 | 14,572,840 | 9,821,383 |
| 0.6 | 4,318,461 | 5,970,119 | 407,710 | 15,185,147 | 15,831,792 | 11,053,461 |
| 0.65 | 5,000,921 | 7,277,023 | 476,287 | 17,272,282 | 18,325,788 | 12,864,726 |
| 0.7 | 6,024,070 | 8,764,044 | 555,533 | 20,306,769 | 19,998,689 | 14,165,080 |
| 0.75 | 6,987,099 | 10,379,561 | 660,470 | 22,420,565 | 23,994,067 | 17,403,424 |
| 0.8 | 8,299,776 | 11,551,749 | 790,161 | 29,016,895 | 28,663,216 | 20,175,681 |
| 0.85 | 10,299,552 | 14,064,224 | 972,481 | 33,390,510 | 32,542,517 | 21,770,233 |
| 0.9 | 13,704,107 | 17,109,285 | 1,196,079 | 43,384,983 | 43,050,312 | 27,959,992 |
| 0.95 | 18,311,356 | 22,554,417 | 1,596,523 | 53,675,673 | 64,545,039 | 36,941,358 |
| 1 | 51,436,265 | 58,420,515 | 33,174,044 | 93,692,234 | 125,288,070 | 111,893,184 |

**Table S45. Effective number of independent positions.** The reported ranges correspond to estimates depending on the population split time of *HST*/*Scladina I-4A* from the *Vindija 33.19* population between 100kya and 140kya.

| | | Altai-like | | Vindija-like | | Ancestral | |
|---|---|---|---|---|---|---|---|
| Neandertal | Dataset | Effective number of independent positions | Total number of positions | Effective number of independent positions | Total number of positions | Effective number of independent positions | Total number of positions |
| HST | All sequences | 1,370-1385 | 1,441 | 1,746-1,755 | 1,847 | 5,548 | 5,796 |
| HST | Deaminated | 534-536 | 544 | 629-630 | 640 | 648 | 655 |
| Scladina I-4A | All sequences | 366-367 | 370 | 518-518 | 527 | 5,485 | 5,714 |
| Scladina I-4A | Deaminated | 121-121 | 127 | 155-155 | 156 | 199 | 200 |

# Note S10. Split time estimates.

## *Estimates under a coalescent divergence model*

Skoglund et al. (*25*) described an approach to estimate population divergence times based on the counts of positions that support the three tree topologies that relate three populations. This approach allowed us to estimate the internode divergence time T (measured in units of effective population size) between the split of the *Altai Neandertal* population from the *Vindija 33.19* population and the split between the *HST* or *Scladina I-4A* population from the *Vindija 33.19* population. A log-likelihood function dependent on T was derived based on the probabilities of topologies that are concordant or discordant with the population history (*95-97*), that we can maximize to compute the maximum likelihood estimate of T. The probabilities of the discordant topologies (the ones that do not support a closer relationship of *HST* or *Scladina I-4A* to *Vindija 33.19*; see counts in Supplementary Note 9, **table S42**) correspond to the probability that *HST* or *Scladina I-4A* do not coalesce with *Vindija 33.19* in the internode population, which happens with probability $e^{-T}$, multiplied by 1/3, as any coalescence happening then in the ancestral population lead to the three topologies with equal probabilities. The probability of the concordant topology is then $1-2e^{-T}/3$ and the log-likelihood is: $log\big(L(T)\big) = G_c \times log\left(1-\frac{2}{3}e^{-T}\right) + G_D \times log\left(\frac{2}{3}e^{-T}\right)$ with $G_c$ and $G_D$ representing the counts of positions supporting the topologies that are concordant and discordant with the population history, respectively. To validate this method, we applied it to five low-coverage Neandertal genomes (**table S46**) for which split times have already been estimated with another method (F(A|B), which we also applied to *HST* and *Scladina I-4A*, as described in the next section).

We then applied this method to the corrected counts presented in Supplementary Note 9, assuming three different constant population sizes (1,500, 2,000 and 2,500 individuals; with 2,000 being closer to the average effective population size estimated with PSMC, (*20*)). We show the corresponding maximum likelihood estimates of T and their approximate 95% confidence intervals in **table S47**. For both *HST* and *Scladina I-4A* we estimate population split times from the *Vindija 33.19* population shortly after the split between the *Altai Neandertal* and *Vindija 33.19* populations (assumed to be 130kya or 145kya), with point estimates varying from 123 to 141kya for *HST* and 109 to 140kya for *Scladina I-4A* depending on the effective population size used. These results suggest that *HST* and *Scladina I-4A* split from the *Vindija 33.19* population shortly after the split with the *Altai Neandertal* population, compatible with the age estimates of these Neandertals (**table S28**).

## *Estimates based on the F(A|B) statistic*

To estimate when the population(s) of *HST* and *Scladina I-4A* split from other modern and archaic populations, we also computed the F(A|B) statistic, which corresponds to the proportion of heterozygous sites in a diploid genome B that share a derived allele with a haploid genome A (*8, 20*). This proportion depends on the relative amount of mutations that were either already present in the common ancestor of population A and B, or specific to population B. The proportion of mutations that are not shared is therefore informative of how long population B has been isolated from population A since the two populations split. This is dependent on the demography of population B, but independent of the demography of population A, making it useful for comparing *HST* and *Scladina I-4A* to high-quality genomes for which the demographic

history was estimated with the Pairwise Sequentially Markov Coalescent (PSMC, (*20*)). Using coalescent simulations of the demographic histories, we can then calibrate the observed F(A|B) values into split time estimates in years before present by using molecular age estimates of the individual from population B ("Branch shortening", **table S48**). The advantage over the previous coalescent model-based method is that we do not assume a constant population size, but rather make use of the estimated variations in population size.

We identified heterozygous sites in four high-coverage genomes (*Denisova 3 (19)*, *Vindija 33.19* (*20*), the *Altai Neandertal* (*8*) and a present-day human from Africa, Mbuti, HGDP00456 (*19*)). Only transversion polymorphisms were considered to avoid recurrent mutations and errors from deamination and the map35_100 filter was applied (*20*). When a position was covered by multiple sequences, only one randomly chosen sequence was retained. Positions with a third allele in the low coverage samples could represent sequencing errors and were filtered out. For computing the F(A|B) values with *Vindija 33.19* or *Altai Neandertal* as individual B while avoiding any reference bias, we used *HST* and *Scladina I-4A* sequences that aligned either to hg19 or its modified version that includes the alleles of *Vindija 33.19* and *Altai Neandertal* (see Supplementary Note 9). To compute confidence intervals, we used a block jackknife resampling approach (**table S49**).

For calibration, we ran 100 coalescent simulations of 100,000 independent sites with different split times, ranging from 0 to 250,000 generations, using ms (*98*), and computed the expected F(A|B) values for each split time. The F(A|B) values were converted into time by assuming a mutation rate of $0.435 \times 10^{-9}$ /bp/year (*74, 99*). Here are three example command lines of coalescent simulations with ms (*98*), used for calibration in this study (SPLITTIME indicates the split time in units of time of 4 Ne at time 0):

- following the *Altai Neandertal* population history:

ms 3 40 -I 2 2 1 0 -ej SPLITTIME 2 1 -t 561.023910668551 -r 110.824678989283 30000000 -en 0.0856 1 1.1287 -en 0.1424 1 1.5616 -en 0.2113 1 2.3855 -en 0.2948 1 3.2320 -en 0.3960 1 4.2048 -en 0.5186 1 5.2280 -en 0.6673 1 5.9954 -en 0.8474 1 6.1151 -en 1.0658 1 5.8135 -en 1.3304 1 5.5096 -en 1.6512 1 5.3295 -en 2.0399 1 5.3460 -en 2.5110 1 5.5491 -en 3.0821 1 5.8810 -en 3.7741 1 6.4238 -en 4.6129 1 7.7458 -en 5.6296 1 10.9397 -en 6.8617 1 16.7727 -en 8.3550 1 24.2142 -en 10.1650 1 30.4875 -en 12.3586 1 33.8998 -en 15.0173 1 34.9102 -en 18.2396 1 34.5669 -en 22.1451 1 33.5579 -en 26.8785 1 31.6513 -en 32.6153 1 26.4952 -en 47.9954 1 87.5315

- modeling the *Vindija33.19* population history:

ms 3 40 -I 2 2 1 0 -ej SPLITTIME 2 1 -t 4223.96290935493 -r 821.604855597291 30000000 -en 0.0121 1 0.1380 -en 0.0202 1 0.2749 -en 0.0299 1 0.3972 -en 0.0416 1 0.5473 -en 0.0558 1 0.7037 -en 0.0730 1 0.7776 -en 0.0937 1 0.7865 -en 0.1187 1 0.7527 -en 0.1490 1 0.7222 -en 0.1855 1 0.7141 -en 0.2297 1 0.6949 -en 0.2831 1 0.6628 -en 0.3477 1 0.6554 -en 0.4257 1 0.6922 -en 0.5200 1 0.7766 -en 0.6340 1 0.9086 -en 0.7717 1 1.1381 -en 0.9381 1 1.5819 -en 1.1393 1 2.3415 -en 1.3824 1 3.3024 -en 1.6763 1 4.1052 -en 2.0314 1 4.5758 -en 2.4606 1 4.8093 -en 2.9793 1 4.7910 -en 3.6062 1 4.3875 -en 4.3638 1 3.3049 -en 6.3862 1 12.4491

- following the Mbuti population history:

ms 3 40 -I 2 2 1 0 -ej 0.SPLITTIME 2 1 -t 10366.0844218972 -r 1544.9246695003 30000000 -en 0.0460 1 1.7122 -en 0.0752 1 1.9574 -en 0.1093 1 2.3100 -en 0.1493 1 3.0406 -en 0.1962 1

3.6222 -en 0.2512 1 3.9734 -en 0.3157 1 4.2422 -en 0.3912 1 4.1372 -en 0.4798 1 3.5879 -en 0.5836 1 2.8960 -en 0.7052 1 2.3558 -en 0.8478 1 2.0076 -en 1.0150 1 1.8131 -en 1.2109 1 1.7295 -en 1.4405 1 1.7156 -en 1.7097 1 1.7506 -en 2.0252 1 1.8435 -en 2.3951 1 2.0393 -en 2.8286 1 2.3988 -en 3.3367 1 2.9436 -en 3.9323 1 3.5732 -en 4.6305 1 4.0212 -en 5.4488 1 4.0508 -en 6.4080 1 3.7299 -en 7.5323 1 3.3645 -en 8.8502 1 3.3691 -en 12.2055 1 10.3767

Note that F(A|B) values can be potentially affected by several factors, for example recurrent mutations and sequencing errors. Recurrent mutations would lead to a misassignment of the ancestral and derived states. For example, if we define ancestral alleles as those that are shared with the chimpanzee genome, any back mutation with allele frequency *q* at a position where a derived mutation reached fixation in the human population would be considered as a polymorphism with derived allele frequency 1-*q*. As a consequence, the estimated F(A|B) equals

$$F(A|B)_C = (1-p)*F(A|B)+p*(1-F(A|B)) \text{ and}$$
$$F(A|B)_{CM} \approx (1-p/2)*F(A|B)+p/2*F(A|B)$$

when computed by defining derived alleles as those that are different from the chimpanzee genome (C), or from the chimpanzee and the macaque genomes (CM), respectively, where *p* indicates the proportion of recurrent mutations. Prüfer et al.,2014 (*8*) introduced a correction to estimate F(A|B) while accounting for recurrent mutations by combining these equations into: $F(A|B) \approx 2*F(A|B)_{CM}-F(A|B)_C$. Since the F(A|B) values are lower than 0.5, $F(A|B)_C$ is expected to always be equal or higher than $F(A|B)_{CM}$ and F(A|B). In very low coverage samples, data might not be sufficient to estimate *p* correctly and this expectation might not be fulfilled. Thus, for *HST* and *Scladina I-4A*, we report the corrected F(A|B) values as well as $F(A|B)_{CM}$, representing an upper boundary for the F(A|B) estimate (**table S50**).

Sequencing errors in a low-coverage genome would inflate the F(A|B) statistics because there are more ancestral alleles that can be misread into derived alleles (the F(A|B) value is usually close to 1/3 for a short divergence time, the exact value depending on the demographic history, and lower for deeper split times) and therefore make the population splits appear more recent. Ascertaining heterozygous sites from high-quality genomes limits the number of errors. By considering any third allele as a sequencing error on *HST* or *Scladina I-4A* sequences at A-T polymorphisms identified in the Mbuti genome, we estimated an error rate of 0.0044 (95% binomial CI: 0.0019-0.0086) for *HST* sequences (8 positions with third alleles among 2,733 positions, which should represent 2/3 of the total number of erroneous substitutions if we assume that any substitution is equally likely) and 0.0076 (95% binomial CI: 0.0016-0.0223) for *Scladina I-4A* sequences (3 positions with third alleles among 588 positions). These error rates are potentially overestimates, as third alleles are not unexpected, and suggest that errors should have negligible effects on our F(A|B) estimates: for instance, for *HST*, ~7 errors would be expected at the 1,609 or 1,652 sites used to estimate to F(A|B) values with *Vindija 33.19* or the *Altai Neandertal*, respectively, and ~3 errors at the 346 or 442 sites used for *Scladina I-4A* (**table S49**).

Although F(A|B) values were computed from sequences that exhibit C-to-T substitutions within the last 3bp of either end, remaining contamination from present-day human DNA may influence our F(A|B) estimates. The deep split of 160kya estimated between the populations of the Altai

and Scladina Neandertals is 15 to 30 ky too old if *Scladina I-4A* belonged to the *Vindija 33.19* population, which split from the Altai population 130-145kya (*20*). Noting that F(Vindija|Altai) = 35.9, F(Mbuti|Altai) = 13.1 and that F(Scladina|Altai) = 35.0, solving the equation: C x 13.1 + (1 - C) x 35.9 = 35.0 leads to a contamination rate C of 4%, which is compatible with the contamination estimate of *Scladina I-4A* after filtering for putatively deaminated sequences (Supplementary Note 8). Our split time estimates should therefore be considered as upper estimates, with the exception of the split time from modern humans, as contamination increases the allele sharing with the Mbuti genome.

**Table S46. Comparison between split time estimates from the Vindija population based on a coalescent divergence model and the F(A|B) statistic for five low-coverage Neandertal genomes.** To be consistent with the published estimates using the F(A|B) statistic (*6*), we report results for deaminated sequences only without correction for reference bias or contamination. Generations are assumed to be 29 years long, the internode time is in units of 2Ne generations, with Ne the effective population size. Lines marked in bold fit best the estimates made using the F(A|B) method because an effective population size (Ne) of 2,000 individuals is closer to the average Ne estimated for Neandertals with PSMC (*20*). We assumed a split time between *Vindija 33.19* and the *Altai Neandertal* of 137kya (average of the estimated 130-145kya (*20*)).

| Neandertal | Inferred internode time | Assumed pop. size | Estimates (kya) | Estimates based on F(A\|B) (kya) |
|---|---|---|---|---|
| *Mezmaiskaya 2* | 0.480 [0.467-0.493] | 1,500 | 95.2 [94.1-96.4] | 70.0 [67.4-74.5] |
| | | **2,000** | **81.3 [79.8-82.8]** | |
| | | 2,500 | 67.4 [65.5-69.3] | |
| *Les Cottés Z4-1514* | 0.519 [0.508-0.529] | 1,500 | 91.8 [91.0-92.8] | 70.0 [67.9-72.4] |
| | | **2,000** | **76.8 [75.6-78.1]** | |
| | | 2,500 | 61.7 [60.3-63.3] | |
| *Goyet Q56-1* | 0.704 [0.683-0.725] | 1,500 | 75.8 [73.9-77.6] | 59.9 [57.8-61.9] |
| | | **2,000** | **55.3 [52.9-57.8]** | |
| | | 2,500 | 34.9 [31.9-38.0] | |
| *Spy 94a* | 0.645 [0.622-0.669] | 1,500 | 80.9 [78.8-82.9] | 62.7 [59.1-64.8] |
| | | **2,000** | **62.2 [59.4-64.8]** | |
| | | 2,500 | 43.5 [40.0-46.8] | |
| *Mezmaiskaya 1* | 0.343 [0.329-0.357] | 1,500 | 107.2 [105.9-108.4] | 98.7 [94.5-102.9] |
| | | **2,000** | **97.2 [95.6-98.8]** | |
| | | 2,500 | 87.3 [85.2-89.3] | |

**Table S47. Split time estimates from the Vindija population based on a coalescent divergence model.** The internode time is in units of 2Ne generations, with Ne the effective population size. To convert these estimates into population split time since present (in kya), we assumed a generation of 29 years, three different effective population sizes and used two split times between the *Altai Neandertal* and *Vindija 33.19* populations of 130kya (cal. with 130kya) and 145kya (cal. with 145kya) that represent the two published estimates (*20*).

| Neandertal | Dataset | Internode time | Assumed pop. size | Split time estimate (cal. with 130kya) | Split time estimate (cal. with 145kya) |
|---|---|---|---|---|---|
| *HST* | Deaminated | 0.054 [0.019-0.092] | 1,500 | 125.3 [122.0-128.3] | 140.3 [137.0-143.3] |
| | | | 2,000 | 123.7 [119.3-127.8] | 138.7 [134.3-142.8] |
| | | | 2,500 | 122.2 [116.7-127.2] | 137.2 [131.7-142.2] |
| *HST* | All sequences | 0.05 [0.029-0.072] | 1,500 | 125.7 [123.7-127.5] | 140.7 [138.7-142.5] |
| | | | 2,000 | 124.2 [121.6-126.6] | 139.2 [136.6-141.6] |
| | | | 2,500 | 122.8 [119.6-125.8] | 137.8 [134.6-140.8] |
| *Scladina I-4A* | Deaminated | 0.058 [0-0.136] | 1,500 | 125.0 [118.2-130.0] | 140.0 [133.2-145.0] |
| | | | 2,000 | 123.3 [114.2-130.0] | 138.3 [129.2-145.0] |
| | | | 2,500 | 121.6 [110.3-130.0] | 136.6 [125.3-145.0] |
| *Scladina I-4A* | All sequences | 0.143 [0.092-0.197] | 1,500 | 117.3 [112.9-122.0] | 132.3 [127.9-137.0] |
| | | | 2,000 | 113.4 [107.1-119.3] | 128.4 [122.1-134.3] |
| | | | 2,500 | 109.3 [101.4-116.7] | 124.3 [116.4-131.7] |

**Table S48. Age estimate for individual B (branch shortening) used to convert the F(A|B) values shown in table S47 into time before present (*20*).**

| Population B | Branch shortening (kya) |
|---|---|
| *Vindija 33.19* | 51.8 |
| *Altai Neandertal* | 122.4 |
| *Denisova 3* | 72 |
| Mbuti (HGDP00982) | 0 |

**Table S49. Summary of the number of sites and blocks used to compute the F(A|B) statistic and CIs.**

| Neandertal | Population B | Number of sites | Number of jackknife blocks |
|---|---|---|---|
| *Scladina I-4A* | *Altai Neandertal* | 346 | 236 |
| *HST* | *Altai Neandertal* | 1,652 | 382 |
| *Scladina I-4A* | *Vindija 33.19* | 394 | 251 |
| *HST* | *Vindija 33.19* | 1,609 | 402 |
| *Scladina I-4A* | *Denisova 3* | 442 | 256 |
| *HST* | *Denisova 3* | 1,830 | 419 |
| *Scladina I-4A* | Mbuti (HGDP00982) | 2,084 | 380 |
| *HST* | Mbuti (HGDP00982) | 8,984 | 512 |

**Table S50. Split time estimates between *HST* or *Scladina I-4A* and different populations (population B) based on the calibration of the F(A|B) statistic.** We report the results for transversions only and assuming a mutation rate of $0.435 \times 10^{-9}$ /bp/year (*74*, *99*). For the F(A|B) with the *Altai Neandertal* or *Vindija 33.19* as representative of population B, we used the alignments to both the original human reference (hg19) and its modified version including alleles from *Vindija 33.19* and the *Altai Neandertal* that differ from hg19. Confidence intervals were obtained by jackknife resampling, using blocks of 5Mb. The Mbuti genome used is HGDP00982 (*8*). $F(A|B)_{CM}$ represents estimates when defining derived alleles as those that are different from both the chimpanzee and the macaque genomes.

| Neandertal | Population B | F(A\|B) [C.I.] (%) | $F(A\|B)_{CM}$ (%) | time ky [C.I.] | time kya [C.I.] |
|---|---|---|---|---|---|
| *Scladina I-4A* | *Altai Neandertal* | 34.7 [29.2-40.2] | 35 | 37.7 | 160.1 [128.8-209.5] |
| *HST* | *Altai Neandertal* | 38.3 [35.8-40.8] | 38.1 | 10.6 | 133 [ 128 -144.7] |
| *Scladina I-4A* | *Vindija 33.19* | 30.3 [25.1-35.5] | 30.2 | 48.2 | 100 [66.4-152.7] |
| *HST* | *Vindija 33.19* | 30.1 [27.5-32.7] | 30.5 | 49.3 | 101.1 [80.2-122.7] |
| *Scladina I-4A* | *Denisova 3* | 14.2 [10.7-17.7] | 14 | 298 | 370 [304.8-493.5] |
| *HST* | *Denisova 3* | 14 [11.8-16.2] | 14.5 | 302 | 373.9 [329.2-440.8] |
| *Scladina I-4A* | Mbuti | 18.2 [16.3-20.1] | 18.2 | 492.3 | 492.3 [394.5-599.7] |
| *HST* | Mbuti | 18 [17.1-18.9] | 18.3 | 501.8 | 501.8 [455.8-553.7] |

# Note S11. Discordance between the nuclear and mitochondrial divergence of *HST* to other Neandertals.

Mitochondrial DNA has a specific mode of inheritance, transmitted solely from a mother to an offspring. This uniparental mode of inheritance leads to a lower effective population size of the mitochondrial DNA compared to the nuclear DNA. As a result, mitochondrial lineages tend to find common ancestors more recently than autosomal lineages because of the reduced pool of ancestors in each generation.

In contrast to this expectation, the mitochondrial genome of *HST* represents a surprisingly divergent lineage (*10*) given the relatively more recent split times observed between *HST* and late European Neandertals (Supplementary Note 10, **table S50**). To test whether this mitochondrial lineage is at odds with the nuclear divergence, we explored the distribution of expected time to the most recent common ancestor (TMRCA) with simulations and using different split times between the populations of *HST* and the *Vindija 33.19* Neandertal (between 55 and 145kya, in steps of 5,000 years). In these simulations, we used the demographic history estimated from PSMC with the nuclear genome of the *Vindija 33.19* Neandertal (see Supplementary Information 7 from (*20*)) and scaled the effective population sizes to account for the lower size expected for the mitochondrial DNA. Although the scaling is often assumed to be one quarter, there may have been differences in male and female effective population sizes in Neandertals due to demographic processes or differences in reproductive success. Indeed, the ratio of females to males has been previously estimated to 1.54 for the *Altai Neandertal* population (*8*), and as this would reduce the difference of population sizes between autosomes and mitochondrial genome we used this estimate as a conservative scaling of the population sizes. If we define $N_{mt}$, $N_f$, $N_m$ and $N_e$ as the mitochondrial, female, male and autosomal effective population sizes respectively, we have the following equations: $\frac{N_f}{N_m} = 1.54$, $N_{mt} = \frac{N_f}{2}$ (assuming equal probability of transmission to a male or a female) and $N_f + N_m = N_e$ leading to the following scaling $N_{mt} = \frac{1}{2} \times \frac{N_e}{1+\frac{1}{1.54}}$.

We report in **table S51** the average TMRCA of 10,000 coalescent simulations (carried out with scrm (*36*)) for each population split time tested. We also computed the probability to have a most recent common ancestor (MRCA) as old as or older than the estimated TMRCA between *HST* and other Neandertals (270kya according to (*10*) and 215kya according to (*6*)) as the proportion of simulated loci having such deep MRCAs. For the TMRCA distribution for each population split time, see **fig. S19**.

Here is an example of a command line for scrm (*36*) used to simulate a population split of 50ky before *Vindija 33.19*, corresponding to ~100 kya:

scrm 2 10000 -L -t 42.51259 -I 2 1 1 -n 1 .3031 -ej 0.507 2 1 -en 0.0436 1 .1362 -en 0.0724 1 .3451 -en 0.1073 1 .5146 -en 0.1494 1 .6491 -en 0.2004 1 .7661 -en 0.2620 1 .8390 -en 0.3365 1 .8559 -en 0.4266 1 .8221 -en 0.5355 1 .7960 -en 0.6671 1 .7934 -en 0.8264 1 .7743 -en 1.0189 1 .7388 -en 1.2516 1 .7291 -en 1.5331 1 .7665 -en 1.8733 1 .8546 -en 2.2848 1 .9960 -en 2.7822 1 1.2441 -en 3.3837 1 1.7204 -en 4.1109 1 2.5346 -en 4.9902 1 3.5889 -en 6.0533 1 4.5119 -en 7.3388 1 5.0719 -en 8.8930 1 5.3460 -en 10.7722 1 5.3395 -en 13.0443 1 4.8967 -en 15.7915 1 3.6552 -en 23.1293 1 13.6043

We find that the occurrence of a mitochondrial MRCA 270kya (or even 215kya) is significantly unlikely given the split time between *HST* and other European Neandertals ~100kya (p=0.012 for a MRCA 270kya and p=0.0496 for a MRCA 215kya). Instead, the probability of a mitochondrial MRCA as old as or older than 270kya becomes greater than 5% for a population that split more than 155kya from other Neandertals (**table S52**). In fact, 270kya is the expected age of the mitochondrial MRCA for a population that split 225kya (**table S52**). These observations are robust to the uncertainties in the Neandertal population sizes estimated with PSMC, as using the upper estimates from the 95% confidence intervals of the population sizes only shifts our estimates by around 5,000 years (**table S53**).

Here is an example of a command line for scrm (*36*) using the upper estimates of the Neandertal population size (*20*) (example again with a population split from the *Vindija 33.19* population 50ky before *Vindija 33.19*):

scrm 2 10000 -L -t 42.51259 -I 2 1 1 -ej 0.507 2 1 -en 0.0436 1 0.149331 -en 0.0724 1 0.387274 -en 0.1073 1 0.539576 -en 0.1494 1 0.716252 -en 0.2004 1 0.853427 -en 0.2620 1 0.89799 -en 0.3365 1 0.925243 -en 0.4266 1 0.901597 -en 0.5355 1 0.874617 -en 0.6671 1 0.841058 -en 0.8264 1 0.823112 -en 1.0189 1 0.767666 -en 1.2516 1 0.776548 -en 1.5331 1 0.797647 -en 1.8733 1 0.915451 -en 2.2848 1 1.02522 -en 2.7822 1 1.30321 -en 3.3837 1 1.79316 -en 4.1109 1 2.61654 -en 4.9902 1 3.77182 -en 6.0533 1 4.61154 -en 7.3388 1 5.18449 -en 8.8930 1 5.47955 -en 10.7722 1 5.45718 -en 13.0443 1 5.00603 -en 15.7915 1 3.80031 -en 23.1293 1 14.117

We conclude that the mitochondrial DNA of *HST* is likely the result of admixture, either with an isolated Neandertal population or a population related to modern humans as described in the main text (**Fig. 3**).

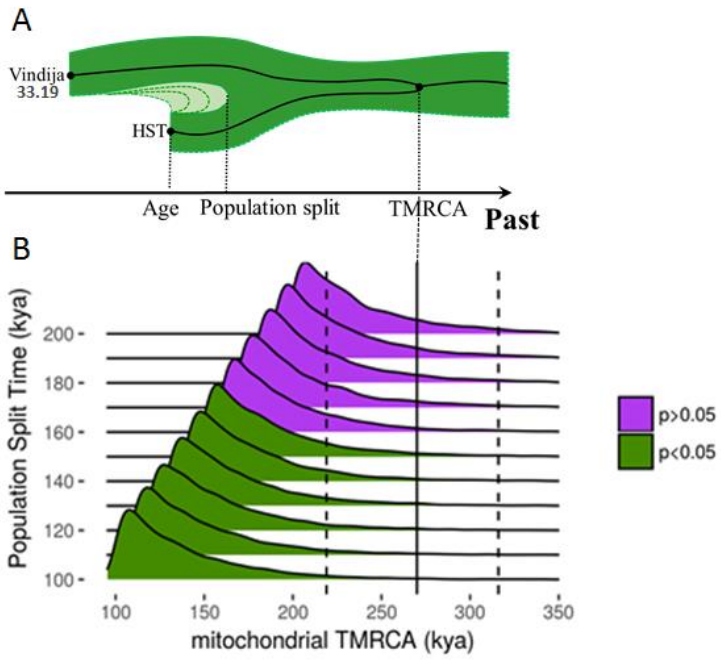


**Fig. S19. Comparison of the expected and observed mitochondrial TMRCA of *HST* with other European Neandertals.** (A) Illustration of the simulated history for two mitochondrial lineages (*HST* and *Vindija 33.19*) with varying population sizes (inferred from the high-coverage *Vindija 33.19* genome) and different population split times (light green). (B) Distribution of TMRCAs from 10,000 simulated loci for each population split time (from 100 to 200kya). Distributions in green correspond to population split times incompatible with the observed TMRCA (vertical solid line; dashed lines correspond the 95% HPD interval bounds of this TMRCA estimate (*10*)) while distributions in purple are not significantly different from the observed TMRCA.

**Table S51. Predictions of the mitochondrial TMRCA given different split times between the populations of *HST* and *Vindija 33.19*.** We performed 10,000 coalescent simulations per split time and recorded the average mitochondrial TMRCA as well as the proportion of loci that share a most recent common ancestor that is older than either 270kya (*10*) or 215kya (*6*). For the simulations, we used the demographic history estimated from PSMC with the nuclear genome of the *Vindija 33.19* Neandertal (see Supplementary Information 7 from (*20*)) and scaled the effective population sizes to account for the lower size expected for the mitochondrial DNA (assuming a female to male ratio of 1.54 for Neandertals (*8*)).

| Population Split Time (years ago) | Average Mitochondrial TMRCA | Probability that TMRCA ⩾ 270,000 years ago | Probability that TMRCA ⩾ 215,000 years ago |
|---|---|---|---|
| 55,000 | 80,661 | 0.0032 | 0.0087 |
| 60,000 | 95,834 | 0.0044 | 0.0138 |
| 65,000 | 103,548 | 0.0067 | 0.0203 |
| 70,000 | 109,729 | 0.0056 | 0.0216 |
| 75,000 | 115,301 | 0.0066 | 0.0266 |
| 80,000 | 119,629 | 0.0064 | 0.0277 |
| 85,000 | 124,245 | 0.0077 | 0.0306 |
| 90,000 | 128,820 | 0.0111 | 0.0357 |
| 95,000 | 134,042 | 0.0104 | 0.0425 |
| 100,000 | 139,237 | 0.012 | 0.0496 |
| 105,000 | 143,842 | 0.015 | 0.0548 |
| 110,000 | 148,870 | 0.0175 | 0.0592 |
| 115,000 | 153,498 | 0.0166 | 0.066 |
| 120,000 | 157,482 | 0.0188 | 0.0736 |
| 125,000 | 163,077 | 0.0221 | 0.0857 |
| 130,000 | 167,442 | 0.027 | 0.099 |
| 135,000 | 172,399 | 0.0283 | 0.1099 |
| 140,000 | 177,882 | 0.0354 | 0.128 |
| 145,000 | 182,910 | 0.0372 | 0.1478 |

**Table S52. Predictions of the mitochondrial TMRCA given different split times between the *Vindija 33.19* population and a hypothetical isolated Neandertal population.** See **table S51** for more details.

| Population Split Time (years ago) | Average Mitochondrial TMRCA | Probability that TMRCA ⩾ 270,000 years ago | Probability that TMRCA ⩾ 215,000 years ago |
|---|---|---|---|
| 150,000 | 188,274 | 0.042 | 0.1726 |
| 155,000 | 193,277 | 0.0485 | 0.1989 |
| 160,000 | 198,569 | 0.0572 | 0.2229 |
| 165,000 | 204,659 | 0.0676 | 0.2602 |
| 170,000 | 208,144 | 0.0736 | 0.2925 |
| 175,000 | 214,595 | 0.0842 | 0.3388 |
| 180,000 | 219,905 | 0.0985 | 0.3861 |
| 185,000 | 226,343 | 0.1123 | 0.4436 |
| 190,000 | 230,573 | 0.1242 | 0.5127 |
| 195,000 | 237,052 | 0.1473 | 0.5853 |
| 200,000 | 241,442 | 0.183 | 0.66 |
| 205,000 | 248,606 | 0.1967 | 0.7686 |
| 210,000 | 254,558 | 0.2289 | 0.8783 |
| 215,000 | 259,306 | 0.2583 | 1 |
| 220,000 | 265,100 | 0.2988 | 1 |
| 225,000 | 271,000 | 0.3319 | 1 |
| 230,000 | 278,646 | 0.3862 | 1 |
| 235,000 | 282,793 | 0.4402 | 1 |
| 240,000 | 290,710 | 0.4874 | 1 |
| 245,000 | 296,796 | 0.56 | 1 |
| 250,000 | 302,336 | 0.6255 | 1 |

**Table S53. Predictions of the mitochondrial TMRCA as done for table S51 but using either the upper or the lower estimates of the Neandertal population size.** We used the lower or upper estimates of the 95% confidence intervals of the population sizes estimated from PSMC with the *Vindija 33.19* genome (100 bootstraps with PSMC default parameters). See **table S51** for more details.

| | Based on the upper estimates of the Neandertal population size | | Based on the lower estimates of the Neandertal population size | |
|---|---|---|---|---|
| Population Split Time (years ago) | Average Mitochondrial TMRCA | Probability that TMRCA ⩾ 270,000 years ago | Average Mitochondrial TMRCA | Probability that TMRCA ⩾ 270,000 years ago |
| 60,000 | 98,724 | 0.0055 | 93,217 | 0.0027 |
| 70,000 | 112,500 | 0.0067 | 107,193 | 0.0038 |
| 80,000 | 123,088 | 0.0098 | 118,740 | 0.0055 |
| 90,000 | 132,361 | 0.0149 | 127,260 | 0.007 |
| 100,000 | 142,208 | 0.0153 | 136,901 | 0.0092 |
| 110,000 | 151,044 | 0.0182 | 147,229 | 0.0137 |
| 120,000 | 159,993 | 0.0246 | 155,964 | 0.0133 |
| 130,000 | 169,799 | 0.0318 | 166,534 | 0.0226 |
| 140,000 | 180,348 | 0.041 | 175,579 | 0.029 |
| 150,000 | 190,316 | 0.054 | 185,647 | 0.0388 |
| 160,000 | 201,079 | 0.0702 | 195,435 | 0.047 |
| 170,000 | 211,698 | 0.0878 | 205,602 | 0.0616 |
| 180,000 | 222,610 | 0.108 | 217,195 | 0.0885 |
| 190,000 | 233,185 | 0.145 | 227,719 | 0.112 |
| 200,000 | 245,455 | 0.1921 | 240,146 | 0.1583 |
| 210,000 | 257,276 | 0.2488 | 250,753 | 0.2082 |
| 220,000 | 269,836 | 0.3164 | 263,867 | 0.2847 |
| 230,000 | 281,027 | 0.4038 | 275,581 | 0.3708 |
| 240,000 | 295,140 | 0.5182 | 286,709 | 0.4776 |

# Note S12. Likelihood of a recent mitochondrial replacement in Neandertals.

To investigate whether an admixture with an early population of modern humans could have happened more recently than 270kya (the estimated time of the Neandertal mitochondrial MRCA according to (*10*)) but before the Neandertals split from each other ~140kya, we calculated the probability that all sampled Neandertal mtDNAs come from an early modern human population, as done previously (Supplementary Note 5 of (*10*)). We assumed a generation time of 29 years, a constant population size (***N***) and an instantaneous admixture event. We first consider a scenario where 23 Neandertal mitochondrial lineages were sampled 40 kya and calculated the probability of there being ***m*** remaining lineages at the time of admixture, ***t***, measured in generations from the time of sampling (*100*, *101*)

$$g_{n,m}(t) = \sum_{i=m}^{n} \frac{(-1)^{k-m}(2i-1)m_{(i-1)}n_{[i]}}{m!\,(i-m)!\,n_{(i)}} e^{\frac{-i(i-1)t}{4N}}$$

where

$$n_{(k)} = n(n+1)\ldots(n+k-1), k \geq 1; n_{(0)} = 1$$
$$n_{[k]} = n(n-1)\ldots(n-k+1); n_{[0]} = 1$$

We then calculated the probability that *j* lineages (out of *m* lineages present at the time of admixture) came from the introgressing population, assuming a binomial sampling with the probability of success, noted *r*, corresponding to the admixture rate (*10*)

$$b(,m,r) = \binom{m}{j} r^j (1-r)^{n-j}$$

The probability that all sampled lineages come from the introgressing population is therefore

$$P(n,r,t) = \sum_{m=1}^{n} g_{n,m}(t) b(m,m,r)$$

We report results with different admixture rates (from 1% to 99%, in steps of 1%) and different mitochondrial effective population sizes (between 100 and 2,000) (**fig. S20**). Because of the estimated low population size in Neandertals (in the order of 500 for the mitochondrial effective population size, assuming a quarter of the autosomal population size of 2,000 (*30*)), the

probability of sampling lineages only from this introgressing population is very close to the admixture rate, even in the scenario of an admixture event happening as recently as 140kya.

Note that in reality, *HST*, *Scladina I-4A* and the *Altai Neandertal* lineages were sampled much earlier than 40kya, around 100-120kya. We therefore modelled a scenario where 3 lineages were first sampled 100kya followed by 20 more lineages sampled 40kya

$$P(n_1 = 20, n_2 = 3, r, t_1, t_2) = \sum_{i=1}^{20} \sum_{m=1}^{i+3} g_{20,i}(t_1) g_{i+3,m}(t_2) b(m, m, r)$$

with $t_1$ the time between the two samplings ($t_1$=60ky), and $t_2$ the time between the first sampling (100kya) and the admixture event (140kya or 270kya; so that $t_2$=40ky or 170ky). With this model, the probability that all sampled Neandertal mtDNAs come from the modern human lineage is lower for a recent admixture but remains close to the admixture rate for an older event (**fig. S21**).

We conclude that an introgression more recent than the Neandertal MRCA (270kya) is possible given the small population size of Neandertals, as long as a sufficient percentage of admixture took place.

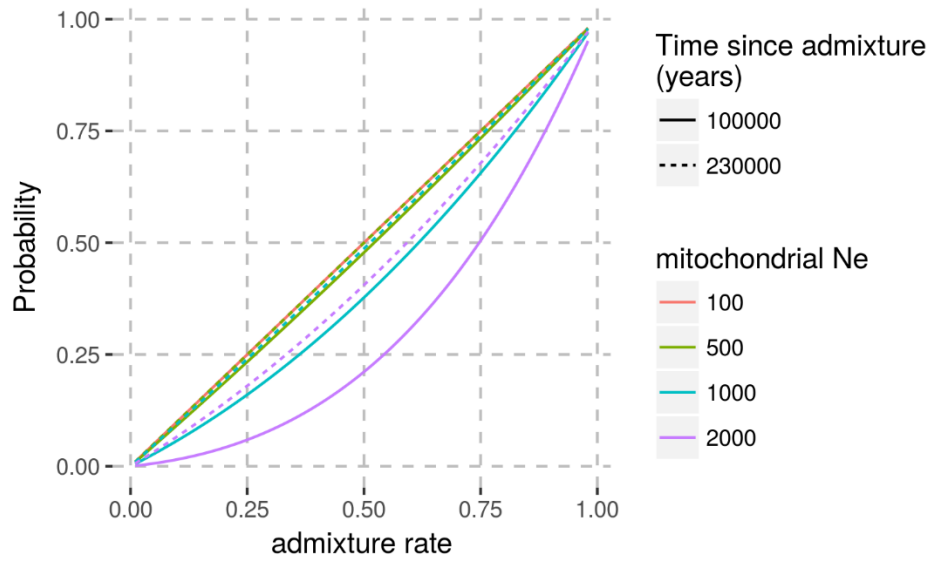


**Fig. S20. Probability that all sampled Neandertal mtDNAs come from an early modern human population as a function of the admixture rate.** We assumed here a sample of 23 Neandertal lineages sampled 40kya, with a constant population size. The time since admixture corresponds to years before the sampling time.

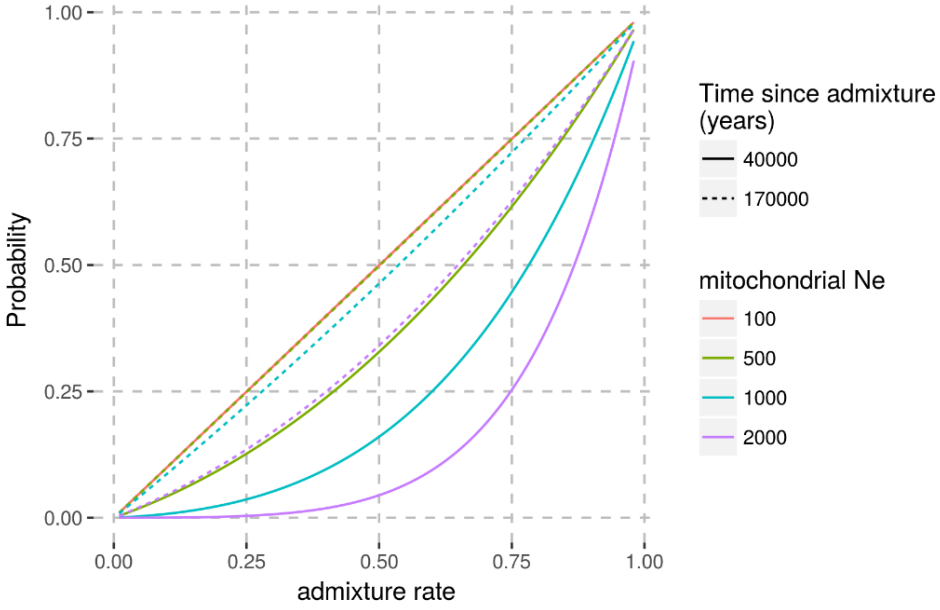


**Fig. S21. Probability that all sampled Neandertal mtDNAs come from an early modern human population as a function of the admixture rate.** We assumed a sample of three lineages 100kya and 20 more lineages 40kya, with a constant population size. The time since admixture corresponds to years before the first sampling time 100kya.